



저작자표시-비영리-변경금지 2.0 대한민국

이용자는 아래의 조건을 따르는 경우에 한하여 자유롭게

- 이 저작물을 복제, 배포, 전송, 전시, 공연 및 방송할 수 있습니다.

다음과 같은 조건을 따라야 합니다:



저작자표시. 귀하는 원저작자를 표시하여야 합니다.



비영리. 귀하는 이 저작물을 영리 목적으로 이용할 수 없습니다.



변경금지. 귀하는 이 저작물을 개작, 변형 또는 가공할 수 없습니다.

- 귀하는, 이 저작물의 재이용이나 배포의 경우, 이 저작물에 적용된 이용허락조건을 명확하게 나타내어야 합니다.
- 저작권자로부터 별도의 허가를 받으면 이러한 조건들은 적용되지 않습니다.

저작권법에 따른 이용자의 권리는 위의 내용에 의하여 영향을 받지 않습니다.

이것은 [이용허락규약\(Legal Code\)](#)을 이해하기 쉽게 요약한 것입니다.

[Disclaimer](#)

A THESIS
FOR THE DEGREE OF DOCTOR OF PHILOSOPHY

**Development of Piezoelectric and Triboelectric
Nanogenerator for Self-powered Device
Applications**

 제주대학교 중앙도서관
BALASUBRAMANIAM SARAVANAKUMAR

Department of Mechatronics Engineering
GRADUATE SCHOOL
JEJU NATIONAL UNIVERSITY

2015. 02

Development of Piezoelectric and Triboelectric Nanogenerator for Self-powered Device Applications

Balasubramaniam Saravanakumar
(Supervised by Professor Sang-Jae Kim)

A thesis submitted in partial fulfillment of the requirement for the degree of Doctor of Philosophy

2014. 12.

This thesis has been examined and approved.

Thesis Director,
Prof. Byung-Gul Lee

Professor, Department of Civil Engineering,
College of Ocean Science, Jeju National University

Thesis Committee Member,
Prof. Jin-Ho Bae

Professor, Department of Ocean System Engineering,
College of Ocean Science, Jeju National University

Thesis Committee Member,
Prof. Sang-Jae Kim

Professor, Department of Mechatronics Engineering,
College of Engineering, Jeju National University

Thesis Committee Member,
Prof. Hyeon Suk Shin

Associate Professor, Department of Chemistry,
Ulsan National Institute of Science and Technology

Thesis Committee Member,
Prof. Sang Min Lee

Assistant Professor, School of Mechanical Engineering,
Chung-Ang University

December 11, 2014.

Department of Mechatronics Engineering

GRADUATE SCHOOL

JEJU NATIONAL UNIVERSITY

REPUBLIC OF KOREA

Dedication

Every challenging work needs self efforts as well as
guidance of elders especially those who were very
close to our heart

My humble effort I dedicate to

My Parents (***Mr. M. Balasubramaniam &***

Mrs. Umavathi)

&

Brother (***Mr. B. Sureshkumar***) Niece (***Dhaksha***)

&

Friends

Along with all hard working and respected

Teachers and Professors

Especially, Late. Dr. Ananth

Contents

	Acknowledgements	xviii
	Abstract in Hangeul	1
	Abstract	2
I	Introduction	
	1.1. Introduction	4
	1.2. Piezoelectricity	6
	1.3. Zinc oxide Nanostructure	7
	1.4. Review of Literature	8
	1.5. Objectives and Scope of the Present Work	9
	1.6. Thesis overview	11
	References	13
II	Microwire based Nanogenerator	
	2.1. Growth of ZnO microwire	18
	2.2. Fabrication of ZnO Microwire based Piezoelectric Nanogenerator	19
	2.3. Fabrication of ZnO Microwire - Polyvinylidene fluoride (PVDF) based inorganic- organic hybrid piezoelectric nanogenerator	30
	2.4. Conclusion	32
	References	33
III	Aligned Nanowire Array based Nanogenerator	
	3.1. Introduction	35
	3.1.1. Synthesis of vertically aligned ZnO nanowire array	35
	3.1.2. ZnO Seed Layer	37

3.1.3. Different Substrate	39
3.1.4. Growth Temperature	41
3.2. Single side Aligned ZnO Nanowire Array Based Nanogenerator	43
3.3. Double side Aligned ZnO Nanowire Array Based Nanogenerator	49
3.3.1. Preparation of ZnO Seed Layer	50
3.3.2. Growth of ZnO Nanowire Array	50
3.3.3. Fabrication of ZnO Nanowire Array Nanogenerator	51
3.3.4. Results and discussion	51
3.4. Conclusion	68
References	70
IV ZnO Nanowall based Nanogenerator	
4.1. Introduction	75
4.2. Experimental Section	
4.2.1. Fabrication of Seed Layer	76
4.2.2. Hydrothermal Growth of ZnO Nanowall	76
4.2.3. Fabrication of Nanogenerator Device	77
4.3. Results and discussion	77
4.4. Conclusion	87
References	88
V Organic – Inorganic Hybrid Composite Nanogenerator	
5.1. Introduction	92
5.2. Experimental Section	
5.2.1. Growth of ZnO Nanowires	93

5.2.2. Fabrication of the Hybrid Composite Nanogenerator	94
5.2.3. Characterization	94
5.3. Results and discussion	95
5.4. Conclusion	111
References	112
VI Carbon based Composite Nanogenerator	
6.1. Introduction	117
6.2. Experimental Section	
6.2.1. Preparation of Graphene Oxide (GO)	118
6.2.2. Preparation of Reduced Graphene Oxide (rGO)	118
6.2.3. Preparation of rGO – ZnO Nanowire Composites	119
6.2.4. Fabrication of the rGO-ZnO Composite Nanogenerator	119
6.2.5. Characterization	119
6.3. Results and discussion	120
6.4. Conclusion	132
References	133
VII Triboelectric Nanogenerator	
7.1. Introduction	136
7.2. Fabrication of Triboelectric Nanogenerator	141
7.3. Results and discussion	141
7.4. Conclusion	144
References	145

VIII	Self-Powered Device Applications	
	8.1. Introduction	148
	8.2. Experimental Section	
	8.2.1. Fabrication of pH sensor	149
	8.2.2. Fabrication of UV Photo sensor	149
	8.3. Results and discussion	
	8.3.1. Self-powered pH sensor	150
	8.3.2. Self-powered UV Photo sensor	156
	8.4. Conclusion	161
	References	162
IX	Summary and Future Direction	164
	Publication and Conference Presentation	166



List of Table

Table.5.1.	Comparison of the performance of other reported PDMS based composite- nanogenerators	104
------------	--	-----



List of Figures

Fig.1.1	Schematic diagram of piezoelectric effect and inverse piezoelectric effect	6
Fig.1.2.	Crystal Structure of ZnO	7
Fig.1.3.	Summary of the development of ZnO based piezoelectric nanogenerator	9
Fig.1.4.	Thesis over view	11
Fig.2.1.	Schematic diagram of the vapor transport growth experimental setup for the growth of ZnO micro/nanowires. The used source materials ZnO, metal Zn, and graphite, with weight ratio of 1.5:0.5:1. The experiment was carried out at 1100°C for 1 hr under elevated condition ($O_2/Ar = 30/350$ sccm).	18
Fig.2.2.	Schematic representation of microwire based nanogenerator device	19
Fig.2.3.	X-ray diffraction (XRD) pattern of ZnO microwire	20
Fig.2.4.	Field emission scanning electron microscopic (FE-SEM) image of ZnO microwire	20
Fig.2.5.	Raman spectrum of single ZnO microwire	21
Fig.2.6.	Schematic diagram of Raman measurement strain and strain free state	22
Fig.2.7.	Raman spectra of ZnO microwire at strain and strain free state	23
Fig.2.8.	ZnO microwire based piezoelectric nanogenerator, a) single wire, b) double wire, c) three wire, and d) four wire	24
Fig.2.9.	Schematic diagram of the force applying setup	24

Fig.2.10.	Schematic diagram of the device connection in forward and reverse connection	25
Fig.2.11.	Single wire nanogenerator, open-circuit voltage and short circuit current under forward and reverse connection condition	26
Fig.2.12.	Two wire nanogenerator, open-circuit voltage and short circuit current under forward and reverse connection condition	26
Fig.2.13.	Three wire nanogenerator, open-circuit voltage and short circuit current under forward and reverse connection condition	27
Fig.2.14.	Three wire nanogenerator, open-circuit voltage and short circuit current under forward and reverse connection condition	28
Fig.2.15.	Mechanism of electrical output generation in ZnO microwire based nanogenerator	29
Fig.2.16.	Schematic diagram of ZnO microwire - PVDF hybrid piezoelectric nanogenerator	30
Fig.2.17.	Raman spectrum of ZnO microwire - PVDF hybrid wire. The inset shows the optical image took in Raman instrument.	31
Fig.2.18.	The electrical output performance of the ZnO microwire- PVDF hybrid nanogenerator, open-circuit voltage and short circuit current under forward and reverse connection condition	31
Fig.3.1.	X-ray diffraction pattern of the as grown nanowire with different seed layer concentrations (0.2, 0.4, 1 M) at 50 mM of Zinc nitrate/HMTA @ 90°C for 6 h.	38
Fig.3.2.	Field emission scanning electron microscopic (FE-SEM) image of ZnO nanowire grown at 50 mM of Zinc nitrate/HMTA @ 90°C for 6 h with different seed layer concentration (0.2, 0.4 and 1 M)	39
Fig.3.3.	XRD pattern of ZnO nanowire array grown on ITO and Si substrate	40

Fig.3.4.	FE-SEM image of ZnO nanowire array grown on ITO and Si substrate	41
Fig.3.5.	Field emission scanning electron microscopic (FE-SEM) image of ZnO nanowire grown at different growth temperature	43
Fig.3.6	Schematic diagram of the aligned ZnO nanowire growth	44
Fig.3.7.	X-ray diffraction pattern of aligned ZnO nanowire array on single side of the PET substrate	45
Fig.3.8.	Raman spectrum of as grown aligned ZnO nanowire array	45
Fig.3.9.	FE-SEM image of aligned nanowire array in-plane view. Insets cross sectional and 20° tilted view.	46
Fig.3.10.	The electrical output performance of the single side ZnO nanowire array nanogenerator, output voltage under forward and reverse connection condition.	47
Fig.3.11.	The electrical output performance of the single side ZnO nanowire array nanogenerator at different pressing speed of 25, 50 mm.s ⁻¹	48
Fig.3.12.	The rectified voltage and current under pressing speed of 50 mm.s ⁻¹ . The digital images of the electronic device powered through nanogenerator.	49
Fig.3.13.	Schematic diagram of the ZnO nanowire growth and nanogenerator device fabrication process	52
Fig.3.14.	XRD pattern of vertically grown ZnO nanowire on PET substrate	53
Fig.3.15.	The optical and FESEM image of a) as grown ZnO nanowire, b) Gold coated ZnO nanowire, c) top view of as grown ZnO nanowire (insert: 20° tilted image), d) top view of gold coated ZnO nanowire (insert: 20° tilted image & higher magnification).	54
Fig.3.16.	a) 3D Schematic representation of the fabricated nanogenerator device. b) Digital image of the real device. c) FESEM image of interface depiction.	55

- Fig.3.17. Electrical measurements of the nanogenerator device, a) open circuit voltage, and b) short circuit current of the PDMS device during the multiple folding and releasing of nanogenerator by fingers. c) Open circuit voltage, and d) short circuit current of the PET device during the multiple folding and releasing of nanogenerator by fingers. 57
- Fig.3.18. Electrical measurement of the nanogenerator device, a) digital image of nanogenerator device when folding and releasing using hand, b) open circuit voltage of the device the during multiple folding and releasing, and c) the enlarged view of the boxed area of voltage and schematic diagram of biased condition (inset), d) closed circuit current of the device during the multiple folding and releasing, and e) the enlarged view of the boxed area of current. 59
- Fig.3.19. Electrical measurement of the nanogenerator device, a) digital image of nanogenerator device when folding and releasing using hand, b) open circuit voltage of the device the during multiple folding and releasing, and c) the enlarged view of the boxed area of voltage and schematic diagram of biased condition (inset), d) closed circuit current of the device during the multiple folding and releasing, and e) the enlarged view of the boxed area of current. 60
- Fig.3.20. Electrical measurement of the nanogenerator device with flat electrode, a) open circuit voltage, and b) short circuit current during the multiple folding and releasing of nanogenerator. 61
- Fig.3.21. Electrical measurement of the nanogenerator device with Au coated ZnO nanowire electrode without PDMS, a) open circuit voltage and, b) short circuit current during the multiple folding and releasing of nanogenerator. 61

- Fig.3.22. Electrical measurement of the nanogenerator device, a) digital image of nanogenerator device when stretching and releasing of finger, b) open circuit voltage of the device during the multiple stretching and releasing, and c) the enlarged view of the boxed area of voltage, d) closed circuit current of the device during the multiple stretching and releasing, and e) the enlarged view of the boxed area of current. 63
- Fig.3.23. Electrical measurements of the nanogenerator device, a) digital image of nanogenerator device when stretching and releasing of finger, b) open circuit voltage of the device the during multiple stretching and releasing, and c) the enlarged view of the boxed area of voltage, d) closed circuit current of the device during the multiple stretching and releasing, and e) the enlarged view of the boxed area of current. 64
- Fig.3.24. Electrical measurements of the nanogenerator device, a) optical image of nanogenerator device when pressing and releasing, b) open circuit voltage of the device during the multiple pressing and releasing, and c) the enlarged view of the boxed area of voltage, d) closed circuit current of the device during the multiple pressing and releasing, and e) the enlarged view of the boxed area of current. 65
- Fig.3.25. a) The output power of the nanogenerator with various load resistances. b) Schematic diagram of full wave bridge rectifier circuit. c) Open circuit voltage of the nanogenerator rectified by a bridge rectifier and enlarged view of one cycle (inset) during the multiple folding and releasing by fingers. d) Short circuit current of the nanogenerator rectified by a bridge rectifier and enlarged view of one cycle (inset) during the multiple folding and releasing by fingers. 66
- Fig.3.26. a) Voltage across the single capacitor during the multiple folding 68

and releasing of nanogenerator by fingers, and b) enlarged portion of the charging curve and extended view of the charging curve for one cycle of folding and releasing of nanogenerator by fingers (inset). c) Snapshot of the LED before and after lighting up using the stored energy.

Fig.4.1.	XRD pattern of ZnO nanowall on PET substrate	78
Fig.4.2.	FE-SEM image of ZnO nanowall On PET substrate, a) lower (Scale bar: 10 μ m), b) higher (Scale bar: 100 nm) magnification.	79
Fig.4.3.	Optical absorbance and transmittance of the ZnO nanowall on both sides of flexible substrate	79
Fig.4.4.	XPS spectrum of ZnO nanowall on flexible substrate, a) survey spectrum, b) Zn- 2p, c) O-1s high resolution core level spectra.	80
Fig.4.5.	Room temperature photoluminescence spectra of ZnO nanowall	81
Fig.4.6.	Electrical property of the ZnO nanowall under dark and under different illumination wavelength (365, 405, 535 nm)	82
Fig.4.7.	Electrical characteristics of nanowall based nanogenerator. a) Open-circuit output voltage of a nanogenerator, c) enlarged view of the marked output voltage. b) Closed- circuit output current, d) enlarged view of the marked output current.	84
Fig.4.8.	a) The voltage and current Vs external load resistance, b) power output Vs external load resistance.	85
Fig.4.9.	a) Circuit diagram of full wave bridge rectifier circuit. b) Rectified voltage. c) Rectified current. Top of the right corner indicates the snapshots of a driving LCD display and light up a commercial green LED.	86
Fig.5.1.	Schematic diagram of the experimental setup for the growth of ZnO micro/nanowires	94

Fig.5.2.	X-ray diffraction (XRD) pattern of as-grown ZnO nanowire.	96
Fig.5.3.	FE-SEM image of ZnO nanowire (Lower and Higher Magnification)	96
Fig.5.4.	Schematic diagram of the fabrication process of the hybrid composite nanogenerator	97
Fig.5.5.	X-ray diffraction (XRD) pattern of the PVDF-ZnO nanowire composite film (the inset shows an enlarged view from 10–30°)	98
Fig.5.6.	Fourier-transform infrared (FTIR) spectra of (a) PVDF, (b) ZnO nanowire, (c) PVDF-ZnO nanowire composite film (d) digital image of the composite film.	98
Fig.5.7.	Field-emission scanning electron microscopy (FE-SEM) image of PVDF-ZnO nanowire composite film, (a) Lower, and (b) Higher magnification. Cross sectional image, (a) Lower, and (b) higher magnification.	99
Fig.5.8.	X-ray photoelectron spectroscopy (XPS), (a) survey spectrum (the inset shows the Zn 2p core-level spectrum). Core-level spectra of (b) C 1s, (c) O 1s, and (d) F 1s of the PVDF-ZnO nanowire composite film.	100
Fig.5.9.	Measured open circuit voltage and short circuit current of hybrid composite nanogenerator under continues bending condition, (a, b) at forward bias, (c, d) at reverse bias respectively. The insets are the enlarged view of the electrical output.	101
Fig.5.10.	Measured open circuit voltage and short circuit current of hybrid composite nanogenerator under different speed of bending/unbending condition, (a, b) at forward bias, (c, d) at reverse bias respectively.	102

Fig.5.11.	Measured open circuit voltage and short circuit current of hybrid composite nanogenerator under different speed of uniaxial pressing / unpressing condition, (a, b) at forward bias, (c, d) at reverse bias respectively.	103
Fig.5.12.	Measured open-circuit voltage and short-circuit current of the hybrid composite nanogenerator for (a, b) folding and (c, d) pressing with fingers.	105
Fig.5.13.	Schematic representation of self-polarization mechanism	106
Fig.5.14.	Power generation mechanism in the hybrid composite nanogenerator	107
Fig.5.15.	a) Open-circuit voltage and b) short-circuit current of the hybrid composite (PVDF-ZnO) nanogenerator after poling at 5.5 kV for 36 h under continuous pressing condition.	108
Fig.5.16.	Measured electrical output of the PVDF nanogenerator: (a) open-circuit voltage, and (b) closed-circuit current.	109
Fig.5.17.	Measured electrical output of the hybrid nanogenerator with ZnO nanoparticle: (a) open-circuit voltage, and (b) closed-circuit current.	109
Fig.5.18.	(a) Schematic diagram of the full-wave Bridge rectifier circuit. (b) Measured rectified open-circuit voltage. (c) Short-circuit current by pressing the fingers. The rectified output was used to drive five green LEDs, which is shown in the top left corner.	110
Fig.6.1.	Graphene Oxide (GO) a) X-ray diffraction (XRD) pattern, b) Field emission scanning electron microscopy (FE-SEM) image, c) Raman spectrum	120
Fig.6.2.	Reduced graphene oxide (rGO), (a) X-ray diffraction (XRD) pattern, (b) Raman spectrum, (c) Field-emission scanning electron microscopy (FE-SEM) image.	121

Fig.6.3.	Schematic representation of composite nanogenerator fabrication	122
Fig.6.4.	Reduced graphene oxide (rGO)-ZnO nanowire composite, (a) X-ray diffraction (XRD) pattern, (b) Fourier Transform Infrared (FTIR) spectrum.	123
Fig.6.5.	Raman Spectrum of rGO-ZnO composite	123
Fig.6.6.	Field-emission scanning electron microscopy (FE-SEM) image, (a) and (b) lower and higher magnified image of rGO-ZnO composite .Cross Sectional view of PDMS- rGO-ZnO composite film, (c) lower, and (d) higher magnification.	124
Fig.6.7.	Measured output performance of the composite nanogenerator under palm impact. a) Schematic representation of the polarity test. The voltage and current under forward connection (b, c) and reverse connection (d, e).	125
Fig.6.8.	Enlarged view of the voltage curve of the composite nanogenerator under forward (a), and reverse (b) connections.	126
Fig.6.9.	Measured output performance of the composite nanogenerator under foot stamp: a) digital image of the foot stamp at different stages, b) output voltage, and c) enlarged view of the voltage signal. d) Output current and e) enlarged view of the current signal.	127
Fig.6.10.	The output performance of the only PDMS, PDMS-ZnO, PDMS-rGO-ZnO composite device with same device size and thickness (a) Voltage, (b) Current. The graphene in the composite enhanced the output voltage and current of the composite device, compare to only ZnO device.	128

Fig.6.11.	(a) Digital image of the constructed bridge rectifier circuit and capacitors. Inset show the digital image of stored voltage in the capacitors (top) b) Snapshot of the LEDs (warm white, green) before and after power up c) Capacitor charging curve under mechanical deformation. d) Snapshot of glowing 15 green and 10 red without storage using large-area nanogenerator.	129
Fig.6.12.	Composite nanogenerator, (a) rectified voltage, and (b) rectified current. (c) Snapshot of the segmented display, (d) Snapshot of the LCD display.	130
Fig.6.13.	Large-area nanogenerator, (a) digital image, (b) snapshots of 12 white and 10 red LEDs glowing, (c) rectified voltage, and (d) rectified current.	131
Fig.7.1.	Traditional Trioelectric generator based on Wimshurst machine and Van de Graaff generator	137
Fig .7.2.	Trioelectric series	138
Fig.7.3.	Four fundamental modes of triboelectric nanogenerators: (a) vertical contact-separation mode; (b) lateral-sliding mode; (c) single-electrode mode; and (d) free standing triboelectric-layer mode	139
Fig.7.4.	Schematic diagram and digital image of the fabricated triboelectric nanogenerator	141
Fig.7.5.	Working mechanism of the triboelectric nanogenerator	142
Fig.7.6.	The measured open-circuit voltage and short circuit current under forward and reverse connection	143
Fig.8.1.	Single ZnO microwire based pH sensor, a) digital image and b)	150

	optical image	
Fig.8.2.	Field emission scanning electron microscopy (FE-SEM) of ZnO microwire device	150
Fig.8.3.	Current-voltage (I - V) characteristics of a ZnO microwire as a function of pH.	151
Fig.8.4.	Current-time (I - t) characteristics of the fabricated ZnO microwire at different pH with constant bias voltage on - 0.5 V	152
Fig.8.5.	Schematic representation of the self-powered pH sensor device	153
Fig.8.6.	Measured electrical output voltage of self-powered pH sensor without any buffer solution.	154
Fig.8.7.	Electrical output as a function of pH across the pH sensor	155
Fig.8.8.	Schematic representation of pH mechanism of the self-powered device	155
Fig.8.9.	Self-powered pH sensor output voltage as a function of different pH values	156
Fig.8.10.	ZnO nanowire film, a) Digital image, and b, c) Optical image of the device	156
Fig.8.11.	FE-SEM image of the ZnO nanowire film, a) Lower, and b) Higher magnification	157
Fig.8.12.	Current – Voltage (I - V) characteristic of the ZnO nanowire photo sensor with different illumination wavelength	157
Fig.8.13.	Schematic representation of the photocurrent generation mechanism in ZnO nanowire photo sensor	158

Fig.8.14.	Schematic diagram of the self-powered UV photo sensor	159
Fig.8.15.	The measured response with and without UV exposes. Inset enlarged portion of pink color mark.	159
Fig.8.16.	The measured response as a function of exposure wavelength.	160
Fig.8.17.	The measured response for the commercial photo sensor	161
Fig.8.18.	a) The digital image of the experimental setup. Inset indicates the glowing red LED during UV expose. b) Circuit diagram of the self-powered UV photo sensor.	161
Fig.9.1.	Overall outlook of the thesis	165



Acknowledgements

I would like to express my sincere thanks to my honorific supervisor, Prof. Sang-Jae KIM, who accepted me as his Ph.D student. He offered me so much advice with patiently and encouraged my research. He guided me in a right direction with courage which grows me as a good researcher. During my tenure, I have learned a lot of things from him, without his help I couldn't finish my thesis successfully. I would like to thank my thesis committee members for letting my defense be an enjoyable moment, and for your brilliant comments and suggestions.

This is the occasion to remember and thank to all of my professors and teachers, who teaches the subject and research. Especially, I would like to thank my physics teacher (Mr. R. Vellingiri) and chemistry teacher (Mr.R.Selvaraj), who make me an interest towards the science at my schooling. After that, my college time, my beloved professors make me tasty to do research. Especially, Late.Dr.Ananth, Dr.P.Christopher Selvin, Dr.R.Kanakaraju, Dr.V.Sathyabama, Dr. M.Karthika, and Dr. Yogeswari.

I would like to thank Prof. P. Kolandaivel, who initiated my research carrier and actively directed me in the research and my personal life. I started my research carrier under the supervision of Prof. V. Rajendran, and he molded me as a good researcher. Under him, I developed my administrative skills and gathered research trends, so I thank him. I would like to thank, Dr. N. Meenakshi Sundaram, Dr.K.Saminathan, Dr.P.Prabu, Dr.Suthan Kissinger, Dr. Ravikumar, Dr. Sathesh and Dr. S.Sudhakar for their constant supports towards scientific discussion.

Without support of other members in the lab, I could not graduate. First, I would like to thank my seniors, specially, Dr. Rajneesh Mohan, Dr. Shrikant Saini, Dr. Gunasekaran and Dr. Anil Khambampatti. They helped a lot during my initial stage in research as well as initial settlement. I am very grateful to my friends and colleague Mr. Ananthakumar Ramadoss, Mr. Kaliannan Thiyagarajan and family, Dr. Sivaprakasam Radhakrishnan, Dr.Karthikeyan, Mr. Veerasubramani Ganesh Kumar, Mr. Nagamelleshwara Rao, Mr. Arunkumar, Ms. Sophia Selvarajan, Mr. Eui-Young Hong, Ms. Shin So Yoon, Mr. Kim Taehyun, Mr. Ko Eunhyung, Ms. Park Minhee and Mr. Seong Mingeon.

Without friends help and motivation, we cannot move forward in the life as well as professional carrier. This is the occasion to thank all of my beloved friends. They stayed with me during the hard part of my life and lifted from that situation with the words of we are always with you lets go. I would like to thanks my friends from childhood, Mr. Arunkumar, Mr. Appadurai, Mrs. Ramya, Mrs.Priya and families. I would like to thank, Dr. Manivasakan and family, Dr. Yuvakkumar and family, Dr. Rajkumar, Dr. Sasipriya, Dr. Dharaneedharan and family, Dr. Sebastian Ananth, Dr.Saranya and Dr. Purush, Dr. Chandramohan and family, Dr. Afeesh, Dr. Suraj Tirupathi, Dr. Navaneethan, Dr. Ganesh Thangaraj, Dr.Sridharan, Dr.Gandhi, Ms. Pavithra, Ms. Kowsalya, Mr. Balaji, Mr. Raja, Mr. Subbiah Ramesh, Mr. Suresh Kannan Balasingam, Mr. MSP. Sudhakaran, Dr. Karuppiah. I would like to thank Jeju friends, they make homely environment during the stay. Dr. Umasuthan and family, Dr. Kalpa, Dr. Nauman, Dr. Khalid, Dr. Murtaza, Dr. Naeem, Dr. Zubair Mr. Kamran Ali, Dr. Adanan Ali, Mr. Mamoon, Mr. Suresh Rai , Mr. Safdar Ali, Mr.

Farrukh, Mr. Razhid, Mr.Sohail, Mr. Junaid Ali, Mr. Siddiqi, Mr. Zahid Manzoor, Mr.Lakmal, Mr. Anushka.

I am also grateful for the Research Instrument facility (RIC) centre for their valuable support and permission given to handle all experimental and characterization facilities. Especially, thanks to Mr. Jeong Eun Koh, he helped a lot for measuring FE-SEM.

Last but certainly not least I thank my father Mr. M. Balasubramaniam, mother Mrs. B. Umavathi and my brother Mr. B. Sureshkumar and family members. They have provided unconditional love and care. Finally, I acknowledge the friends those are not mentioned here they helped me a lot at different occasions.



Balasubramaniam Saravanakumar

Abstract in Hangeul

기술의 급격한 성장과 나노기술의 영향으로 인해 소자의 크기는 몰라보게 줄어들었으며 구동 전력 또한 감소하게 되었다. 심도깊은 연구를 통해 다목적으로 활용할 수 있는 기능성 재료와 소자들이 개발되었다. 하지만, 모든 소자들은 외부 구동전원이 있어야 작동하기 때문에 모든 조건에서 사용할 수 없다는 문제가 생기게 된다. 짧은 수명 시간과 큰 크기를 가진 에너지 저장소자 때문에 축소화된 소자에 집약될 수 없기 때문에 에너지 저장 장치를 없애거나 환경에서 에너지를 수확하는 것이 필요해졌다. 자가발전 구동을 하기 위해서, 나노발전소자와 같은 에너지하베스터가 위와 같은 소자에 구성되었다. 에너지하베스터는 주변환경에서 에너지를 수확하여 별도의 전원 없이 전자기기를 구동시킨다. 이 학위논문에서는 ZnO 마이크로/나노와이어를 유연 기관 위에 증발전달방식을 통해 단면 또는 양면에 일렬로 정렬하거나 ZnO nanowall을 저온열수 방법과 같은 물리적 방법을 통해 합성하였다. 성장시킨 ZnO마이크로와이어와 나노와이어 배열은 나노발전소자를 제작하는 데 사용되었다. 가장 처음에는, 마찰과 압전효과가 같이 공존하는 소자구조를 제작하여 출력 성능을 향상시켰다. 두 번째로는, 넓은 크기의 소자에서 출력 값을 향상시키기 위해서 PVDF를 혼합한 나노발전소자를 개발하였다. 여기서 PVDF는 압전효과를 추가적으로 발생시키면서 또한 ZnO 필름을 만드는 역할을 한다. PVDF 배열에 ZnO가 존재하여 혼합한 필름에 자가편광 하였다. 더불어, 산화그래핀-ZnO를 바탕으로 한 혼합 나노발전소자를 실험하였다.. 마지막으로, 실험을 통해 발광다이오드(LED)와 액정디스플레이(LCD)와 같은 전자소자를 나노발전소자로 구동시켜 그 가능성을 확인하였다. 더불어 ZnO마이크로와이어 pH센서와 ZnO나노와이어 포토센서를 나노발전소자와 결합시켜 자가발전소자의 활용을 확인하였다. 이 논문에서는 자가발전 소자로서 나노발전소자를 사용하였고 환경모니터링을 위한 바이오센서 또는 스마트, 웨어러블, 진동 센서에 확장하여 미래에 실현 가능할 수 있음을 확인하였다.

Abstract

The rapid technical growth and the influence of nanotechnology in the device fabrication incredibly reduced the device dimension as well as the operating power. The intensive research has been carried out to develop a new functional materials and devices with multipurpose applications. However, all the fabricated devices are operated by external power sources, which is not favor for all conditions. Due to large size and short life time of the energy storage device, compare to active devices which hinders their integration in miniaturized device. It is highly required to operate without energy storage device (or) harvest the required energy from the environment. To obtain the self-powered operation, energy harvester such as nanogenerator has been integrated with those active devices. The energy harvester harvests the energy from environment and power up the electronic devices without any external power. This thesis provides the solid background about the synthesis of ZnO micro/nanowires through physical method such as vapor transport method and vertically aligned nanowire array on one side and double sides of the flexible substrate and as well as ZnO nanowall through low temperature hydrothermal process. The grown ZnO microwire and nanowire array was used to fabricate the nanogenerator device. At first time, we demonstrated the coexistence of tribo and piezoelectric effect in the same device architecture, which improved the output performance. Secondly, to improve the output performance and extent to large area device, we have investigated composite based nanogenerator using PVDF, in which PVDF provides the additional piezoelectric output as well as to make ZnO film. The presences of ZnO in PVDF matrix self-polarize the composite film. Further, we have

examined the reduced graphene oxide-ZnO based composite nanogenerator. Finally, we have showed the capability of the nanogenerator by powering commercial electronic devices such as light emitting diodes (LEDs), liquid crystal displays (LCDs). Further, we have investigated self-powered device application by integrating the nanosensors such as ZnO microwire pH, ZnO nanowire photosensors with nanogenerators. This thesis demonstrates the feasibility of using a nanogenerator as a self-powered device that can be extended for use as a biosensor for environmental monitoring and/or as a smart, wearable, vibration sensor in future applications.



CHAPTER -I

Introduction

1.1. Introduction

The introduction of nanotechnology minimized the device size and improved the property of the materials. It is nothing but any technology at nanoscale that has a real application. It emphasizes that the production of materials at nanoscale and apply to physical, chemical, and biological systems. At nanoscale, the material has extraordinary physical, chemical, optical and electrical property than their counterpart in bulk. The exceptional properties of materials at nanometer scale makes the interest to work in this field and developed varies rapidly. The increment of technological development and using this technology improved the performance of the devices in all field of science and technology.

The energy crisis is one of the most important problems facing society, due to the diminishing availability of fossil fuels and the shortfall of existing technology to efficiently convert renewable energy sources [1]. Numerous renewable energy sources are available, including solar, biomass, wind, geothermal, hydro, and tidal energy; however, these sources can be variable and tend to depend on environmental conditions such as time and place [2]. On the other hand, a huge amount of reliable energy sources are available in the form of vibration, heat, which exists regardless of place and time [3], may provide the means to counter growing energy deficits. After a lot of efforts, the scientists find a way to harvest those energy using piezoelectric, pyroelectric, and triboelectric materials [4]. Prof. Wang and his team have been creatively developed a concept of nanogenerator consisting of diverse nanostructured

materials [5]. The nanogenerator was capable of converting low-frequency irregular vibration, mechanical motion, and heat into electrical energy through different physical mechanisms based on the piezoelectric, pyroelectric and triboelectric effects. The human body also provides energy in the form of heat and mechanical energy during human activities. This energy can be used to drive various devices without the need of external power source. As such, there continues to be great interest in self-powered portable and wearable device applications. For these device applications, mechanical energy is the most reliable, independent energy source [6]. Fabrication of the self-powered system can be achieved by combining electronic devices with an energy-harvesting device such as a nanogenerator; additionally, the nanogenerator itself can act as a sensor to detect the signals [7–9]. Numerous studies have investigated energy harvesting from irregular mechanical sources, including air flow, heartbeat, body movement, hydraulic energy, respiration, or air/liquid pressure [8,10], and have used this energy to successfully power liquid crystal displays (LCDs), light-emitting diodes (LEDs), implantable biosensors, and many portable personal electronic devices [11,12]. Various nanostructured materials, such as ZnO [13–15], GaN [16], lead zirconium titanate (PZT) [17,18], BaTiO₃ (BTO)[19,20], NaNbO₃[21], (1-x)Pb(Mg_{1/3}Nb_{2/3})O₃-xPbTiO₃ (PMN-PT) [22], ZnSnO₃ [23,24], polyvinylidene fluoride (PVDF) [10], and polytetrafluoroethylene (PTFE) [25] have been widely used for nanogenerator fabrication in a variety of forms, such as micro/nanowires, nanobelts, and particles. Among them, ZnO is lead-free, biocompatible, and has piezo and semiconducting properties [26, 27]; its non-centrosymmetric nature has proven to be advantageous for nanogenerator applications. Specifically, ZnO played an important role in the nanogenerator

progress with diverse nanogenerator device configurations (e.g., lateral, vertical, radial, integration, stacked and composite nanogenerator forms) [28].

1.2. Piezoelectricity

In 1880, the piezoelectric effect was discovered by Jacques Curie and Pierre Curie. The discovery of this phenomenon created revolution in the technological development. The piezoelectric effect is nothing but when applying pressure on certain crystals (piezoelectric materials) aligns the dipole over the surface generates electrical output. At initially this effect was observed in tourmaline, quartz, topaz, cane sugar, and Rochelle salt. It have converse effect that is when electric field applied to this materials, it change the shape and size through expansion or contraction. Fig.1.1 shows the schematic representation of the piezoelectric effect and inverse piezoelectric effect.

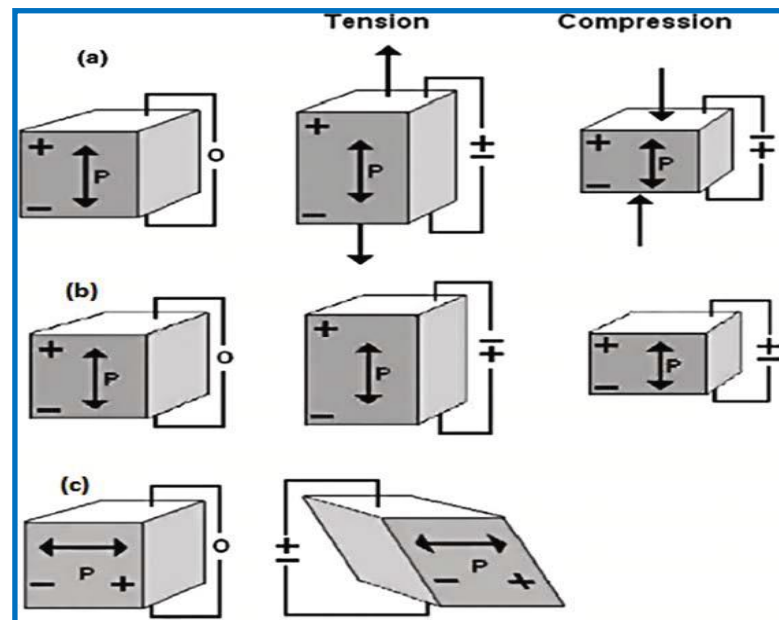


Fig.1.1 Schematic diagram of piezoelectric effect and inverse piezoelectric effect

1.3. Zinc oxide nanostructure

ZnO is a promising material which has extensively studied for all technical application from olden days. The main driving force for using ZnO in electronic application was due to existence of wide band gap structure, near-UV the spectral region, which opens the usage of this material for light emitting diode, transistor and all other electronic applications. At room temperature, it have larger free- exciton binding energy of around 60 meV, which is good to use in high emission application. ZnO is an III-V and II-VI compound semiconductor, with crystal structure of hexagonal wurtzite and cubic zinc blende structure $P6_3mc$. The cubic zinc blende structure is not stable under ambient condition, so most probable stable structure is wurtzite structure, in which each anion is surrounded by four cations at the corners [29, 30]. The crystal structure of the ZnO was shown in Fig.1.2.

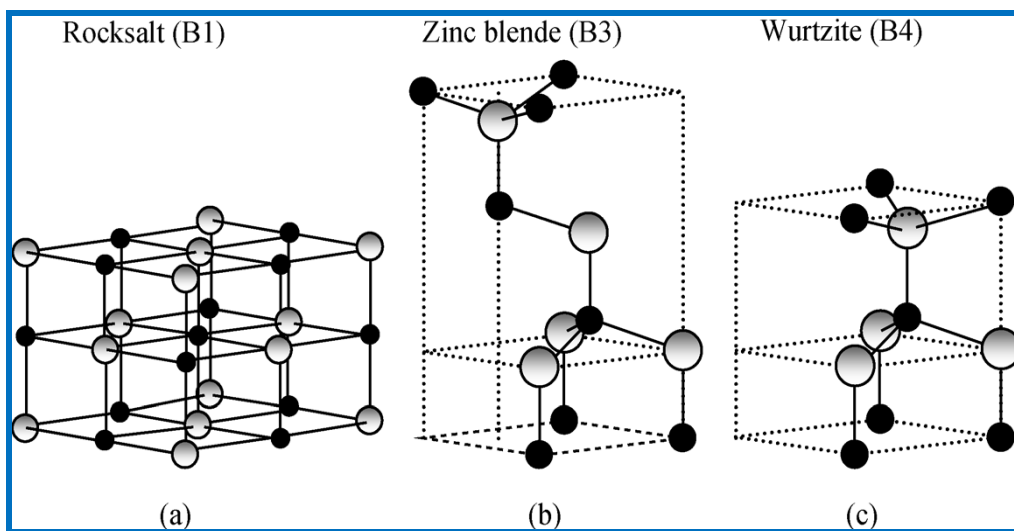


Fig.1.2. Crystal Structure of ZnO

ZnO have wide range of application based on the physical, chemical, optical, electrical properties and few of the properties discussed here.

1. The wide direct band gap and large excitation binding energy of the ZnO, makes this material for light emitting and transparent conducting application
2. Due to presents of the non-centrosymmetric crystal structure, this material has additional property of piezoelectricity. Which wider this material application into sensors and transducers.
3. ZnO is a non-toxic and biocompatible nature makes this material to use in biologically application
4. Compare to all other semiconducting and piezoelectric materials, this is easy to grow in any substrate in different shape at elevated temperature.

1.4. Review of Literature

In the year of 2006, Prof. Wang and his team developed an innovative way to produce the electrical signal through mechanical deflection in the 1D ZnO nanowire structure by piezoelectric effect. In this, they used AFM tip to deflect the nanowire as well as to measure the output signal. Later on new designs were inputted to improve the output performance of the piezoelectric nanogenerator. After that the vertically aligned ZnO was used to assemble the nanogenerator, which improved the output rapidly [4]. The roadmap of the development of ZnO based piezoelectric nanogenerator was shown in Fig.1.3. At last the higher output voltage of 57 V achieved for patterned vertically aligned ZnO nanowire array nanogenerator.

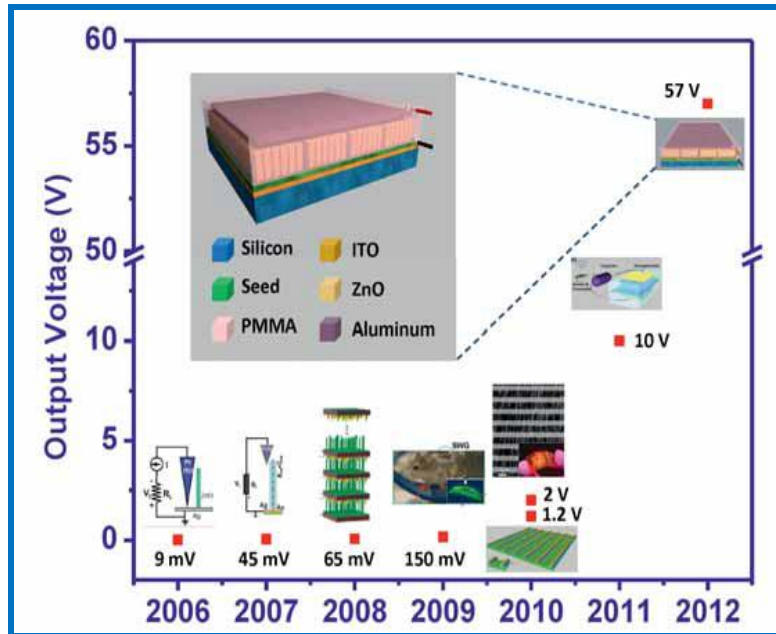


Fig.1.3. Summary of the development of ZnO based piezoelectric nanogenerator



Other than this Prof. Park et.al developed the innovative way to fabricate large area nanogenerator with higher output. He developed composite nanogenerator at low cost with simple fabrication process [17, 23, 24].

1.5 Objectives and scope of the present work

Recently, energy requirements have escalated exponentially due to increasing populations and industrial growth, while at the same time; fossil fuel availability has steadily decreased. Thus, scientists have been focused on increasing the utilization of renewable energy sources in an effective way. The commonly available renewable energy sources such as solar, wind, hydro, geothermal and biomass are place and time dependent. A numerous irregular energy sources are available in the living environment include sound, friction, motion, wind, and noise; these energies exist

enormously in everywhere, which is small and have the potential for use as future power sources for smart, wearable electronic devices. The objective of this thesis is to develop an innovative device structure to harvest the mechanical vibration from environment. A lot of reports are available for vibration energy harvesting from the environment, but further, research required to improve the conversion efficiencies and output power of the device. In this regard, an intensive research required to fabricated energy harvesting device. Based on the pioneering research, we have developed new types of device structure to harvest the mechanical energy with higher output performance.

In the present investigation, we have fabricated energy harvesting device using ZnO micro/nanostructure with different architecture to harvesting mechanical energy as well as human based energy harvester. The harvested energy was used to operate the commercial electronic devices.

The wearable as well as smart electronic devices and low -power sensor systems required long term operation without interruption. In those devices, the life time reduced because of the draining of energy, which is used to drive those systems. To overcome this problem, self-powered device is one of the remedy to operate the electronic device without external power.

In this view, we investigated and fabricated the self-powered pH sensor and UV photosensors using ZnO nanostructures, which coupled with energy harvester to achieve the self-powered operation. The fabricated devices were operated with external power.

1.6. Thesis overview



Fig.1.4. Thesis Overview

The detailed thesis overview is shown in the Fig.1.4. The main focus of this thesis is to develop a piezoelectric and triboelectric nanogenerator for self-powered device applications. Thesis consists of nine chapters which includes introduction and summary of the thesis.

The chapter -2 demonstrates the growth of ZnO microwire through vapor transport method and describes about the fabrication and measuring output of the piezoelectric nanogenerator and its output performance. The next chapter (chapter-3) provides the details about the growth of vertically aligned ZnO nanowire arrays over the various substrates. The vertically grown ZnO nanowire array on flexible substrate at one side and double side was used to fabricate the piezoelectric nanogenerator. The fabricated device was used to harvest the energy from human body movement. The next chapter (chapter-4) proposes the growth of aligned nanowall on the flexible substrate and fruitfully applied for energy harvesting. In chapter-5, explains the growth of nanowires in vapor transport method. The fabricated ZnO was used to make PVDF based composite film, which was finally applied for energy harvesting application. In next chapter (chapter-6), provides the synthesis of reduced graphene oxide and reduced graphene oxide- ZnO composite. The synthesized composite was used to fabricate hybrid composite film by adding into PDMS polymer. The fabricated film was used to make nanogenerator and fabricated device was characterized. The next chapter (chapter-7), explains the fabrication of triboelectric nanogenerator and its mechanism, electrical output measurements. In next chapter (chapter-8), describes the fabrication of self-powered device and its measurements. The last chapter of the thesis provides the outlook of the work and summaries all of work.

References

- [1] T. H. Oh, S. Y. Pang, S. C. Chua, Energy Policy and Alternative Energy in Malaysia: Issues and Challenges for Sustainable Growth. *Renewable Sustainable Energy Rev.* 14 (2010), 1241–1252.
- [2] S. Priya, D. J. Inman, *Energy Harvesting Technologies*. Springer Science, New York 2009.
- [3] S. P. Beeby, M. J. Tudor, N. M. White, Energy Harvesting Vibration Sources for Microsystems Applications. *Meas. Sci. Technol.* 17 (2006), R175.
- [4] Z. L. Wang, G. Zhu, Y. Yang, S. Wang, C. Pan, Progress in Nanogenerators for Portable Electronics. *Mater. Today* 15 (2013), 532-543.
- [5] Z. L. Wang, J. Song, Piezoelectric Nanogenerators Based on Zinc Oxide Nanowire Arrays. *Science* 312 (2006), 242-246.
- [6] S. Lee, R. Hinchet, Y. Lee, Y. Yang, Z. H. Lin, G. Ardila, L. Montès, M. Mouis, Z. L. Wang, Ultrathin Nanogenerators as Self-Powered/Active Skin Sensors for Tracking Eye Ball Motion. *Adv. Funct. Mater.* 24 (2013), 1163-1168.
- [7] Y. Hu, Y. Zhang, C. Xu, L. Lin, R. L. Snyder, Z. L. Wang, Self-Powered System with Wireless Data Transmission. *Nano Lett.* 11 (2011), 2572-2577
- [8] Z. Li, Z. L. Wang, Air/Liquid-Pressure and Heartbeat-Driven Flexible Fiber Nanogenerators as a Micro/Nano-Power Source or Diagnostic Sensor. *Adv. Mater.* 23 (2010), 84-89.
- [9] Y. Hu, C. Xu, Y. Zhang, L. Lin, R. L. Snyder, Z. L. Wang, A Nanogenerator for Energy Harvesting from a Rotating Tire and its Application as a Self-Powered Pressure/Speed Sensor. *Adv. Mater.* 23 (2011), 4068-4071.

- [10] C. L. Sun, J. Shi, D. J. Bayerl, and X. D. Wang, PVDF Microbelts for Harvesting Energy from Respiration. *Energy Environ. Sci.* 4 (2011), 4508-4512.
- [11] Y. Hu, Y. Zhang, C. Xu, G. Zhu, Z. L. Wang, High-Output Nanogenerator by Rational Unipolar Assembly of Conical Nanowires and Its Application for Driving a Small Liquid Crystal Display. *Nano Lett.* 10 (2010), 5025–5031.
- [12] Z. L. Wang, Self-Powered Nanosensors and Nanosystems. *Adv. Mater.* 24 (2012), 280–285.
- [13] B. Saravanakumar, R. Mohan, K. Thiyagarajan, S. J. Kim, Fabrication of a ZnO Nanogenerator for Eco-friendly Biomechanical Energy Harvesting. *RSC Adv.* 3 (2013), 16646-16656.
- [14] B. Saravanakumar, S. Soyoon, S. J. Kim, Self-Powered pH Sensor based on a Flexible Organic-Inorganic Hybrid Composite Nanogenerator, *ACS Appl. Mater. Interfaces.* 27 (2014), 13716-13723.
- [15] B. Saravanakumar, S. J. Kim, Growth of 2D ZnO Nanowall for Energy Harvesting Application, *J. Phys. Chem. C* 118 (2014), 8831–8836.
- [16] C. T. Huang, J. Song, W. F. Lee, Y. Ding, Z. Gao, Y. Hao, L. J. Chen, Z. L. Wang, GaN Nanowire Arrays for High-Output Nanogenerators. *J. Am. Chem. Soc.* 132 (2010), 4766–4771.
- [17] K. I. Park, C. K. Jeong, J. Ryu, G. T. Hwang, K. J. Lee, Flexible and Large-Area Nanocomposite Generators Based on Lead Zirconate Titanate Particles and Carbon Nanotubes. *Adv. Energy Mater.* 3 (2013), 1539.

- [18] L. Gu, N. Cui, L. Cheng, Q. Xu, S. Bai, M. Yuan, W. Wu, J. Liu, Y. Zhao, F. Ma, Y. Qin, Z. L. Wang, Flexible Fiber Nanogenerator with 209 V Output Voltage Directly Powers a Light-Emitting Diode. *Nano Lett.* 13(2013), 91–94.
- [19] K. I. Park, S. Xu, Y. Liu, G. T. Hwang, S. J. L. Kang, Z. L. Wang, K. J. Lee, Piezoelectric BaTiO₃ Thin Film Nanogenerator on Plastic Substrates. *Nano Lett.* 10 (2010), 4939–4943.
- [20] Z. H. Lin, Y. Yang, J. M. Wu, Y. Liu, F. Zhang, Z. L. Wang, BaTiO₃ Nanotubes-Based Flexible and Transparent Nanogenerators. *J. Phys. Chem. Lett.* 3 (2012), 3599–3604.
- [21] Y. Yang, J. H. Jung, B. K. Yun, F. Zhang, K. C. Pradel, W. Guo, Z. L. Wang, Flexible Pyroelectric Nanogenerators using a Composite Structure of Lead-Free KNbO₃ Nanowires. *Adv. Mater.* 24 (2012), 5357–5362.
- [22] S. Xu, G. Poirier, N. Yao, PMN-PT Nanowires with a Very High Piezoelectric Constant. *Nano Lett.* 12 (2012), 2238–2242.
- [23] J. M. Wu, C. Xu, Y. Zhang, Y. Yang, Y. Zhou, Z. L. Wang, Flexible and Transparent Nanogenerators Based on a Composite of Lead-Free ZnSnO₃ Triangular-Belts. *Adv. Mater.* 24 (2012), 6094–6099.
- [24] K. Y. Lee, D. Kim, J. H. Lee, T. Y. Kim, M. K. Gupta, S. W. Kim, Unidirectional High-Power Generation via Stress-Induced Dipole Alignment from ZnSnO₃ Nanocubes /Polymer Hybrid Piezoelectric Nanogenerator. *Adv. Funct. Mater.* 24 (2012), 37-43.
- [25] S. H. Bae, O. Kahya, B. K. Sharma, J. Kwon, H. J. Cho, B. Özyilmaz, J. H. Ahn, Graphene-P(VDF-TrFE) Multilayer Film for Flexible Applications. *ACS Nano* 7 (2013), 3130–3138.

- [26] B. Saravanakumar, R. Mohan, S. J. Kim, An Investigation of the Electrical Properties of p-type Al:N Co-doped ZnO Thin Films. *J. Korean Phys. Soc.* 61 (2012), 1737-1741.
- [27] B. Saravanakumar, R. Mohan, K. Thiyagarajan, S. J. Kim, Investigation of UV Photoresponse Property of Al, N Co-doped ZnO Film. *J. Alloys Compd.* 580 (2013), 538–543.
- [28] Z. L. Wang, W. Wu, Nanotechnology-Enabled Energy Harvesting for Self-Powered Micro-/Nanosystems. *Angew. Chem. Int. Ed.* 51 (2012), 11700-11721.
- [29] A. Janotti, C. G. Van de Walle, Fundamentals of Zinc Oxide as a Semiconductor, *Rep. Prog. Phys.* 72 (2009), 126501.
- [30] H. Morkoç, Ü. Özgür, *Zinc Oxide: Fundamentals, Materials and Device Technology*. 2009, WILEY-VCH.

CHAPTER -II

Microwire Based Nanogenerator

In this chapter demonstrates the synthesis of ZnO microwire through vapor transport method. The synthesized ZnO microwires were characterized through XRD, FE-SEM and Raman spectroscopy to check the structure and morphology of ZnO microwire. We fabricated piezoelectric nanogenerator using those microwires. In additionally, we have tested the performance of the nanogenerator with different number of wires. In this study, we have studied comparatively by adding microwires until 4 wires. To improve the performance, I fabricated hybrid device using PVDF coated ZnO microwire.



2.1. Growth of ZnO microwire

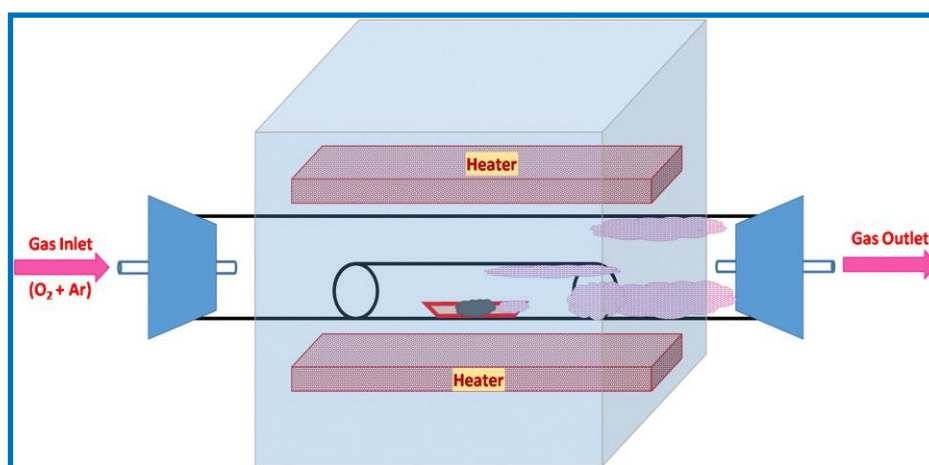


Fig.2.1. Schematic diagram of the vapor transport growth experimental setup for the growth of ZnO micro/nanowires. The used source materials ZnO, metal Zn, and graphite, with weight ratio of 1.5:0.5:1. The experiment was carried out at 1100°C for 1 hr under elevated condition ($O_2/Ar = 30/350$ sccm).

ZnO microwires were synthesized using a vapor transport method [1-3].

Fig.2.1 shows a schematic diagram of the experimental setup for the growth of the ZnO micro/nano wires. In typical growth, a horizontal quartz tube furnace was used. The source material consisted of a mixture of ZnO, metal Zn, and graphite, having a weight ratio of 1.5:0.5:1. The mixture of the source material with ethanol was continuously pulverized in a mortar to obtain the proper mixture. The mixed source material was then loaded into an alumina boat and dried in an oven overnight at 100°C. After, the alumina boat was placed inside a small quartz tube and then placed in the center of a long quartz tube (1.5 m). The source material was heated to 1100°C at a heating rate of 360°C/h under a constant argon flow of 350 sccm. Once the temperature reached 550–600°C, oxygen gas was introduced at a flow rate of 30 sccm. The furnace was maintained under these conditions for 1 h, and then cooled to room temperature. The ZnO microwires and nanowires were collected from source

boat and the end of the quartz tube, respectively, in the up flow direction of the gas flow.

2.2. Fabrication of ZnO Microwire based piezoelectric nanogenerator

The piezoelectric nanogenerator was fabricated by using the as synthesized ZnO microwires. At first, the ZnO microwires were attached to the Au patterned substrate, which was schematically shown in Fig.2.2.

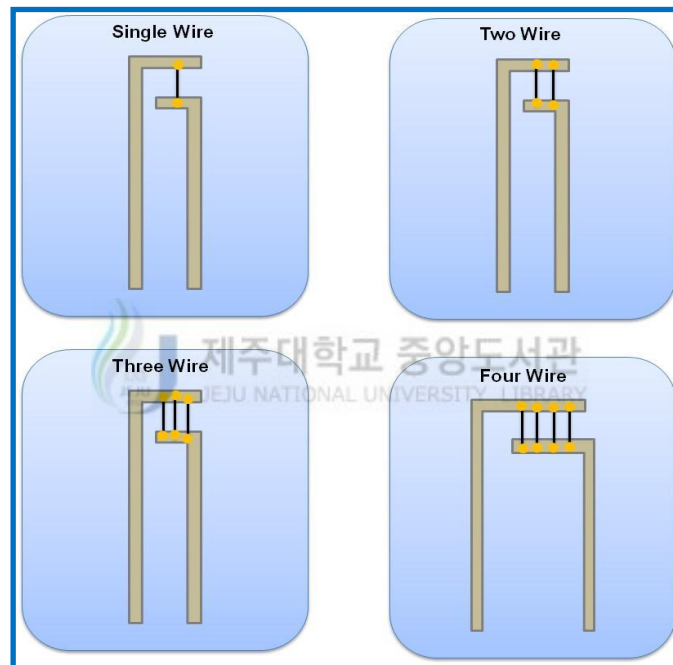


Fig.2.2. Schematic representation of microwire based nanogenerator device

ZnO microwire was grown using vapor transport method. In this experiment, ZnO microwire was collected from the source boat (Aluminium crucible). The quality of the collected microwire was characterized by X-ray diffractometer. The measured XRD pattern was shown in Fig. 2.3 and it confirms the high crystalline nature with lattice constants of $a = 3.25$ and $c = 5.21 \text{ \AA}$. The observed diffraction peaks are well matched with standard JCPDS file (36-1451) and from the ZnO

hexagonal wurtzite structure [2]. Fig.2.3 shows a typical XRD pattern and two SEM images of the as-grown ZnO microwires.

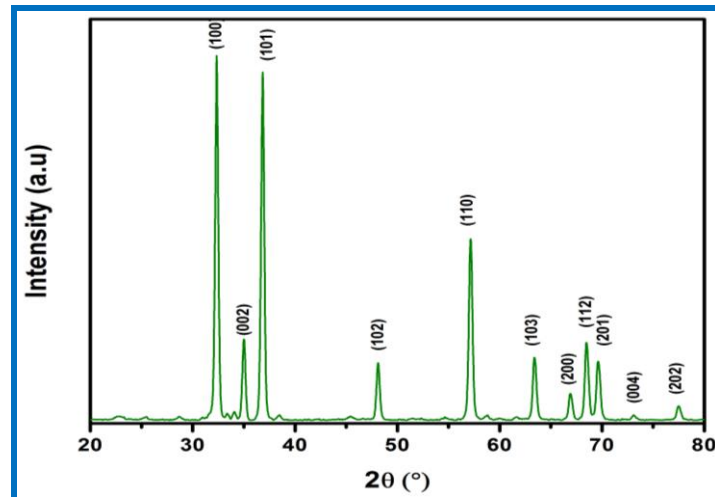


Fig.2.3. X-ray diffraction (XRD) pattern of ZnO microwire

Fig. 2.4 shows a FE-SEM image of ZnO microwires. The average length and diameter of these ZnO microwires are several millimeter meter and 50 – 60 μm , and cross section of ZnO microwires are well-defined hexagons, reflecting the wurtzite structure of ZnO (shown in the inset).

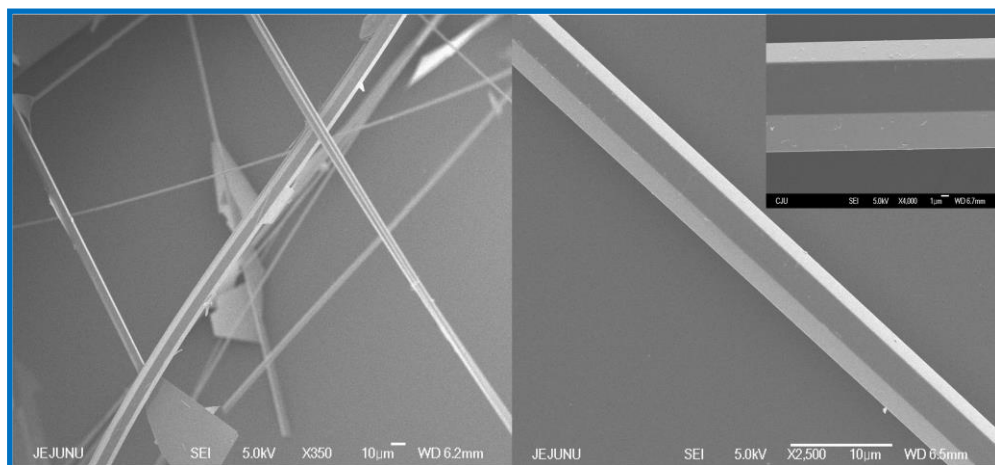


Fig.2.4. Field emission scanning electron microscopic (FE-SEM) image of ZnO microwire

The Raman spectroscopy is a good analytical tool to analysis the micro structural and chemical properties of the nanomaterials such as orientation, crystallinity, defects and impurities [4]. Fig.2.5. illustrates the Raman spectrum of ZnO microwire and demonstrates the high crystalline wurtzite crystal structure, which belongs to the C_{6v} space group ($P6_3mc$). According to group theory, the ZnO have 12 phonon modes which includes nine optical and three acoustic phonon modes,

$$\Gamma_{opt} = A_1 + 2B_1 + E_1 + 2E_2 \text{ ----- (1)}$$

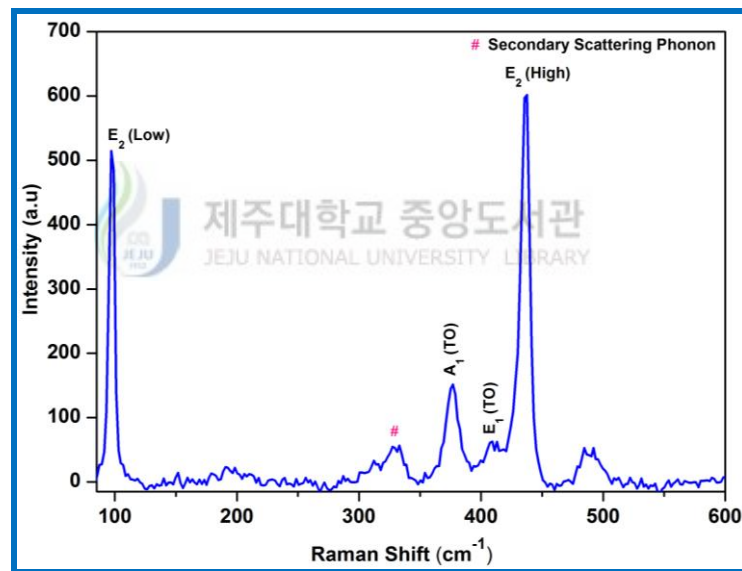


Fig.2.5. Raman spectrum of single ZnO microwire

where, A_1 , E_1 , E_2 modes are Raman active, and B_1 are silent. The A_1 and E_1 modes are polar which split into transverse (A_1 (TO) and E_1 (TO)) and longitudinal optical (A_1 (LO) and E_1 (LO)) optical components. E_2 mode consists of two modes such as E_{2L} (low), E_{2H} (high) with low and high frequency phonons. E_{2L} (low), E_{2H} (high) phonons are associated with the non-polar vibration of the heavy Zn sub lattice and lighter oxygen atoms, respectively. The E_2 (low), E_2 (high),

E_1 (TO), A_1 (TO) and secondary scattering phonon peaks were observed in the as synthesized single ZnO microwire.

Recently, strain engineering of semiconductor nanostructures has attracted great interest towards the tuning properties of nanostructure. Raman spectroscopy is an important tool to study strain engineering of nanostructures. For measuring Raman spectra, we have lay down a single ZnO microwire over the semi cured PDMS film and cured. The schematic diagram (Fig.2.6.) shows the experimental setup used to measure Raman spectra with and without strain, which is a quantitative analysis. The Raman spectra of the ZnO microwire under the strain and strain free state were measured by a micro-Raman microscopy system (LabRAM HR, Horiba). The Raman spectra were excited by a 514 nm Ar^+ ion laser with a power of ~ 3.75 mW at room temperature. For applying strain, we have stretched the PDMS film and hold by both side of the film by tape and measured the Raman spectrum under strained condition. In Raman spectra, we have observed E_2 low (E_{2L}) and E_2 high (E_{2H}) phonon frequency peaks of ZnO structure in ZnO microwire, around 97 and 436 cm^{-1} respectively.

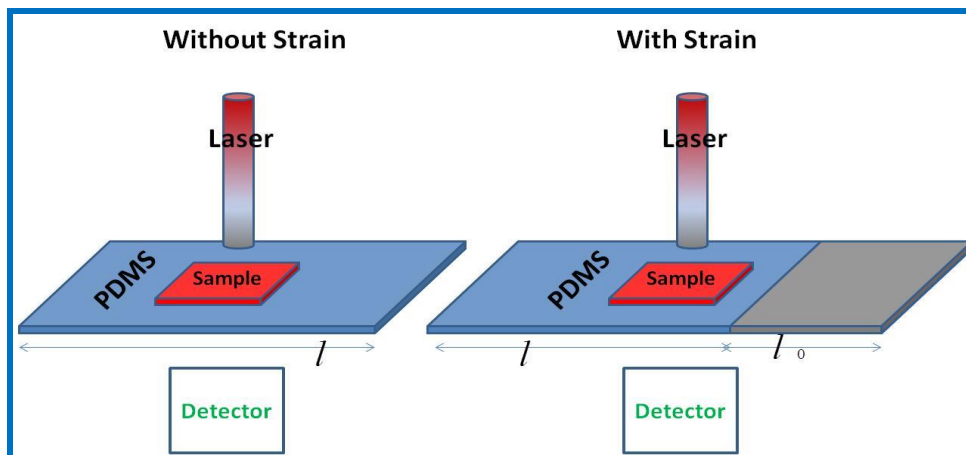


Fig.2.6. Schematic diagram of Raman measurement strain and strain free-state

There is no obvious Raman shift was observed in E_{2LH} phonon frequency of ZnO microwire under strain and strain free state. In ZnO nanowire, E_{2L} phonon frequency is observed at 106.49 cm^{-1} , which is downshifted to 103.82 cm^{-1} after applying strain. The down shift in shift in E_{2L} phonon frequency was mainly due to the experience of tensile strain under strain condition [5], which was shown in Fig.2.7.

The piezoelectric nanogenerator was fabricated using as grown ZnO microwire, which was schematically represented in Fig.2.2. The digital image of the fabricated device was shown in the Fig.2.8. The experimental setup used for applying force to the device was shown in Fig.2.9. The one end of the device fixed with support and other end was free movement. When applying the force at free end it will bend which creates the strain over the ZnO microwire.

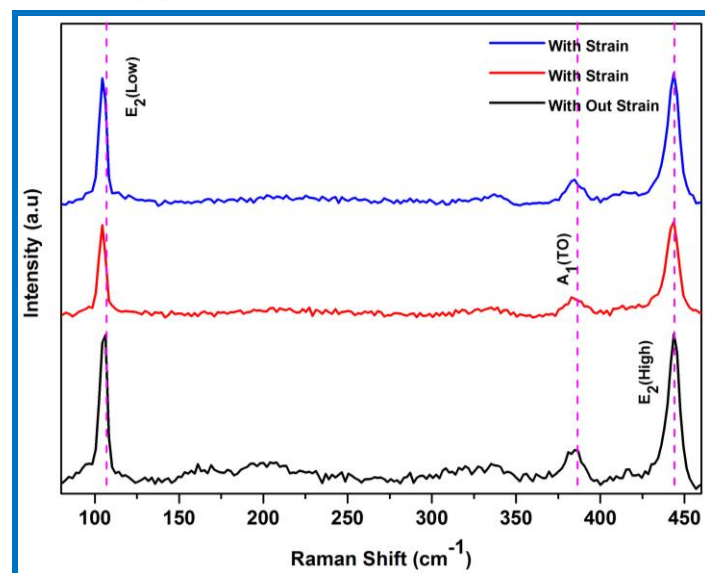


Fig.2.7. Raman spectra of ZnO microwire at strain and strain free state.

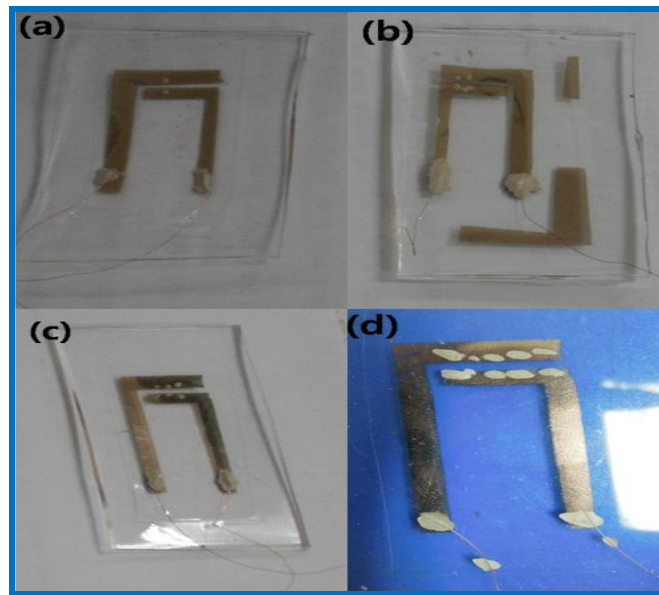


Fig.2.8. ZnO microwire based piezoelectric nanogenerator, a) single wire, b) double wire, c) three wire, and d) four wire

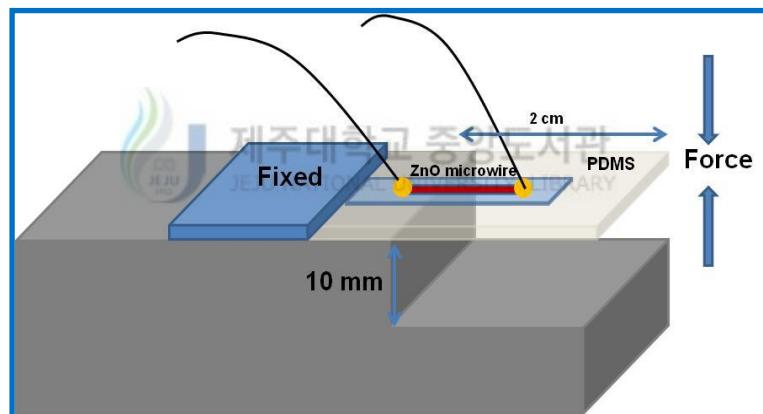


Fig.2.9. Schematic diagram of the force applying setup

At first open-circuit voltage was measured under forward connection by connecting the positive and negative terminal of the measurement system to the positive and negative end of the nanogenerator. The schematic representation of the connection configuration was shown in Fig.2.10. In order to check the real output from the device, we have performed the switching-polarity test. At reverse connection, the positive and negative end of the nanogenerator was connected to the negative and positive terminal of the measurement system. At forward connection,

the positive peaks corresponding to the stretching states of the microwire when the free end of the substrate is bended downward. When the substrate is released, the microwire returns to original state, which results negative peak in the measurement. At the reverse connection, the peaks are reversed, the stretching peaks at negative side and release peak at positive side. The same trend was observed in both open-circuit voltage and short circuit current. Here, we have fabricated different device with various no of microwire such as 1 wire, 2 wires, 3 wires and 4 wires. At first, we have measured electrical output of the single wire piezoelectric nanogenerator which was shown in Fig.2.11. For single microwire based piezoelectric nanogenerator generated the maximum open-circuit voltage of around 9 mV and 5.5 mV under forward and reverse connection respectively.

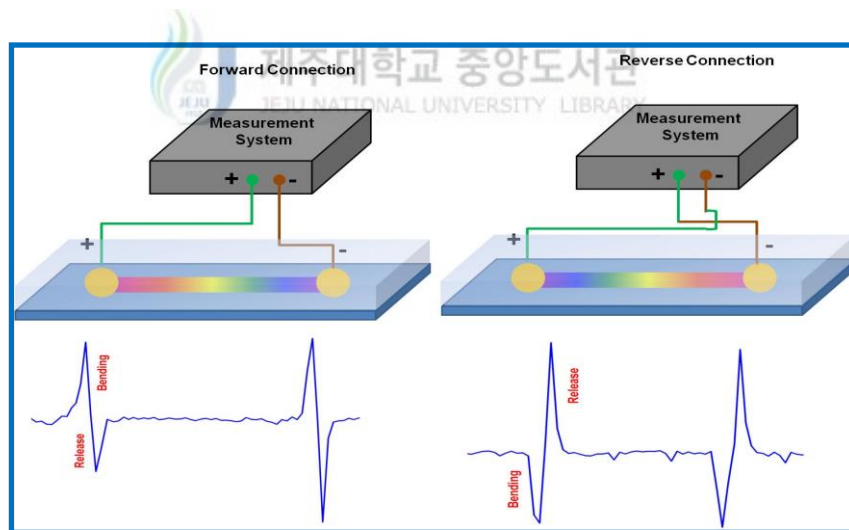


Fig.2.10. Schematic diagram of the device connection in forward and reverse connection

The maximum short-circuit current was produced in this device was around 0.6 nA under both forward and reverse connection. When integrating with two microwires, the generated open-circuit voltage and short-circuit current was

increased to 20 mV and 3 nA respectively. The electrical output performance of the two piezoelectric nanogenerator was shown in Fig.2.12.

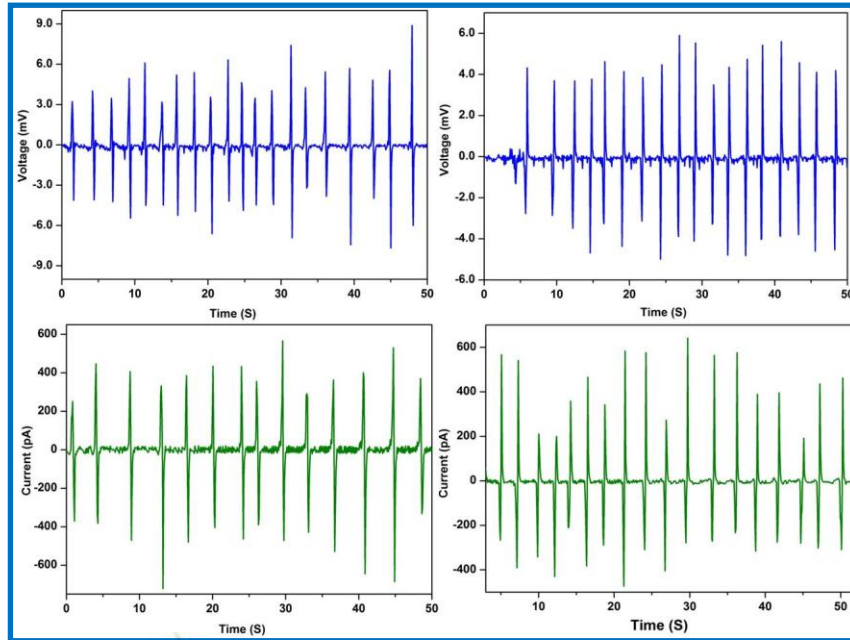


Fig.2.11. Single wire nanogenerator, open-circuit voltage and short circuit current under forward and reverse connection condition

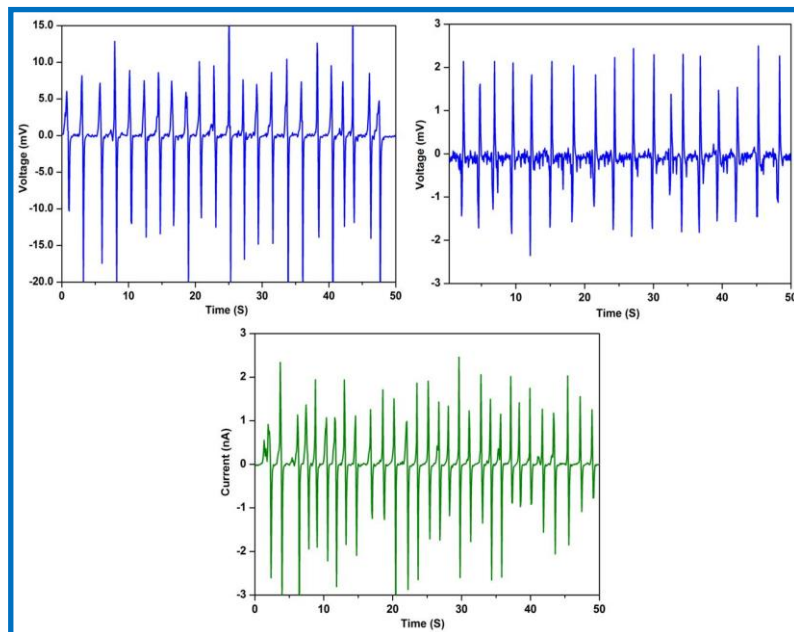


Fig.2.12. Two wire nanogenerator, open-circuit voltage and short circuit current under forward and reverse connection condition

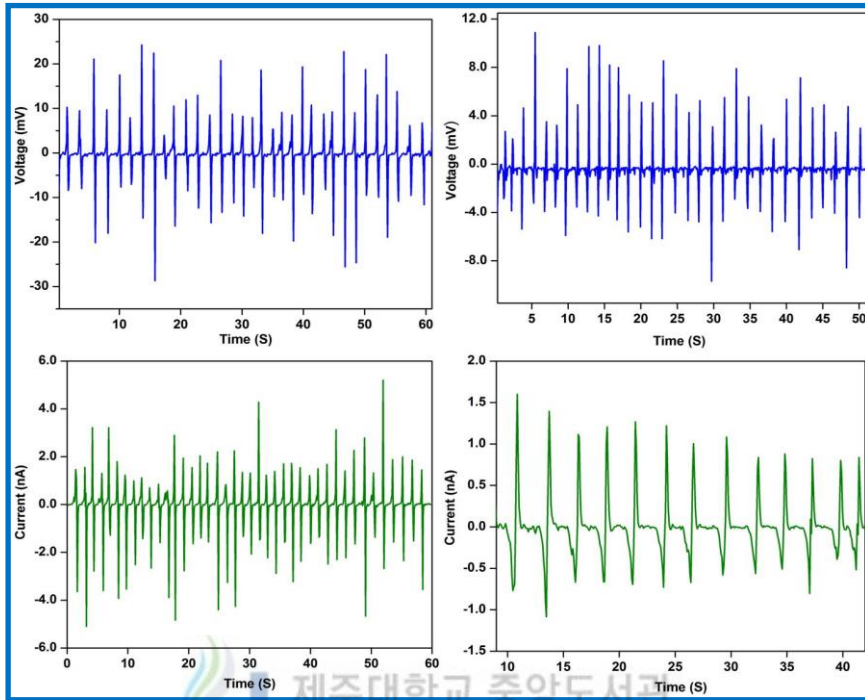


Fig.2.13. Three wire nanogenerator, open-circuit voltage and short circuit current under forward and reverse connection condition

Likewise, integrating the more number of wires in the device increased the output voltage and current in linearly. In this study we have integrated totally four number of wire which produced maximum open-circuit voltage and short-circuit current of 60 mV and 3 nA respectively. The output performance of the three and four wire nanogenerator was shown in Figs.2.13 and 2.14.

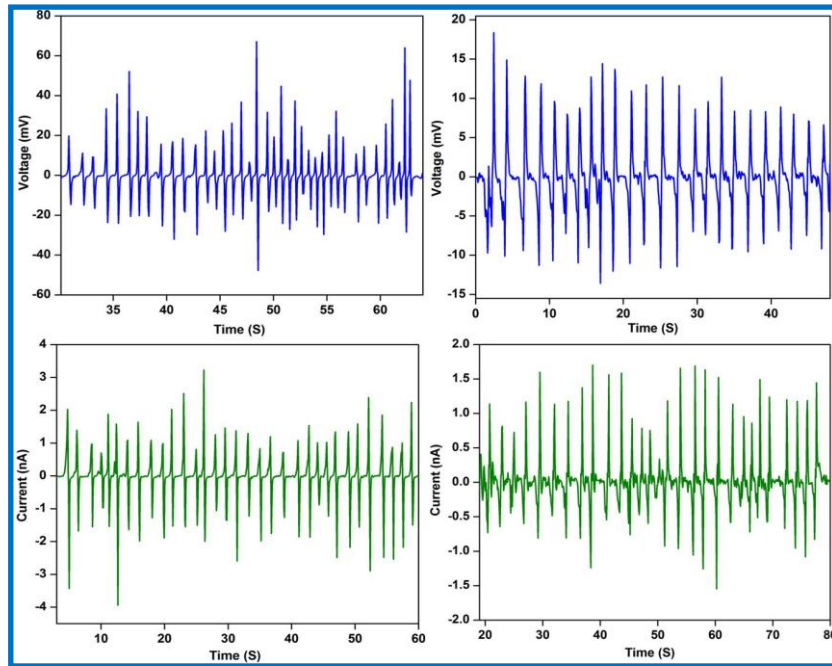


Fig.2.14. Three wire nanogenerator, open-circuit voltage and short circuit current under forward and reverse connection condition

The mechanism for output generation in the microwire was explained by the generation of piezo-potential over the nanowire [6-8]. The detailed mechanism was shown in Fig.2.15. Due to existence of schottky at the one end of microwire restrict the flow of electron from nanowire because of higher local resistance. When apply external force to bend or stretch the microwire piezo-potential was generated along the microwire surface due to polarization of atoms in the crystal to create ionic charges. The polarized ions in the microwires are non-movable; it remains until release of strain. The positive and negative piezo-potential was generated at schottky barrier end and other side (ohmic) of the wire respectively. The presents of schottky contact will raise the energy of the Fermi level of electrode at ohmic contact side to ZnO conduction band, which gives raise to flow of electron ohmic contact electrode to high resistance schottky side through external load. The flown electrons accumulate at the interfacial region between the schottky barrier electrode and the

wire, and this accumulation process was continued until to get the balance of generated piezoelectric potential and accumulated electron potential. When releasing the strain, the generated piezo-potential was disappearing to attain equilibrium the accumulated electron at schottky barrier side move to other side electrode through external circuit.

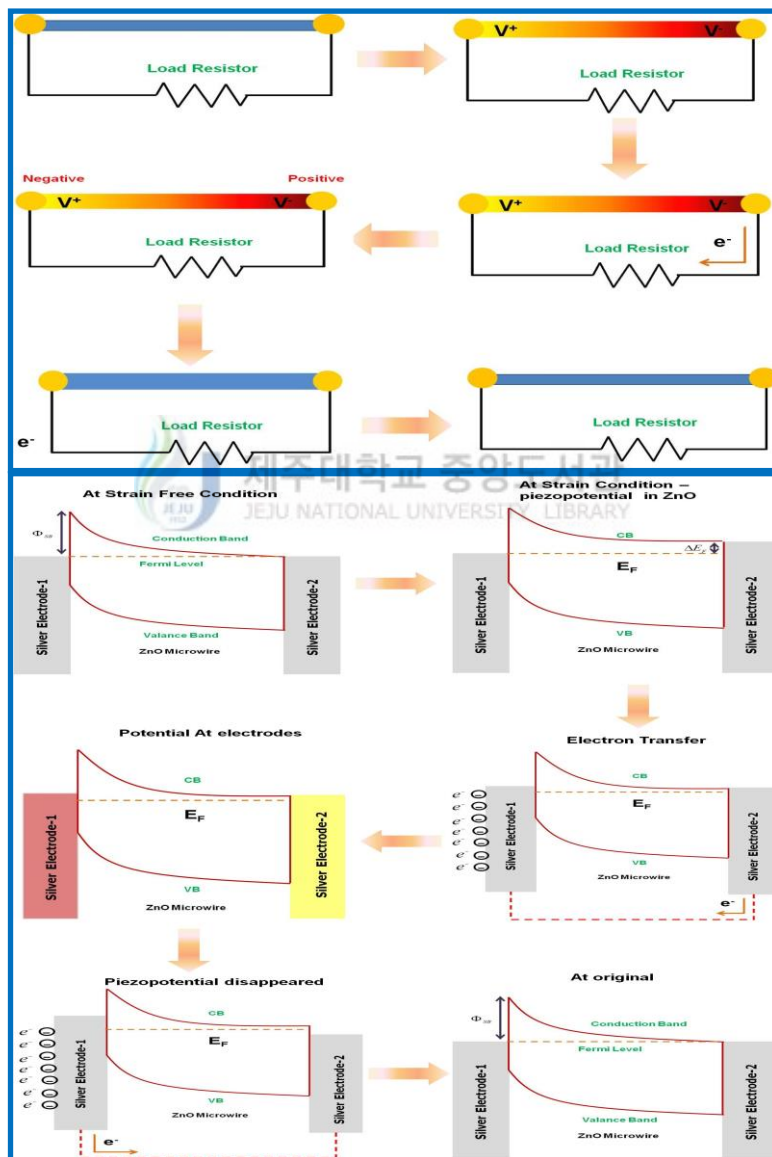


Fig.2.15. Mechanism of electrical output generation in ZnO microwire based nanogenerator

2.3. Fabrication of ZnO Microwire - Polyvinylidene fluoride (PVDF) based inorganic- organic hybrid piezoelectric nanogenerator

To improve the output of the microwire based nanogenerator, we have fabricated inorganic-organic core-shell structure. For this purpose, we have coated polyvinylidene fluoride (PVDF) over the half of the ZnO microwire by dip coating method. The PVDF coated microwire was lay down on the flexible substrate. The fabricated hybrid device was allowed to dry at 60°C for 12 h at hot air oven. After drying the device, we have made electrical contact using Cu wire and silver paste. The one connection was taken from ZnO microwire and another one from PVDF. After make contact, the whole device was packed with PDMS. The schematic diagram of the fabricated device was shown in Fig.2.16.

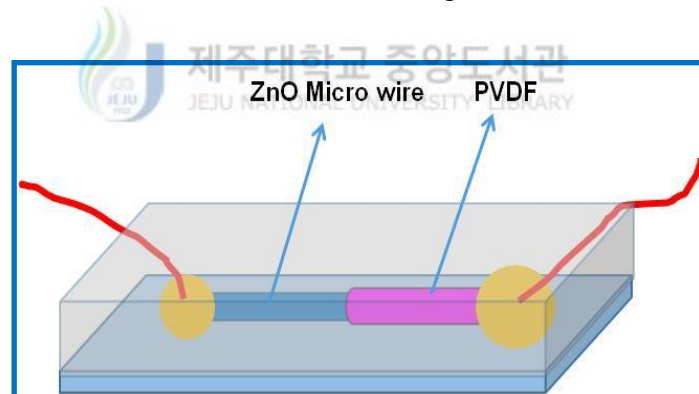


Fig.2.16. Schematic diagram of ZnO microwire - PVDF hybrid piezoelectric nanogenerator

To confirm the PVDF coating over the ZnO microwire, we have measured Raman spectrum at the interface of ZnO-PVDF. The inset shows the optical image of hybrid structure, which is not clearly showing the PVDF coating over the microwire due to thin layer of PVDF over the microwire. To further, confirm we measured Raman spectrum, which clearly indicating the coating of β - phase of PVDF. The existence of β - phase PVDF give the additional piezo-potential during the applying

strain. The Fig.2.17 shows the Raman spectrum of the ZnO microwire-PVDF hybrid wire.

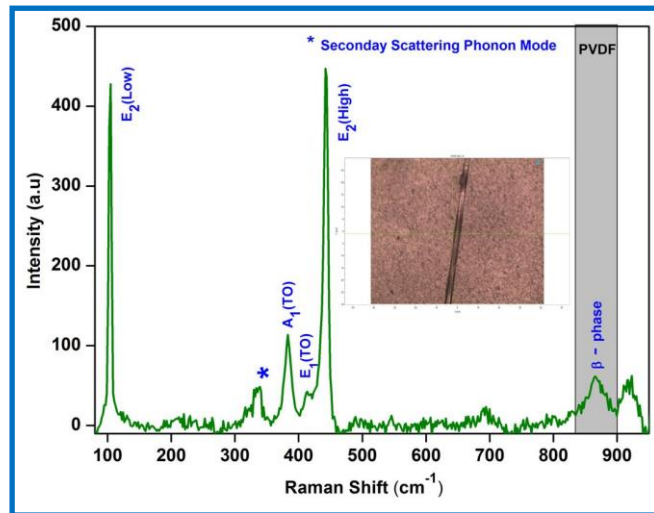


Fig.2.17. Raman spectrum of ZnO microwire - PVDF hybrid wire. The inset shows the optical image took in Raman instrument

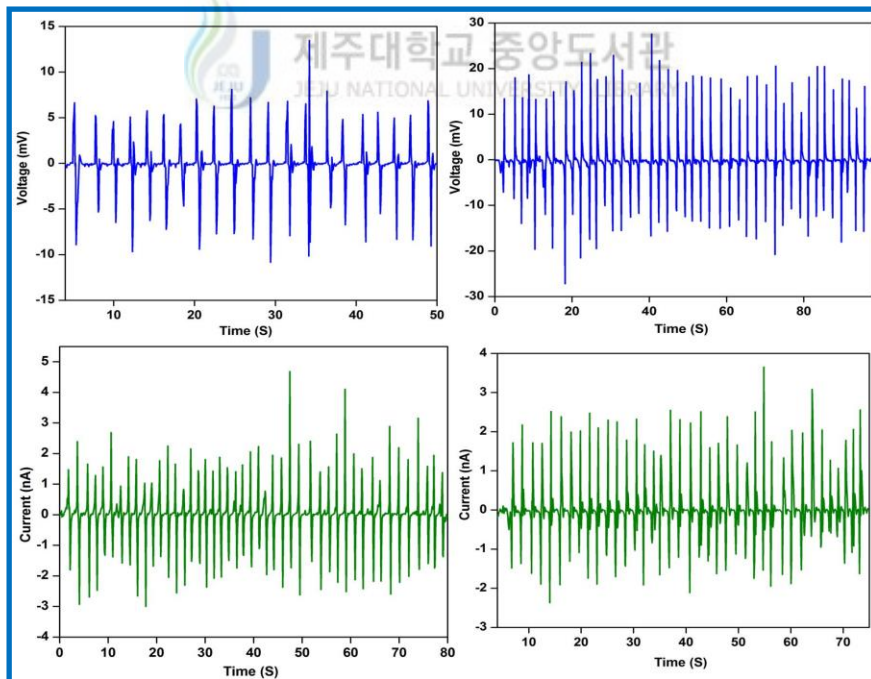


Fig.2.18. The electrical output performance of the ZnO microwire- PVDF hybrid nanogenerator, open-circuit voltage and short circuit current under forward and reverse connection condition

We have fabricated the piezoelectric nanogenerator using the ZnO microwire-PVDF hybrid wire. The measured open-circuit voltage and short-circuit current of

the hybrid device under forward connection is shown in Fig.2.18. The fabricated device generated open-circuit voltage and short circuit current of 10 mV, 20 mV and 2.5 nA under forward and reverse connection respectively. The fabricated device showed higher output than bare ZnO based device. The mechanism of energy generation in the hybrid device was explained based on the piezoelectric effect. Due to presents of PVDF in the device increase the schottky barrier height and reduced the leakage current through schottky barrier, which improved the output performance of the device.

2.4. Conclusion

This chapter discusses the detailed growth of ZnO microwire through vapor transport method. The grown microwire was characterized with XRD, FE-SEM, and Raman spectrum. Finally, the piezoelectric nanogenerator was fabricated by using these microwires. Here, we have studied the performance of nanogenerator when increasing no wires. We have studied until four wires and results concluding that the output increases with increase of number of nanowire. To further improve output, we have fabricated hybrid device using PVDF as a shell over the microwire. The coating of PVDF improved the output performance of the nanogenerator by reducing leakage current and increase Schottky barrier height.

Reference

- [1] R. Mohan, K. Karthikeyan, S.J. Kim, Enhanced Photocatalytic Activity of Cu-doped ZnO Nanorods, *Solid State Commun.* 152 (2011), 375-380.
- [2] R. Mohan, K. Karthikeyan, S.J. Kim, Diameter Dependent Photocatalytic Activity of ZnO Nanowires Grown by Vapor Transport Technique, *Chem. Phys. Lett.* 539 (2012), 83-88.
- [3] R. Mohan, G.S. Kim, S.J. Kim, ZnO Nanostructures in Vapor Transport Growth Method, *Sci. Adv. Mater.* 6 (2014), 336-342.
- [4] J.B. Park, W.K. Hong, T.S. Bae, J.I. Sohn, S.N. Cha, J.M. Kim, J. Yoon, T. Lee, Strain Effects in a Single ZnO Microwire with Wavy Configurations, *Nanotechnology* 24 (2013), 455703.
- [5] X.W. Fu, Z.M. Liao, R. Liu, J. Xu, D. Yu, Size-Dependent Correlations between Strain and Phonon Frequency in Individual ZnO Nanowires, *ACS Nano* 7 (2013), 8891–8898.
- [6] R. Yang, Y. Qin, C. Li, Guangzhu, Z.L. Wang, Converting Biomechanical Energy into Electricity by a Muscle-Movement-Driven Nanogenerator, *Nano Letters.* 9 (2009), 1201-1205.
- [7] R. Yang, Y. Qin, C. Li, L. Dai, Z.L. Wang, Characteristics of Output Voltage and Current of Integrated Nanogenerators, *Appl. Phys. Lett.* 94 (2009), 022905.
- [8] R. Yang, Y. Qin, L. Dai, Z.L. Wang, Power Generation with Laterally-packaged Piezoelectric Fine Wires, *Nat. Nanotechnol.* 4 (2009), 34-39.

Chapter -III

Aligned Nanowire Array Based Nanogenerator

This chapter presents the growth of vertically align ZnO nanowire array on flexible substrate using low temperature hydrothermal method. The grown ZnO nanowire was well characterized using X-ray diffraction pattern, FE-SEM. We fabricated piezoelectric nanogenerator using vertically aligned ZnO nanowire on one side and double side. The detailed analysis of nanogenerator characteristics was discussed. Further, We fabricated a new device structure consists of double side grown ZnO nanowire array sandwiched between gold coated ZnO nanowire arrays using polydimethylsiloxane and this devices was effectively used to energy harvesting from human body movement.

3.1. Introduction

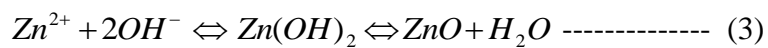
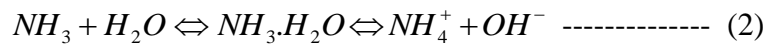
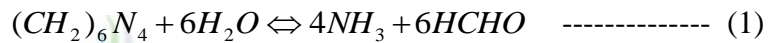
Recent years, quasi-one dimensional nanostructures are created enormous interest towards their technical application and in-depth analysis over their properties because of unique properties than their bulk counterparts. It is an ideal system to explore a novel phenomenon at the nanoscale relating with size, dimension and directional. One dimensional nanostructure is expected to play an important role in the development of science and engineering. The one-dimensional nanostructures such as rod, wire, springs/rings and belt received more attention in many applications including field effect transistors [1, 2], UV lasers [3], light emitting diodes [4], solar cells [5], photodetectors [6], nanogenerators [7], and piezotronics [8], catalysis etc. To demonstrate the various applications, synthesis of one dimensional nanostructure with control over size, aspect ratio, orientation and density are significant and much needed one. There are main methods are available to grow one dimensional nanostructures such as physical vapor deposition [9, 10], MOVCD [11], MBE [12], chemical vapor deposition [13], pulsed layer deposition (PLD) [14] and the wet chemical method [15]. For large scale, low cost and easy fabrication, hydrothermal method is one of the fascinating methods to fabricate one dimensional nanostructure with controlled aspect ratio and orientation with higher crystallinity at low temperature (< 100 °C).

3.1.1. Synthesis of vertically aligned ZnO nanowire array

The ZnO nanowire array was grown through seed mediated hydrothermal method on various substrates such as Si, ITO coated glass/PET and PET substrate. To optimize the experimental condition and explore the experimental parameters, we

have chosen only flexible substrate. The substrates were cleaned by ultrasonication consecutively in different solution such as ethanol, acetone, and isopropyl alcohol and deionised water each for 15 min. Initially, substrates were dried by nitrogen gas blew and in oven for 1 hr at 60°C. The ZnO seed layer was coated on the cleaned substrate by spin coating method. The ZnO nanowire array was grown on the substrate using hydrothermal method. For hydrothermal reaction, the solution was prepared by dissolving equal concentration of zinc nitrate hexahydrate and hexamethylenetetramine (HMTA) in de-ionized water.

The ZnO nanowire was grown during hydrothermal reaction based on the following reactions,



At the start of hydrothermal reaction, HMTA hydrolyzes into ammonia and formaldehyde as per equation (1). The existence of ammonia in the solution increased the pH of the growth solution. Here, HMTA release ammonia in controlled and slowly to reaction solution, which hold the constant pH over the reaction period, simply it act as a buffer. Then, ammonia reacts with water molecules, which form ammonium hydroxide. Then, Zn^{2+} react with OH^- released from ammonium hydroxide form different kinds of hydroxide monomers such as $Zn(OH)^+$, $Zn(OH)_2$, $Zn(OH)_3^-$, $Zn(OH)_4^{2-}$, like equation (2)&(3). Finally, ZnO nuclei are formed by the

dehydration of zinc hydroxide at the seed layer surfaces as equation (3). The rapid hydration followed by condensation of zinc hydroxide forms ZnO nanowire. The existence of HMTA and ammonia observed over the particular planer surface of ZnO nanocrystals, which hinders their growth along that direction and it meant grow only certain direction. Even though, the exact mechanism and role of HMTA during the ZnO nanowire growth is still unclear.

The controlling of the chemical equilibrium of the reaction solution helps to control the size, aspect ratio, density and orientation of nanowires and crystallinity. The equilibrium of the reaction was controlled by changing reaction parameters, such as reactants concentration and growth duration. By adjusting concentration of the reactant solution controls the density of the nanowires and aspect ratio, morphology of the nanowires was controlled by growth time and temperature. In this part, we detail analyzed about the vertical growth of ZnO nanowire array over different substrate, seed solution concentration, growth time and concentration.

3.1.2 ZnO Seed layer

To explore the relation between ZnO seed layer concentration and crystallinity, morphology of the nanowire, we have performed a serious of experiment with different concentration of seed layer concentration at constant hydrothermal reaction solution concentration (50 mM) and growth temperature, time of 90° C, 6 h.

The ZnO sol-gel precursor was prepared as follows: the different concentration (0.2, 0.4, 1 M) of ZnO seed solution was prepared as follows; an equal

mole of zinc acetate and monoethanolamine was dissolved in 50 ml of 2 – methoxyethanol. The solution mixture was stirred for 30 min at 60 °C and then the solution was allowed to cool down to room temperature under stirring condition. The prepared transparent solution was aged at ambient condition for 48h to check the stability of the solution. The aged seed solution was spin coated at 2000 rpm for 20 s on flexible substrate and dried at 100 °C for 10 min in a hot air oven. The Fig.3.1 shows the XRD pattern of the as grown ZnO nanowire array on flexible PET substrate with different seed layer concentration. From these results, we conclude that the higher concentration of seed layer solution formed a good crystalline nanowire array compared to other concentration.

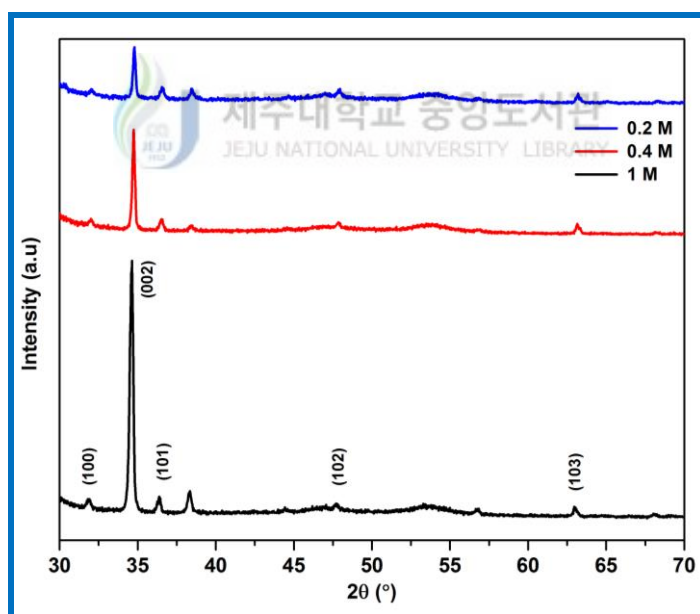


Fig.3.1. X-ray diffraction pattern of the as grown nanowire with different seed layer concentrations (0.2, 0.4, 1 M) at 50 mM of Zinc nitrate/HMTA @ 90°C for 6 h

Fig.3.2 shows the FE-SEM image of vertically grown ZnO nanowire array on different concentration seed layer. The higher concentration of seed solution results smaller and orientated nanowire array compare to 0.2 and 0.4 M concentration. At

lower concentration, the nanowire diameter was small and also in mixed structure which contains, sheets and higher diameter nanowires. The higher concentration of seed solution is optimum for growing well aligned nanowire array.

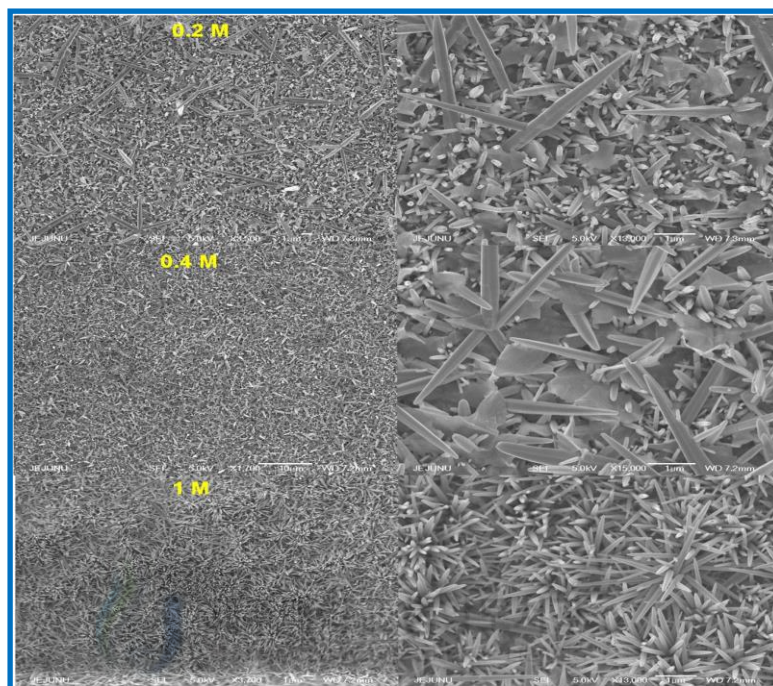


Fig.3.2. Field emission scanning electron microscopic (FE-SEM) image of ZnO nanowire grown at 50 mM of Zinc nitrate/HMTA @ 90°C for 6 h with different seed layer concentration (0.2, 0.4 and 1 M)

3.1.3. Different Substrate

To study the effect of substrate on the nanowire growth, we have grown ZnO nanowire array on Si and ITO coated glass substrate. A Si / ITO coated glass substrates were cleaned by a standard cleaning progress. First, the substrate was sonicated consecutively in acetone, ethanol and de-ionized water each for 10 minutes, then substrate was dried by nitrogen gas blew and then baked in oven to remove moisture and remain water. Then, 0.2 M ZnO seed layer was coated on the substrate by spin coating method. The spin coating process was carried out for 3 times and after each coating the substrate was dried at 100°C for 5 min and finally,

annealed at 500°C for 1 hr. The ZnO nanowire was grown by hydrothermal method, which is described in detail as follows. An equimolar (0.075 M) aqueous solution of Zinc nitrate ($\text{Zn}(\text{NO}_3)_2 \cdot 6\text{H}_2\text{O}$) and Hexamethylenetetramine (HMTA, $(\text{CH}_2)_6\text{N}_4$) was dissolved in 50 ml of DI water with molecular ratio of 1:1. The prepared solution was transferred to 100 ml Teflon container and the seed layer coated substrate was hanged in Teflon container. Hydrothermal reaction was performed at 95°C for 6 h. Finally, the samples were rinsed in DI water and then dried in air at 60 °C for 5 min.

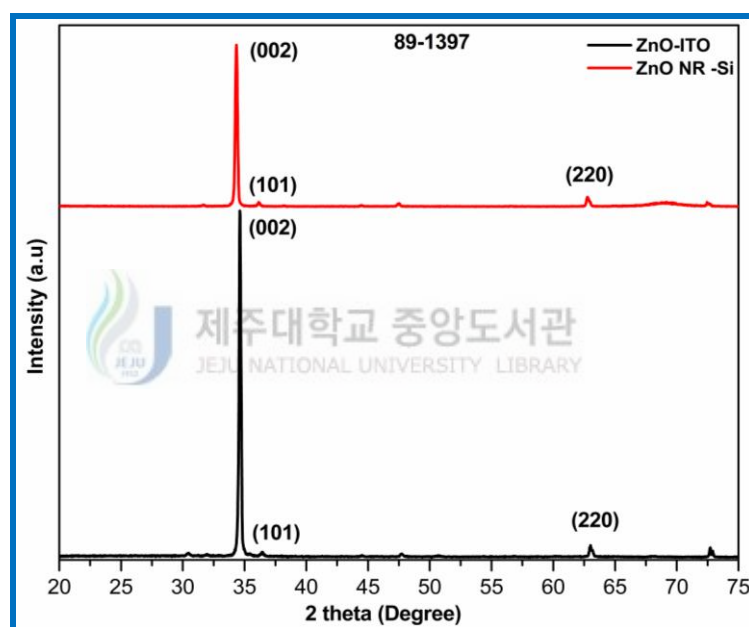


Fig.3.3. XRD pattern of ZnO nanowire array grown on ITO and Si substrate

Fig.3.3. shows the X-ray diffraction pattern of ZnO nanowire array grown on ITO/Si substrate. From diffraction pattern, we observed one dominant peak at 34.36° which corresponds to ZnO (0 0 2) plane and another peak at 72.32° this corresponds to ZnO (0 0 4) plane (JCPDS 65-3411). The ZnO (0 0 2) plane was corresponds ZnO wurtzite structure. The higher crystallinity was observed in ITO substrate than Si substrate. The morphology of the ZnO nanorods were analyzed through FESEM

which shown in Fig.3.4. The FESEM result was conformed the vertical orientation, highly dense nanorods and uniformly orientated in whole sample area. The length and diameter of the grown ZnO nanorods was measured from FESEM which have the diameter of 180 – 300 nm and 2-3 μm of length.

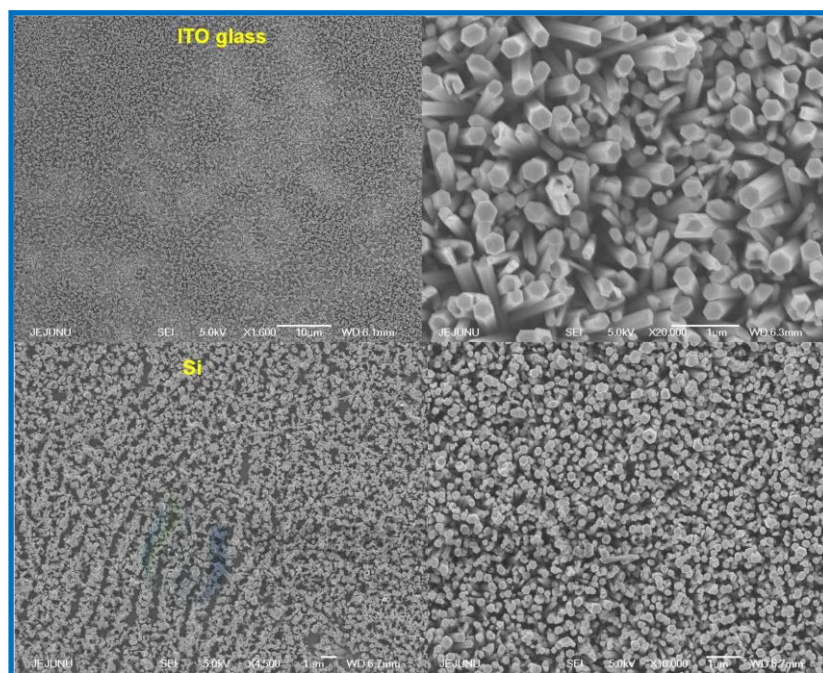


Fig.3.4. FE-SEM image of ZnO nanowire array grown on ITO and Si substrate

3.1.4. Growth temperature

To explore the relation between growth temperature and aspect ratio and orientation of nanowire, we have performed a series of experiments with different growth temperatures at constant hydrothermal reaction solution concentration (50 mM) for 6 h.

The 1 M ZnO seed layer was coated on the flexible substrate by spin coating method. The spin coating process was carried out for 3 times and after each coating the substrate was dried at 100°C for 5 min. An equimolar (0.05 M) aqueous solution

of Zinc nitrate ($\text{Zn}(\text{NO}_3)_2 \cdot 6\text{H}_2\text{O}$) and Hexamethylenetetramine (HMTA, $(\text{CH}_2)_6\text{N}_4$) was dissolved in 50 ml of DI water. The prepared solution was transferred to 100 ml Teflon container and the seed layer coated substrate was hanged in Teflon container. Hydrothermal reaction was performed at different temperature such as 60, 70, 80 and 90°C for 6 h.

At the various growth temperatures, the growth of non polar surface is almost compared to polar surface growth that means the variation of diameter almost constant for different growth temperature. But in case of length increased with increasing temperature and also density, orientation of nanowire were higher at 90°C, which is shown in Fig.3.5. From this experimental study we concluded that 1 M seed layer concentration with growth solution concentration of 50 mM at 90°C for 6 h were optimum condition to grow the vertically aligned nanowire array over the flexible substrate.



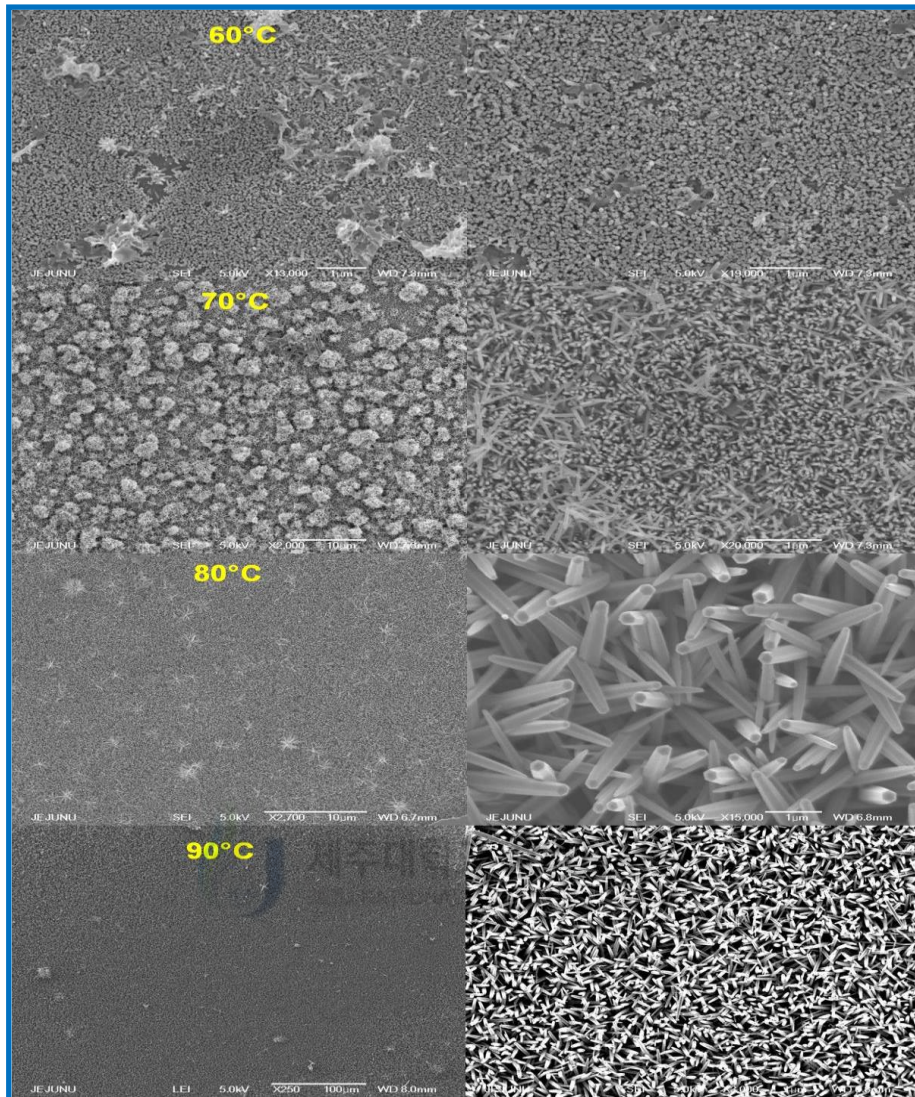


Fig.3.5. Field emission scanning electron microscopic (FE-SEM) image of ZnO nanowire grown at different growth temperature

3.2. Single side Aligned ZnO Nanowire array based nanogenerator

Fig. 3.6 represents detailed process of aligned ZnO nanowire array growth over flexible IT coated PET substrate by low temperature hydrothermal method. The seed layer (1 M) was coated over the cleaned ITO substrate by spin coating method. The nanowire was grown through hydrothermal reaction and reaction was carried out in equimolar zinc nitrate/HMTA solution (50 mM) at 95°C for 8 h.

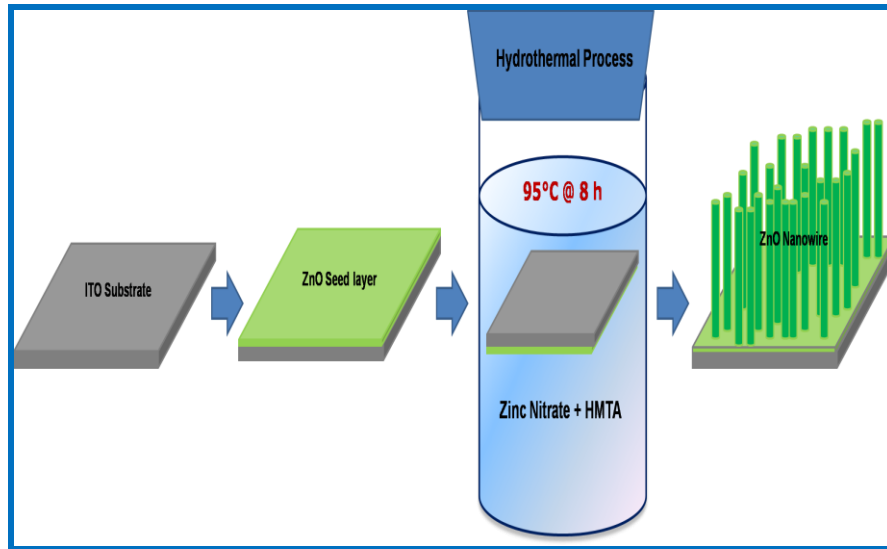
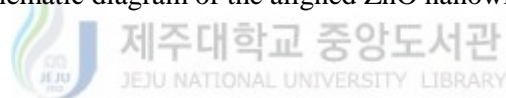


Fig.3.6. Schematic diagram of the aligned ZnO nanowire growth



The crystallinity and orientation of the grown ZnO nanowire array were measured through X-ray diffraction pattern, which is shown in Fig.3.7. The observed XRD pattern is well agreement with standard JCPDS (JCPDS card - 36-14510). In XRD pattern, a predominant peak observed at 2θ of 34.4, which is originated from the (002) plane of ZnO NWs. Micro-Raman analysis was carried to analysis the microstructure of the aligned nanowire array. According to group theory, ZnO have nine optical phonon modes and three acoustic phonon modes. The available phonon modes such as E_2 (low and high), A_1 [(TO) transverse optical and (LO) longitudinal optical] and E_1 (TO and LO) are Raman active, which expressed as [16].

$$\Gamma_{opt} = 1A_1 + 2B_1 + 1E_1 + 2E_2 \quad \text{----- (1)}$$

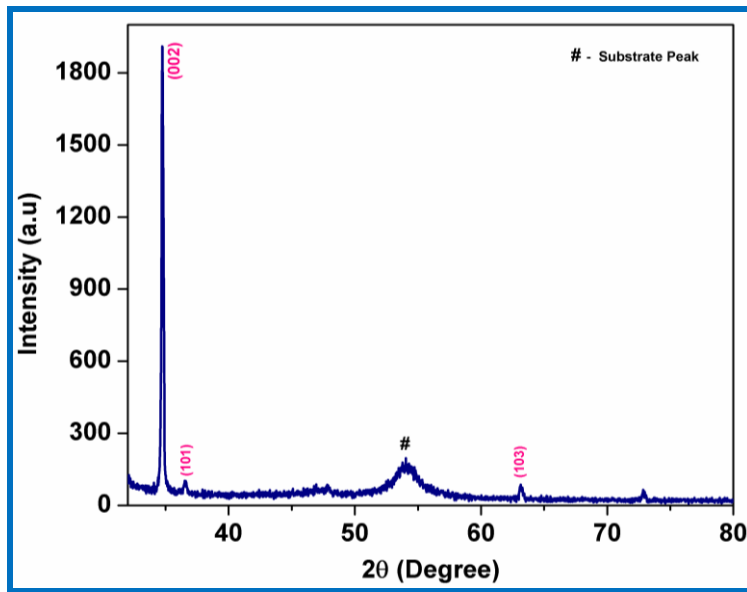


Fig.3.7. X-ray diffraction pattern of aligned ZnO nanowire array on single side of the PET substrate

In as grown aligned nanowire (Fig.3.8), we observed only E_2 (low), E_2 (high), which confirms the wurtzite structure of ZnO. The existence of higher intensity of E_2 (high) indicates the high crystalline nature of the nanowire.

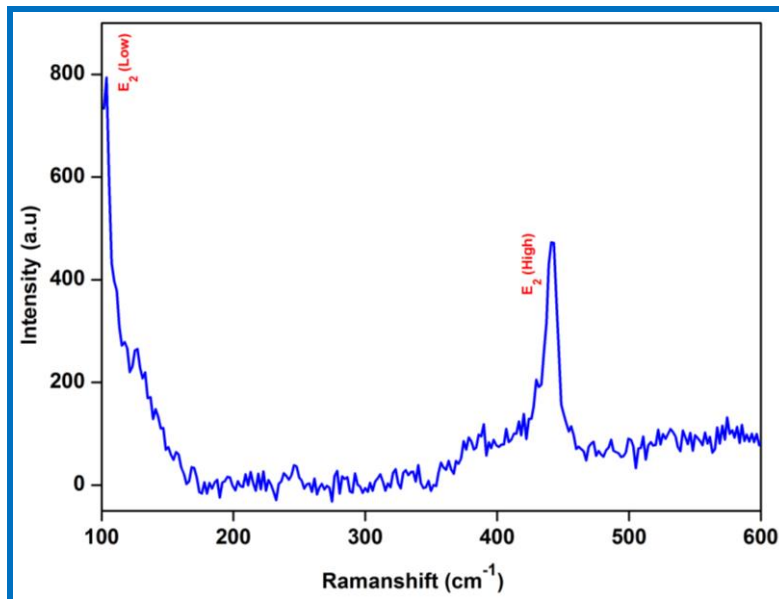


Fig.3.8. Raman spectrum of as grown aligned ZnO nanowire array

The surface morphology of the aligned nanowire array was analyzed through field emission scanning electron microscopy (FE-SEM), which is shown in Fig.3.9. The image indicates the homogeneous and uniform growth of nanowire over the whole substrate. The nanowires are well-aligned and vertically oriented with average diameter of $\sim 60\text{--}100\text{ nm}$ and $\sim 3\text{--}4\text{ }\mu\text{m}$ in length.



Fig.3.9. FE-SEM image of aligned nanowire array in-plane view. Insets cross sectional and 20° tilted view.

The piezoelectric nanogenerator was fabricated using aligned nanowire array by coating poly (methyl methacrylate) (PMMA) over the nanowire array through spin coating and Au top electrode was fabricated through thermal evaporator. The connection was taken out from top Au and bottom ITO electrode through Cu wire. The whole device was packed with polydimethylsiloxane (PDMS), to avoid breaking of device during measurement. The performance of the fabricated nanogenerator device (active area $1.5 \times 1.5\text{ cm}^2$) was tested through bending tester under pressing condition.

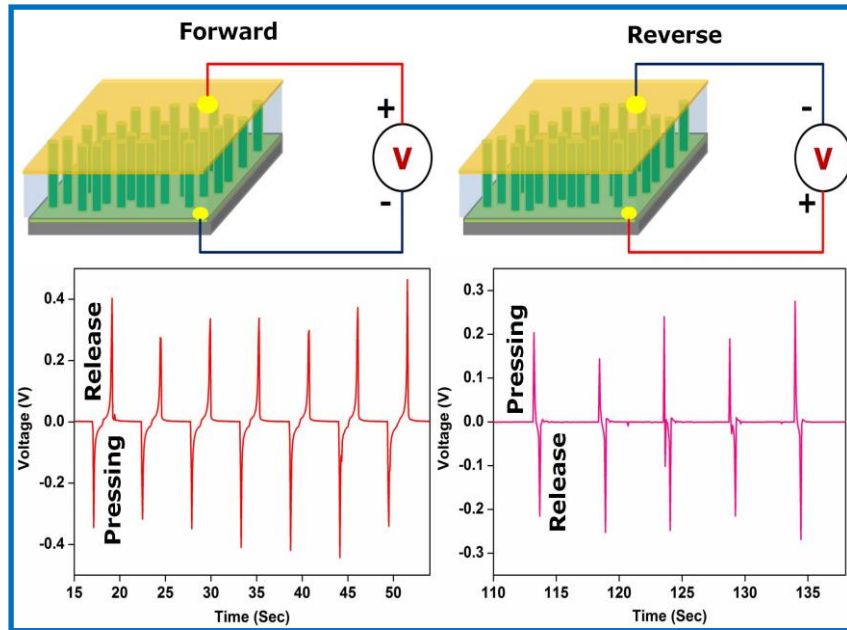


Fig.3.10. The electrical output performance of the single side ZnO nanowire array nanogenerator, output voltage under forward and reverse connection condition.

The Fig.3.10 represents the measured output voltage (V) from nanogenerator under forward and reverse connection. The origin of generating voltage was verified by conduct the polarity test (reverse bias). The result revealed that the generated voltage in forward bias condition is a negative voltage side. When change the polarity of the device, the voltage changes to the positive voltage side which confirms the generated voltage is only from the nanogenerator. The maximum voltage generator under forward and reverse connection are 0.4, 0.2 V under the pressing speed of 25 mm.s^{-1} .

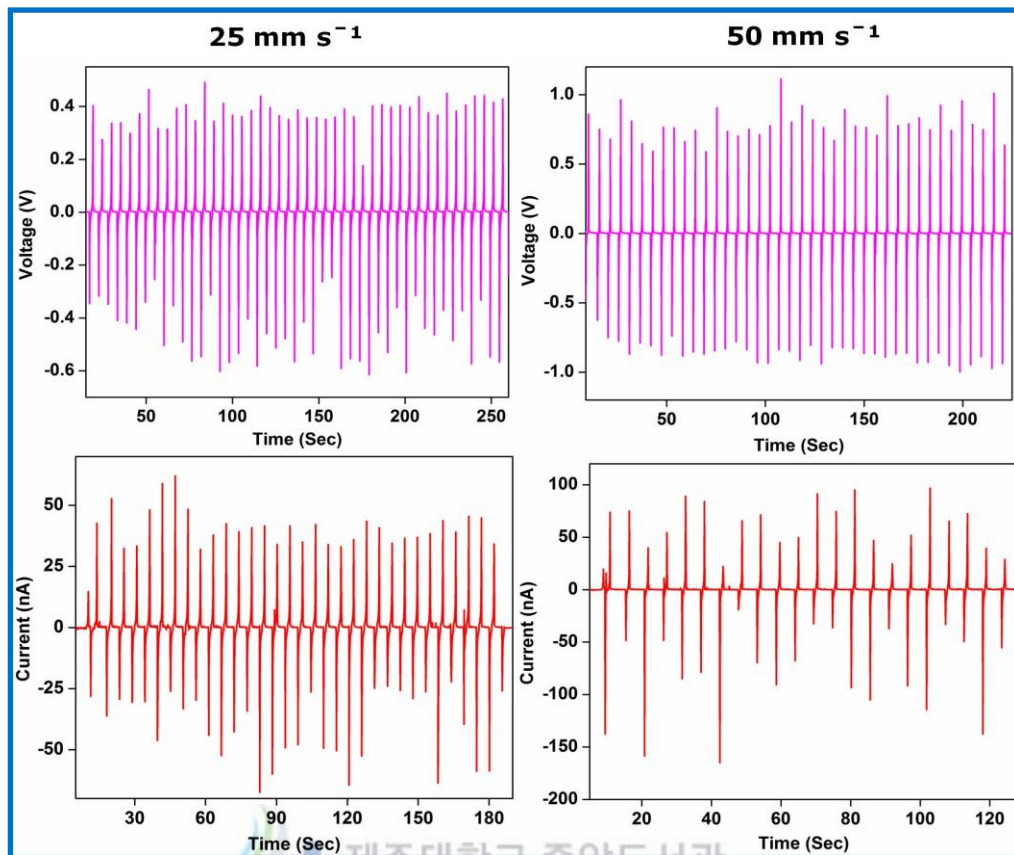


Fig.3.11.The electrical output performance of the single side ZnO nanowire array nanogenerator at different pressing speed of 25, 50 mm.s⁻¹.

To check effect of the pushing speed on the output performance of nanogenerator, we have tested under different pushing speed of 25, 50 mm.s⁻¹. When increasing pushing speed the output of the nanogenerator increased due to increase of higher force over the nanowire, which was shown in Fig.3.11. The maximum output voltage and current was observed at 50 mm.s⁻¹, which are 1 V and 0.18 μ A.

The mechanism for voltage and current generation in the device is based on the piezoelectric effect. When the device is deformed by an external force, a piezoelectric potential generated in the ZnO nanowire. The existence of a potential gradient over nanowire from top to bottom will induces the charges over the top and bottom electrode. The induced charges in the top and bottom electrode have a

potential difference which will drive the electron in the external circuit to get equilibrium under strain condition. When applied force is released, the generated piezo-potential over the nanowire will vanish, which disturb equilibrium again. To attain the equilibrium, electron flow back in the opposite direction.

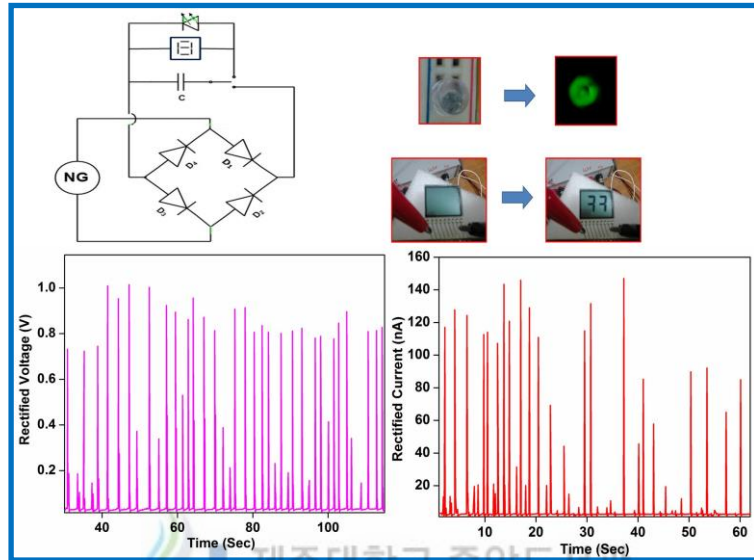


Fig.3.12. The rectified voltage and current under pressing speed of 50 mm.s^{-1} . The digital images of the electronic device powered through nanogenerator.

To demonstrate the application of nanogenerator, we have constructed bridge rectifier circuit, which consists of four diodes. The constructed rectifier rectified the nanogenerator output, which was shown in the Fig.3.12. The maximum rectified output of the nanogenerator was 1 V and $0.15 \mu\text{A}$. the rectified output was stored in commercial capacitor ($1 \mu\text{F}$) to drive the green light emitting diode (LED) and liquid crystal display (LCD). The harvested energy was successfully stored in capacitor and applied to LED and LCD to power up.

3.3. Double side Aligned ZnO Nanowire array based nanogenerator

In this section, we demonstrate new device architecture to harvest the mechanical vibration into electric energy using both piezoelectric effect from

vertically aligned zinc oxide nanowire (ZnO NW) and triboelectric effect from PDMS. Vertically aligned ZnO nanowire was grown on both sides of the flexible substrates and sandwiched between the gold coated vertically aligned ZnO nanowire electrode substrate using PDMS. The gold coated ZnO NW array was used as an electrode to enhance the effective contact between the electrode and nanogenerator. This modified novel structure have potential to extract more energy from the device due to unevenly aligned nanowire surface creates the more contact area as well as the introduction of inductance charges in PDMS layer by triboelectric effect.

3.3.1 Preparation of ZnO seed layer

The flexible polyethylene terephthalate (PET) substrate was used for fabricating ZnO nanogenerator. First, the flexible substrate was cleaned with ethanol and deionized (DI) water in bath sonicator for 30 min respectively. ZnO seed layer was coated by sol-gel spin-coating method. The ZnO seed solution was prepared as follows, equal mole of zinc acetate (1 M) and monoethanolamine was dissolved in 50 ml of 2-methoxyethanol. The solution mixture was stirred for 30 min at 60 °C after that solution allowed to cool ambient temperature under stirring condition. The prepared transparent solution was aged at ambient condition for 48 hr for checking any precipitation formation. The aged solution was spin coated at 2000 rpm for 20 s on flexible PET substrate and dried at 100 °C for 10 min in hot air oven. This process was repeated for five times. The seed layer was coated for both sides for active layer and electrode layer coated on one side.

3.3.2 Growth of ZnO nanowire array

An equimolecular (25 mM) aqueous solution of zinc nitrate hexahydrate and hexamethylenetetramine and 0.5 ml of directional agent polyethylenimine (PEI) was

dissolved in 50 ml of DI water with molecular ratio of 1:1. The prepared solution was transferred to 100 ml Teflon container and seed layer coated substrate was hanged in Teflon container. Hydrothermal reaction was performed at 90 °C for 6 h. Finally, the samples were rinsed with DI water to remove the residual present on the surface and then dried in air at 100 °C for overnight. The ZnO nanowire was grown in both side of the flexible PET substrate its act as an active layer for nanogenerator. For electrodes the ZnO NW array were also grown on single side of two other flexible PET substrates with similar procedure. The gold electrodes were coated over these one sided grown ZnO NW array using thermal evaporation. These two one sided gold coated ZnO NW array will act as top and bottom electrodes for the prepared nanogenerator.

3.3.3 Fabrication of ZnO nanowire nanogenerator

The double side grown ZnO nanowire substrate was sandwiched between the gold coated ZnO nanowire substrate using PDMS. The sandwiched device was pressed using 150 g weight over the top of the device it will help to attach properly. The device was dried at 70 °C for overnight in oven. The electrical contact was taken from top and down side of gold coated ZnO nanowire through Cu wire using silver paste. After drying the whole device wrapped with scotch tab to prevent peel off problems.

3.3.4. Results and discussion

The detailed step by step process of ZnO NW growth and fabrication of the nanogenerator device was schematically presented in Fig.3.13. The low temperature

hydrothermal method was used to grow vertically aligned ZnO NW array on the flexible substrate for fabrication of the nanogenerator device.

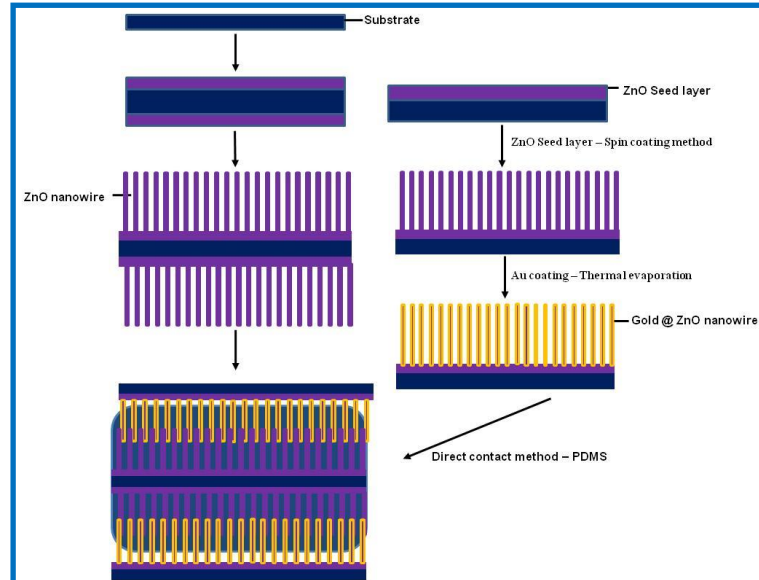


Fig.3.13. Schematic diagram of the ZnO nanowire growth and nanogenerator device fabrication process



The crystallinity and orientation of the grown ZnO NW array on the PET substrate were studied through X - ray diffraction method, which is depicted in Fig.3.14. The observed XRD pattern is well matched and indexed with standard JCPDS (JCPDS card - 36-14510) [17]. In XRD pattern, a predominant peak at 34.4° is originated from the (002) plane of ZnO NWs. The (002) orientation indicates the c-axis growth of ZnO, which is normal to the substrate surface. Since few nanowires are bent randomly, therefore few small peaks corresponding to other crystalline planes of ZnO were also observed. ZnO NW arrays were uniformly grown on both sides of the substrate, as evident from the optical image of a grown ZnO NW array on the PET substrate shown in Fig.3.15a. The optical image of the gold coated ZnO NW (ZnO NW @ Au) array is shown in Fig.3.15b. The ZnO NW @ Au array on two

separate flexible PET substrates was served as metal electrode for top and downside of the nanogenerator.

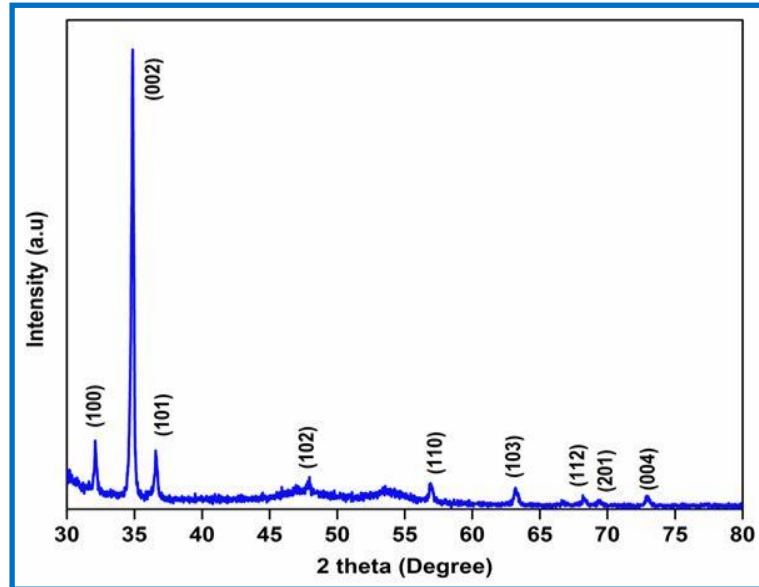


Fig.3.14. XRD pattern of vertically grown ZnO nanowire on PET substrate

The surface morphology of the grown ZnO NW array on a flexible PET substrate from normal view and 20° tilted view (insert) was imaged through FESEM, which is reported in Fig.3.15 c and d. The FESEM images confirm the vertical orientation of ZnO NW, which is densely packed over the whole substrate. The 20° titled view of ZnO NW on a flexible substrate shown in the inset of Fig.3.15c, which clearly indicates the c-axis orientation of the ZnO NW. The average length and diameter of as grown ZnO nanowire was 2 – 3 μm and 70 – 100 nm respectively. The FESEM image of the gold coated ZnO NW array is publicized in Fig.3.15d, which depicting each ZnO nanowire is fully covered by gold like core shell structure (more clear in insets).

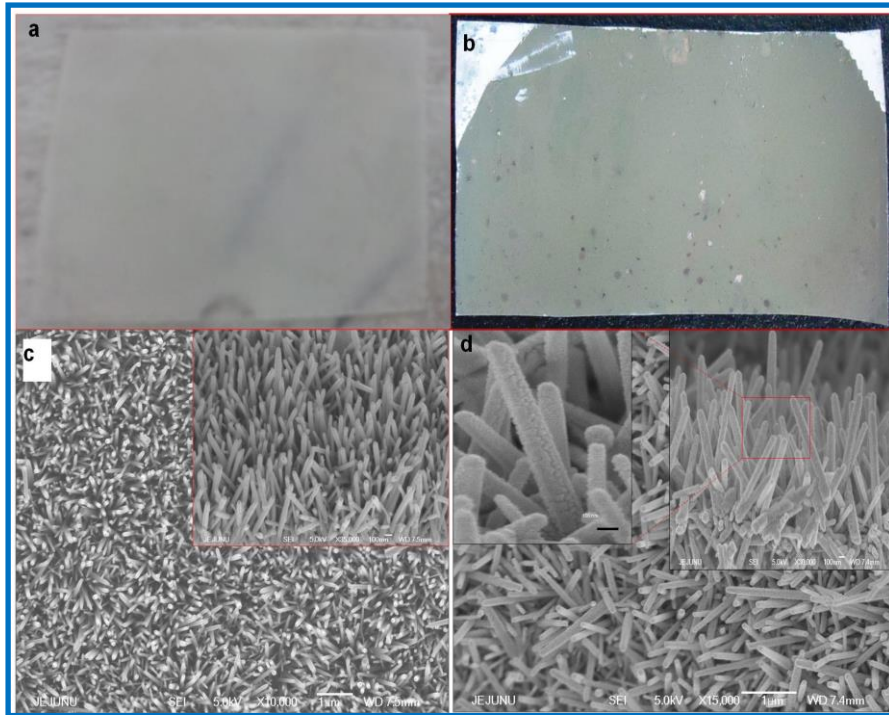


Fig.3.15. The optical and FESEM image of a) as grown ZnO nanowire, b) Gold coated ZnO nanowire, c) top view of as grown ZnO nanowire (insert: 20° tilted image), d) top view of gold coated ZnO nanowire (insert: 20° tilted image & higher magnification).

Fig.3.16a represents the 3-dimensional schematic diagram embodies the hybrid device structure of the fabricated nanogenerator. The digital image and interface manifestation of the fabricated nanogenerator was represented in Fig.3.16 b, c respectively. The top and bottom ZnO NW @ Au act as an array of tips to deflect the ZnO NW array grown on another flexible substrate on both sides. The piezoelectric and semiconducting properties of ZnO were coupled for charge creation and accumulation, transfer respectively [18]. The strain will occur in the uncoated ZnO NW array by the deflection or bending of electrode when it experience stress from the environment at any direction. Because of these stresses on the nanowire, the piezo-potential was generated on both sides of the uncoated ZnO nanowire and extracted and then transported through electrode. The non-uniform lengths of gold coated nanowire arrays have created more interface contact when it bend /fold, which

increase the transfer efficiency effectively. In this study, the nanogenerator device with four layer structure includes two ZnO NW @ Au array and two uncoated ZnO NW array. The double side grown ZnO NW was entangled with ZnO NW @ Au array on both sides.

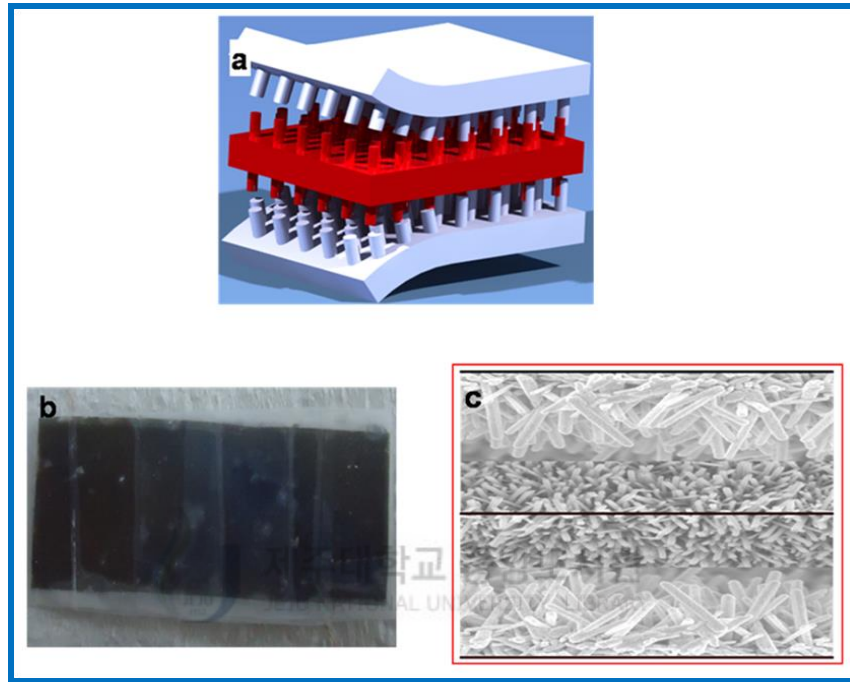


Fig.3.16. a) 3D Schematic representation of the fabricated nanogenerator device. b) Digital image of the real device. c) FESEM image of interface depiction.

The output voltage and current generated in this architecture can be explained via two mechanisms that are piezoelectric and triboelectric principles. The piezoelectric potential is generated by the strain applied to nanogenerator such as bending, pressing. It was assumed that ZnO NW array behave like a film oriented along c-axis. In case of bending, the double sided nanowire array will subjected to tensile strain on one side due to stretching in nanowire film and compressive strain on the other side owing to compression in nanowire film. In case of ZnO NW @ Au array will not be generated the piezo-potential due to the metallic conductivity of the surface, which will nullify the polarization of charges. When the substrate is being

bent (top to a downside), then tensile and compressive stress will generate on top and bottom side of the nanogenerator respectively. Due to tensile stress on top side (ZnO NW @ Au substrate) results in the compressive strain along the c-axis direction of ZnO NW. The compressive strain generates the piezo-potential distribution which drops from root to top of the nanowire. At the same time bottom-side of the NW array experiences compressive stress, which produce tensile strain along c-axis. The higher piezo-potential generated at the tips of the nanowires in bottom side. The potential difference between top and bottom side of nanowire array is same, then the potential is added constructively. The generated piezo-potential introduces the induced charge on a ZnO NW @ Au electrode, which will derive the electron in an external load. The bending and pressing of nanogenerator creates friction at nanowire and PDMS interface due to stretching and compression of nanowires. Friction of the nanowires induces the electrostatic charge on PDMS surface by triboelectric effect. Simultaneously, opposite charge was induced on the ZnO NW @ Au surface which will derive the electron in an external load [19].

The as grown ZnO nanowire have a higher surface defect mostly oxygen related defects, which generates free electron in crystal lattice as well as the reactive center for chemisorptions process. These native defects affect the piezo-potential distribution in the nanowire [20]. In this device PDMS play an important role. Firstly, it passivates the ZnO NW and reduces depletion layer formation due to chemisorptions. Because of the passivation improved the nanogenerator performance which was already reported by Y.Hu et al [21]. Then due to capillary force and the force applied due to the weight PDMS flow inside the nanowire and fill the gap

between nanowires. These PDMS holds the nanowire as stiff like film when stretching.

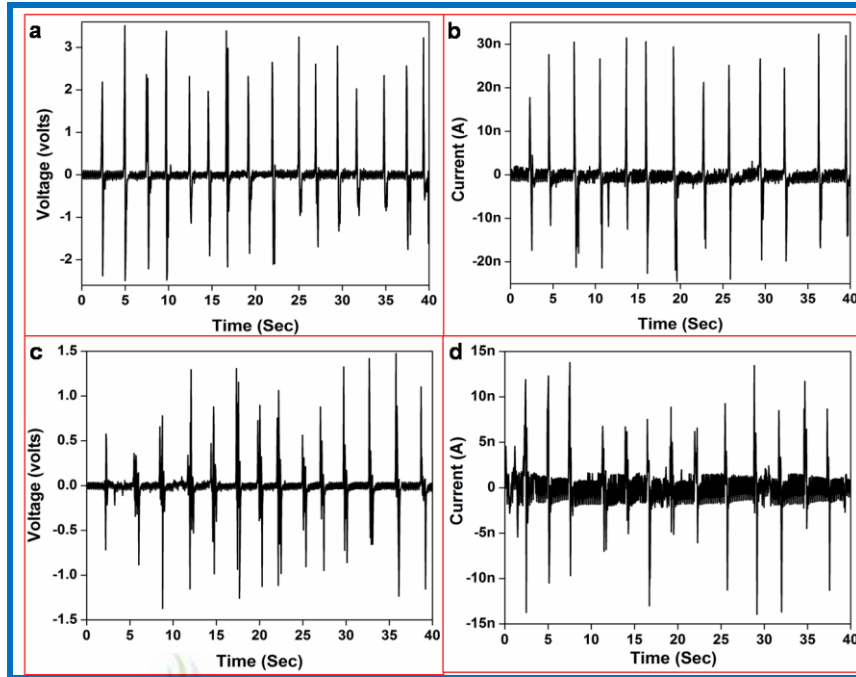


Fig.3.17. Electrical measurements of the nanogenerator device, a) open circuit voltage, and b) short circuit current of the PDMS device during the multiple folding and releasing of nanogenerator by fingers, c) Open circuit voltage, and d) short circuit current of the PET device during the multiple folding and releasing of nanogenerator by fingers.

In case strain applied by pressing, the top side ZnO NW @ Au substrate applies compressive stress to the uncoated ZnO NW substrate. At the same time bottom nanowire array felt compressive stress from downside electrode. The applied compressive stress produces tensile strain along the ZnO growth direction and generates the piezo-potential gradient from root to top of the nanowire. The same potential gradient was generated in top and bottom side of the substrate. This potential difference derives the transient flow of inductance charges [19]. The presence of PDMS in the device increases the inductance charge due to triboelectric effect. We checked the contribution of the triboelectric effect of our device by making a separate device made by PDMS film and PET substrate separately with the

same device area. This device generated low electrical power output compared to nanogenerator made by ZnO NW. The measured voltage and current was shown in Fig.3.17. From these results we confirmed that the generated voltage is combined effect of the piezoelectric from ZnO NW and triboelectric effect of PDMS and PET substrate. At this point, ZnO nanowire playing dual role to generating piezo-potential as well as templates for desired shape to PDMS [22]. In our device, PDMS plays an important to produce the triboelectric effect and also act as a dielectric between two ZnO NWs as well as it passivate the ZnO NW surface.

The human body contains enormous quantities of energy in the form of heat, fat, kinetic energy from physical movement. This creates interest to exploit this enormous power in an effective way. The development of low power devices opens this possibility to use human as a self-powered system to power up the wearable electronic devices. Here, we demonstrate the energy harvesting from human body movement by converting biomechanical energy to electrical energy using ZnO NW nanogenerator. The body movements like folding, pressing and stretching of finger were effectively utilized for generating strain on the nanogenerator. We have measured the output power generated by the nanogenerator with periodic bending and unbending conditions. The performance of the fabricated nanogenerator device (active area $1.4 \times 4.4 \text{ cm}^2$) was tested by fixing the device on above and down of the finger for energy harvesting from the movement of a finger. The Fig.3.18a represents the real time picture of bend created by periodic stretching and releasing of fingers and measured the open-circuit voltage (V_{oc}) and closed circuit current (I_{sc}).

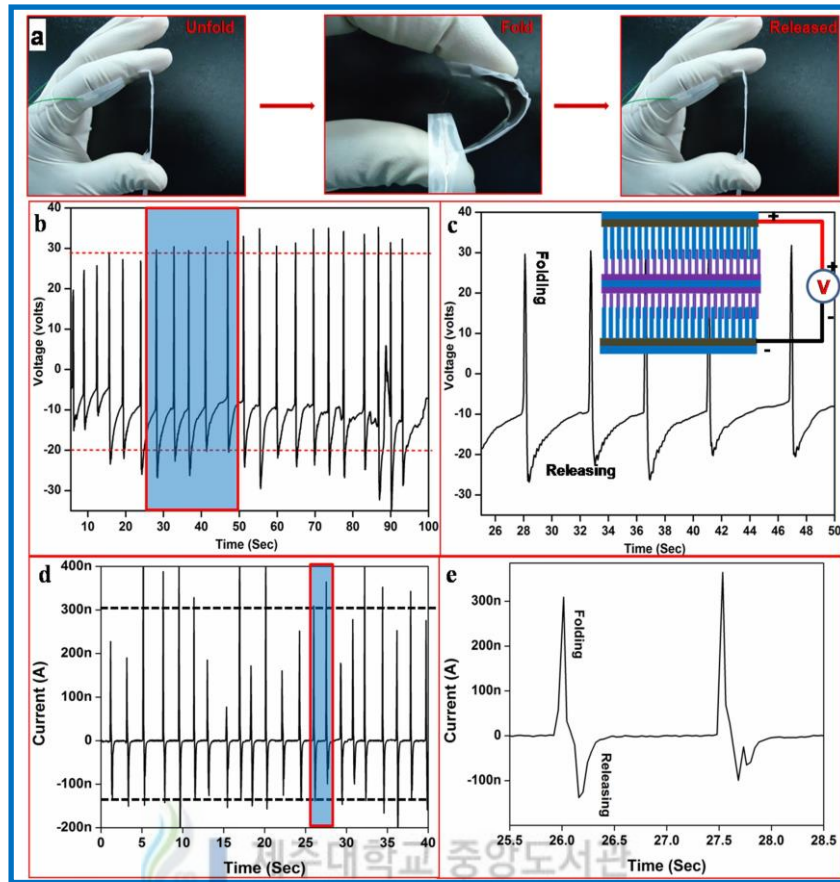


Fig.3.18. Electrical measurement of the nanogenerator device, a) digital image of nanogenerator device when folding and releasing using hand, b) open circuit voltage of the device the during multiple folding and releasing, and c) the enlarged view of the boxed area of voltage and schematic diagram of biased condition (inset), d) closed circuit current of the device during the multiple folding and releasing, and e) the enlarged view of the boxed area of current.

The generated voltage and current were shown in Fig.3.18 b, d and enlarged view of the voltage and current (Fig.3.18 b, d) for forward bias, which corresponds to the folding and unfolding state of the device. The origin of generating voltage and current was verified by conduct the polarity test (reverse bias) [23]. The result revealed that the generated voltage in forward bias condition is a positive voltage side. When change the polarity of the device, the voltage changes to the negative voltage side which confirms the generated voltage is only from the nanogenerator.

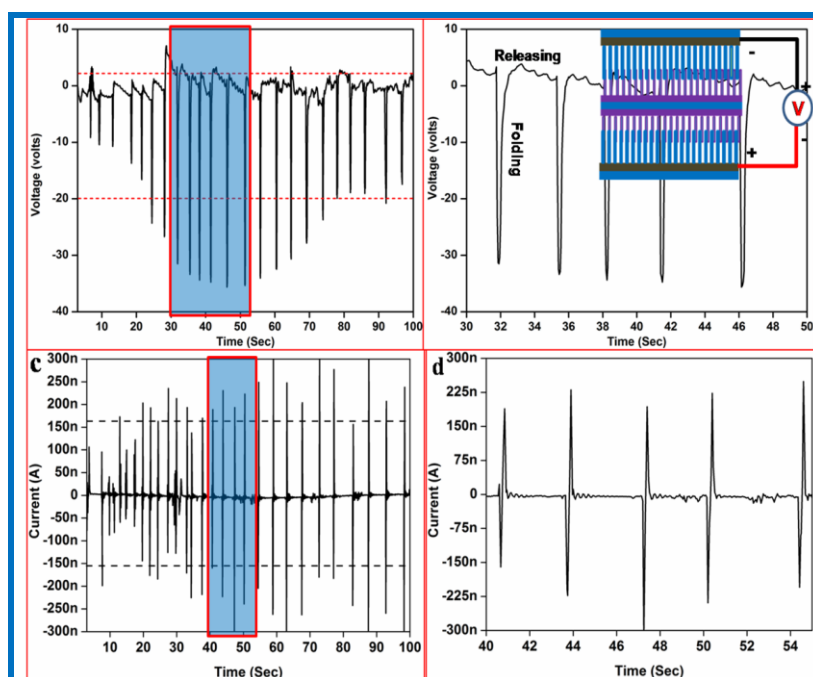


Fig.3.19. Electrical measurement of the nanogenerator device, a) digital image of nanogenerator device when folding and releasing using hand, b) open circuit voltage of the device the during multiple folding and releasing, and c) the enlarged view of the boxed area of voltage and schematic diagram of biased condition (inset), d) closed circuit current of the device during the multiple folding and releasing, and e) the enlarged view of the boxed area of current.

The average peak to peak at voltage and current were generated in nanogenerator when folding the finger was 30 V to – 20 V and 300 nA to - 150 nA (average current density 48.70 nA/cm²) in forward bias. Peak to peak at voltage and current in the reverse biased condition was 2 V to – 20 V and - 150 nA to 150 nA, which is opposite polarity with reduced voltage (Fig.3.19). The output power densities of the nanogenerator in forward and reverse bias are 0.390 and 0.130 mW/cm² respectively. Height of the voltage peak was different in folding and releasing condition, which is due to different strain rate [23-26]. The average peak current of the device was same, which confirms the similar amount of charge transferred at folding and releasing conditions [26]. The non-symmetric behavior observed in voltage and current before and after switching the polarity because of

non-uniform strain rate was experienced in nanogenerator device when folding and releasing the device [27].

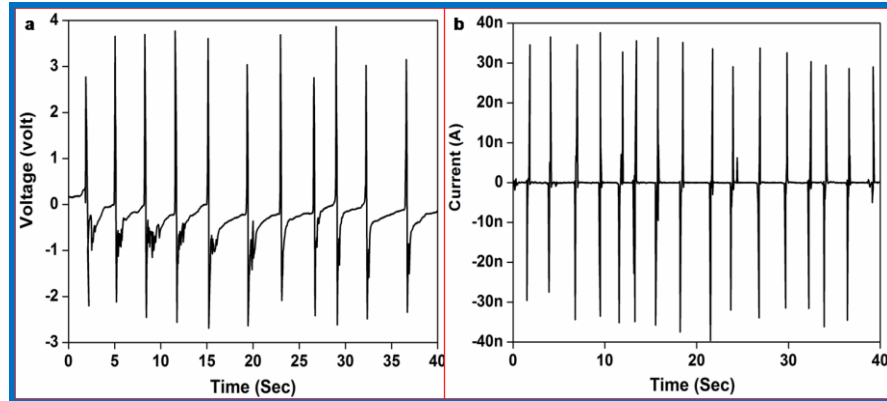


Fig.3.20. Electrical measurement of the nanogenerator device with flat electrode, a) open circuit voltage, and b) short circuit current during the multiple folding and releasing of nanogenerator.

We compared our device performance with normal flat electrode nanogenerator and Au coated nanowire nanogenerator without PDMS. The performance of this device increased nearly 10 times higher than conventional flat electrode as well as ZnO NW @ Au electrode. This dramatic increase in the device efficiency is attributed due to the combined piezo and triboelectric effects of ZnO NWs and PDMS respectively. The results are shown in Figs.3.20 and 3.21.

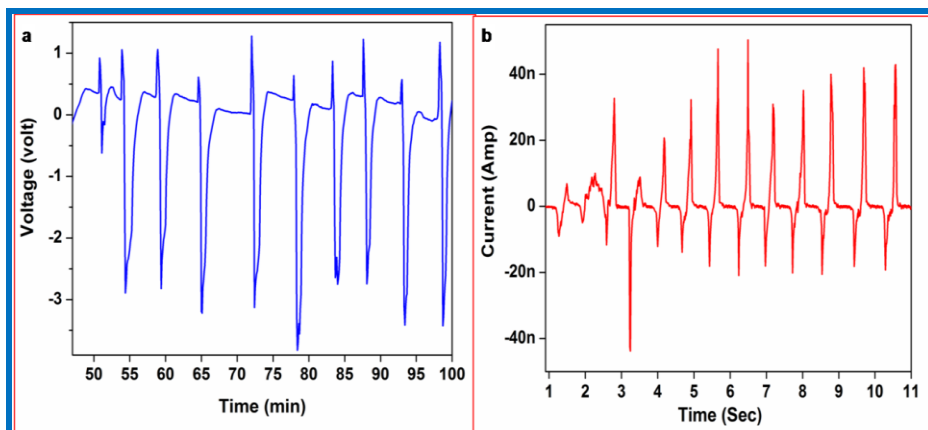


Fig.3.21. Electrical measurement of the nanogenerator device with Au coated ZnO nanowire electrode without PDMS, a) open circuit voltage and, b) short circuit current during the multiple folding and releasing of nanogenerator.

The main aim of this work scavenges the energy from human body movement. So we tested the performance of our device for practical application using the stress generated by finger movement. Here, we fixed our device in two different places of the finger. First, we fixed the device down of index finger, and we tested the performance of the device when twisting the finger. The nanogenerator device was firmly attached to the finger using scotch tape, so that the device could experience enough strain when twisting the finger. The Fig.3.22a shows the optical image of the nanogenerator in the stretched and un-stretched (released) state. The average voltage and current generated by twisting of index finger is 5 V to -1 V and 2 nA to -1.8 nA (average current density 0.325 nA/cm^2) with an output power density of 9.492 nW/cm^2 . The generated output voltage is higher than previously reported values for other device structures [28, 29]. The generated voltage and current are shown in Fig.3.22b and d and enlarged view of the voltage and current (Fig.3.22 b and d) which corresponds to the stretching and relaxed state of the index finger.

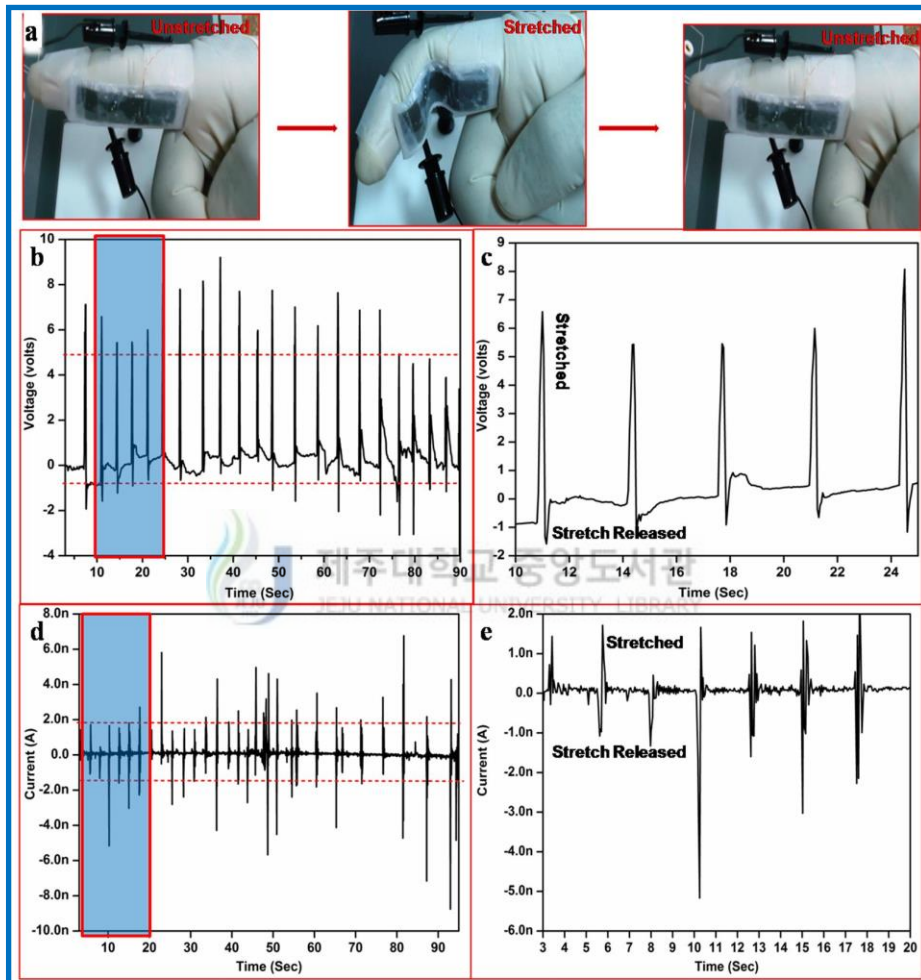


Fig.3.22. Electrical measurement of the nanogenerator device, a) digital image of nanogenerator device when stretching and releasing of finger, b) open circuit voltage of the device during the multiple stretching and releasing, and c) the enlarged view of the boxed area of voltage, d) closed circuit current of the device during the multiple stretching and releasing, and e) the enlarged view of the boxed area of current.

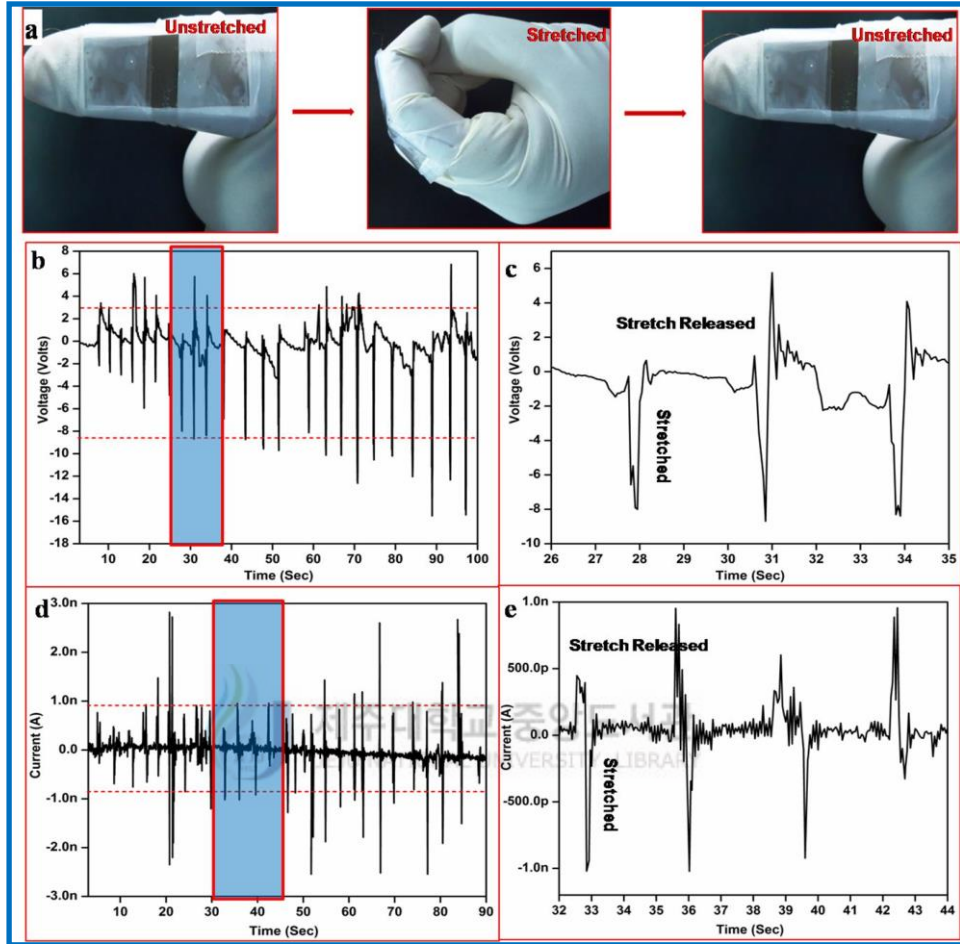


Fig.3.23. Electrical measurements of the nanogenerator device, a) digital image of nanogenerator device when stretching and releasing of finger, b) open circuit voltage of the device the during multiple stretching and releasing, and c) the enlarged view of the boxed area of voltage, d) closed circuit current of the device during the multiple stretching and releasing, and e) the enlarged view of the boxed area of current.

In the second measurement, we fixed the device on top of the index finger as shown in Fig.3.23a. The performance of the device is shown in Fig.3.23 b and d with an enlarged view in Fig.3.23 c and e. The measured voltage and current value of the device when folding and unfolding condition was 2.5 V to - 8.5 V and - 1 nA to 1 nA (current density 0.146 nA/cm²) with power density of 8.19 nW/cm².

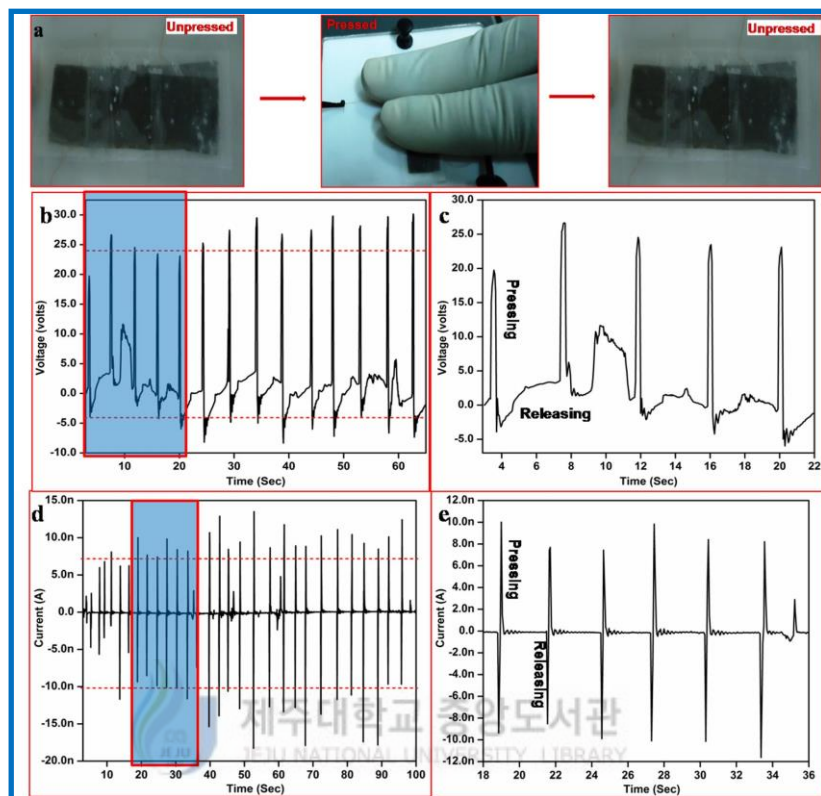


Fig.3.24. Electrical measurements of the nanogenerator device, a) optical image of nanogenerator device when pressing and releasing, b) open circuit voltage of the device during the multiple pressing and releasing, and c) the enlarged view of the boxed area of voltage, d) closed circuit current of the device during the multiple pressing and releasing, and e) the enlarged view of the boxed area of current.

Finally, we tested the fabricated nanogenerator device by pressing with two fingers, as shown in Fig.3.24a. The average voltage and current generated through compressive stress applied by pressing the fingers on the nanogenerator is shown in Fig.3.24 b and d and enlarged view of the same is shown in Fig.3.24 c and e. The measured output voltage and current is 24 V to – 4.5 V and 7.5 nA to – 10 nA (current density 1.22 nA/cm²) with an output power density of 0.115 μW/cm² respectively.

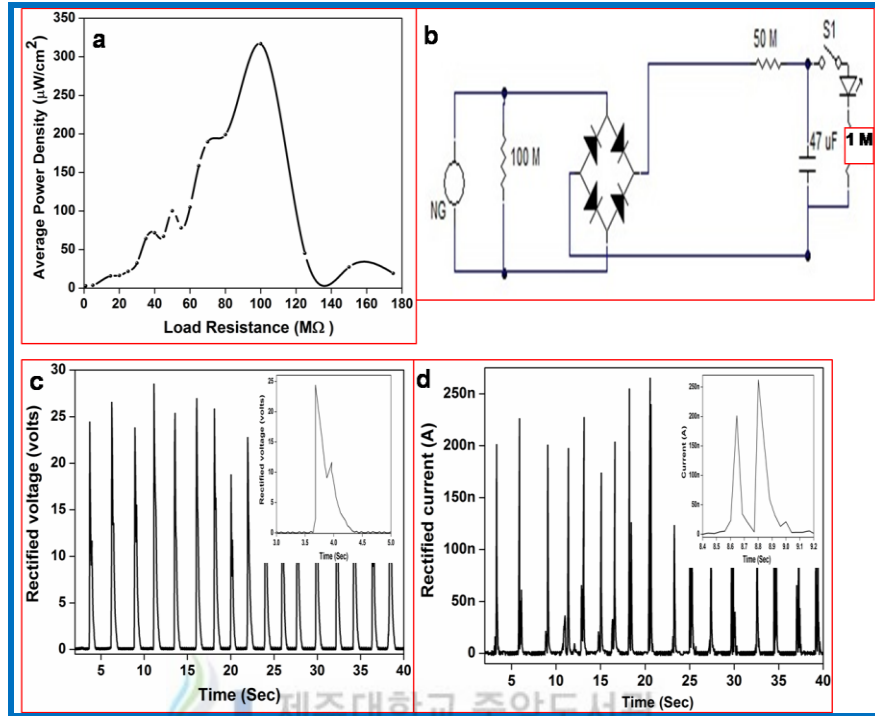


Fig.3.25. a) The output power of the nanogenerator with various load resistances. b) Schematic diagram of full wave bridge rectifier circuit. c) Open circuit voltage of the nanogenerator rectified by a bridge rectifier and enlarged view of one cycle (inset) during the multiple folding and releasing by fingers. d) Short circuit current of the nanogenerator rectified by a bridge rectifier and enlarged view of one cycle (inset) during the multiple folding and releasing by fingers.

To derive the electronic device using nanogenerator or other power source, the load resistance was important this must match with electronic device load resistance. We have measured the output power of the nanogenerator with different load resistances. The results clearly indicating that when increasing the load resistance from 1 M to 100 M Ω output voltage and current was increased and further increase reduce the voltage and current. The maximum output power was attained at 100 M ohm which is 0.317 mW/cm^2 (Fig.3.25a). To utilize entire electrical energy generated in nanogenerator for one cycle of mechanical deformation by using full

wave rectifier circuit, which rectify both positive and negative voltage and current generated by folding and unfolding. The rectified voltage and current of 25 V and 200 nA respectively was shown in Fig.3.25 c, d, which validates the full wave rectification of the input signal. The inset figures indicate the one complete cycle of mechanical deformation created by folding and unfolding.

To demonstrate the practical application of nanogenerator, it is necessary to store the generated power in external device like a capacitor, supercapacitor or battery. Here, we stored generated voltage in a capacitor and used to drive the commercial LED. The output energy was stored in commercial capacitor with the help of a bridge rectifier circuit, which is shown in Fig.3.25 b. The charging and discharging of capacitor through nanogenerator output was shown in Fig.3.26 a. The capacitor can be charged to 1.6 V by continuous stretching of nanogenerator for 710 s, which is enough for deriving commercial LED (Fig.3.26 c). The enlarged view of charging curve showed discrete steps with increment voltage of 2 mV which is shown in Fig.3.26 b. The inset Fig.3.26 b indicating the time taken to store 2 mV in the capacitor (453 ms), which is one complete cycle of the nanogenerator (folding & unfolding). The present idea of integrating ZnO nanogenerator improved the performance of the nanogenerator device compared to conventional flat electrode. In future the performance of the device will be increase by improving the charge extraction and transport efficiency.

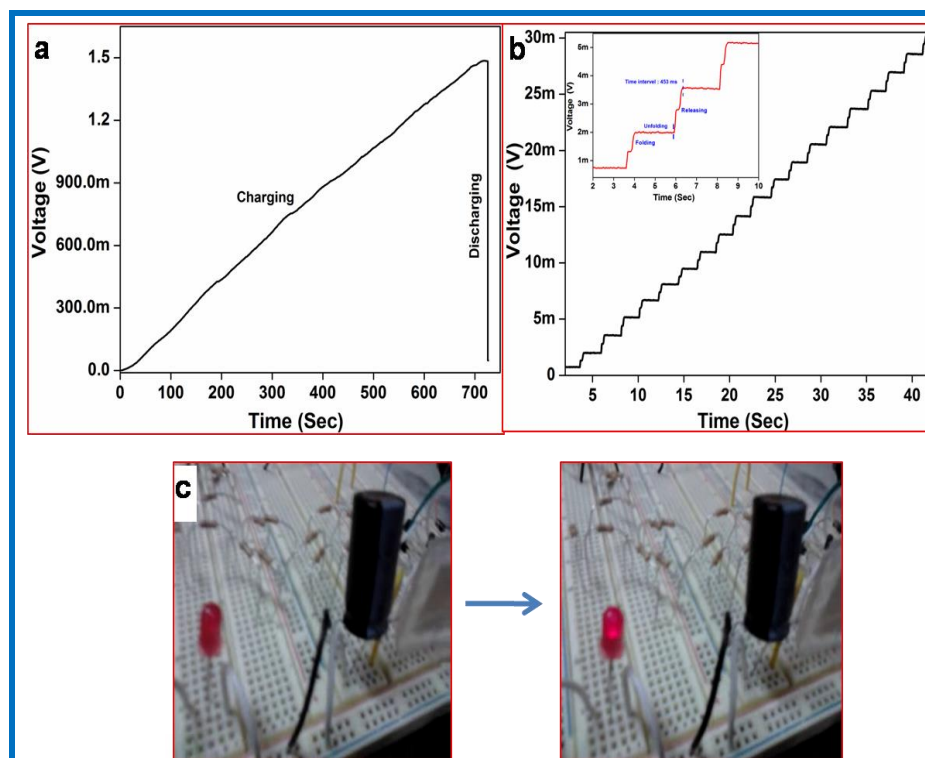


Fig.3.26. a) Voltage across the single capacitor during the multiple folding and releasing of nanogenerator by fingers, and b) enlarged portion of the charging curve and extended view of the charging curve for one cycle of folding and releasing of nanogenerator by fingers (inset). c) Snapshot of the LED before and after lighting up using the stored energy.

3.4. Conclusion

In this chapter, a detail discussed about the growth of aligned ZnO nanowire array over the various substrates and experimental conditions. The detailed growth of aligned nanowire array on one side double side of flexible substrate is discussed. Finally, this chapter concluding the optimum condition for aligned nanowire growing on flexible substrate was seed layer solution concentration of 1 M with hydrothermal reaction solution concentration of 50 mM (zinc nitrate & HMTA) at 95°C for 6 h. The secondly, this chapter described the fabrication and measurement of nanowire array based nanogenerator.

Finally, the novel device structure consists of four layers of the vertically aligned crystalline ZnO nanowire array. The vertically aligned ZnO nanowires on the flexible substrate were grown through hydrothermal method. The ZnO nanowire array grown on the both sides (top and bottom) of the PET substrates were sandwiched between two gold coated ZnO nanowire electrodes. This novel device was working in both piezoelectric and triboelectric effect. The fabricated device successfully applied for biomechanical energy harvesting from human body activities like folding, stretching, and pressing. It showed good performance against applied activities.



Reference

- [1] U. Ozgur, Y. I. Alivov, C. Liu, A. Teke, M.A. Reshchikov, S. Dogan, V. Avrutin, S.J. Cho, H.A. Morkoc, Comprehensive Review of ZnO Materials and Devices. *J. Appl. Phys.* 98 (2005), 041301.
- [2] D.C. Look, Recent Advances in ZnO Materials and Devices. *Mat. Sci. Eng. B-Adv.* 80 (2001), 383–387.
- [3] M.H. Huang, S. Mao, H. Feick, H.Q. Yan, Y.Y. Wu, H. Kind, E. Weber, R. Russo, P.D. Yang, Room-temperature Ultraviolet Nanowire Nanolasers. *Science* 292 (2001), 1897–1899.
- [4] W. I. Park, G. C. Yi, Electroluminescence in n-ZnO Nanorod Arrays Vertically Grown on p-GaN. *Adv. Mater.* 16 (2004), 87–90.
- [5] M. Law, L. E. Greene, J. C. Johnson, R. Saykally, P. D. Yang, Nanowire Dye-Sensitized Solar Cells. *Nat. Mater.* 4 (2005), 455–459.
- [6] C. Soci, A. Zhang, B. Xiang, S.A. Dayeh, D P.R. Aplin, J. Park, X.Y. Bao, Y. H. Lo, D. Wang, ZnO Nanowire UV Photodetectors with High Internal Gain, *Nano Lett.* 7 (2007), 1003–1009.
- [7] Z.L. Wang, J.H. Song, Piezoelectric Nanogenerators Based on Zinc Oxide Nanowire Arrays. *Science* 312 (2006), 242–246.
- [8] Z.L. Wang, The New Field of Nanopiezotronics. *Mater. Today* 10 (2007), 20–28.
- [9] Z.W. Pan, Z.R. Dai, Z.L. Wang, Nanobelts of Semiconducting Oxides. *Science* 291 (2001), 1947–1949.

- [10] W.I. Park, G.C. Yi, M.Y. Kim, S.J. Pennycook, ZnO Nanoneedles Grown Vertically on Si Substrates by Non-catalytic Vapor-Phase Epitaxy. *Adv. Mater.* 14 (2002), 1841–1843.
- [11] H. Yuan, Y. Zhang, Preparation of Well-aligned ZnO Whiskers on Glass Substrate by Atmospheric MOCVD. *J. Cryst. Growth* 263 (2004), 119–124.
- [12] Y.W. Heo, V. Varadarajan, M. Kaufman, K. Kim, D.P. Norton, F. Ren, P.H. Fleming, Site-specific Growth of ZnO Nanorods Using Catalysis-Driven Molecular-Beam Epitaxy. *Appl. Phys. Lett.* 81 (2002), 3046–3048.
- [13] S.Y. Bae, H.W. Seo, J. Park, Vertically Aligned Sulfur-Doped ZnO Nanowires Synthesized via Chemical Vapor Deposition, *J. Phys. Chem. B*, 108 (2004), 5206–5210.
- [14] Y. Sun, G.M. Fuge, M.N.R. Ashfold, Growth of Aligned ZnO Nanorod Arrays by Catalyst-free Pulsed Laser Deposition Methods. *Chem. Phys. Lett.* 396 (2004), 21–26.
- [15] S. Xu, Y. Wei, M. Kirkham, J. Liu, W. Mai, D. Davidovic, R.L. Snyder, Z.L. Wang, Patterned Growth of Vertically Aligned ZnO Nanowire Arrays on Inorganic Substrates at Low Temperature without Catalyst. *J. Am. Chem. Soc.* 130 (2008), 14958–14959.
- [16] O. Lupan, T. Pauporté, L. Chow, B. Viana, F. Pellé, L.K. Ono, B. Roldan Cuenya, H. Heinrich, Effects of Annealing on Properties of ZnO Thin Films Prepared by Electrochemical Deposition in Chloride Medium, *Appl. Surf. Sci.* 256 (2010), 1895- 1907.
- [17] S. Xu, Z.L. Wang, One-Dimensional ZnO Nanostructures: Solution Growth and Functional Properties. *Nano Res.* 4 (2011), 1013–1098.

- [18] J.H. Song, J. Zhou, Z.L. Wang, Piezoelectric and Semiconducting Coupled Power Generating Process of a Single ZnO Belt/Wire: A Technology for Harvesting Electricity from the Environment. *Nano Lett.* 6 (2006), 1656 - 1662.
- [19] F.R. Fan, L. Lin, G. Zhu, W. Wu, R. Zhang, Z.L. Wang, Transparent Triboelectric Nanogenerators and Self-Powered Pressure Sensors Based on Micropatterned Plastic Films. *Nano Lett.* 12 (2012), 3109–3114.
- [20] G. Mantini, Y. Gao, A. D'Amico, C. Falconi, Z.L. Wang, Equilibrium Piezoelectric Potential Distribution in a Deformed ZnO Nanowire. *Nano Res.* 2 (2009), 624–629.
- [21] Y. Hu, L. Lin, Y. Zhang, Z.L. Wang, Replacing a Battery by a Nanogenerator with 20 V Output. *Adv. Mater.* 24 (2012), 110–114.
- [22] G. Zhu, A.C. Wang, Y. Liu, Y. Zhou, Z.L. Wang, Functional Electrical Stimulation by Nanogenerator with 58 V Output Voltage. *Nano Lett.* 12 (2012), 3086–3090.
- [23] X.D. Wang, J. Liu, J.H. Song, Z.L. Wang, Integrated Nanogenerators in Biofluid. *Nano Lett.* 7 (2007), 2475–2479.
- [24] S. Xu, Y. Qing, C. Xu, Y.G. Wei, R.S. Yang, Z.L. Wang, Self-powered Nanowire Devices. *Nat.Nanotechnol.* 5 (2010), 366–373.
- [25] M. Lee, J. Bae, J. Lee, C.S. Lee, S. Hong, Z.L. Wang, Self-powered Environmental Sensor System Driven by Nanogenerators. *Energy Environ. Sci.* 4 (2011), 3359 - 3363.
- [26] R. Yang, Y. Qin, L. Dai, Z.L. Wang, Power Generation with Laterally Packaged Piezoelectric Fine Wires. *Nat. Nanotechnol.* 4 (2009), 34 – 39.

- [27] J.H. Jung, M. Lee, J.I. Hong, Y. Ding, C.Y. Chen, L.J. Chou, Z.L. Wang, Lead-Free NaNbO₃ Nanowires for a High Output Piezoelectric Nanogenerator. ACS Nano 5 (2011), 10041 – 10046.
- [28] R. Yang, Y. Qin, C. Li, G. Zhu, Z.L. Wang, Converting Biomechanical Energy into Electricity by a Muscle-Movement-Driven Nanogenerator. Nano Lett. 9 (2009), 1201 - 1205.
- [29] H. Kim, S.M. Kim, H. Son, H. Kim, B. Park, J.Y. Ku, J.I. Sohn, K. Im, J.E. Jang, J.J. Park, O. Kim, S.N. Chax, Y.J. Park, Enhancement of Piezoelectricity via Electrostatic Effects on a Textile Platform. Energy Environ. Sci. 5 (2012), 8932 - 8936.

CHAPTER - IV

ZnO Nanowall based nanogenerator

In this chapter describes about a novel and facile way to grow the vertically aligned ZnO nanowall on both sides of the flexible substrate through low temperature, cost-effective hydrothermal method and their application toward energy harvesting application. The fabricated nanogenerator device structure consists of a ZnO nanowall structure on the both sides of the flexible substrates covered with poly(methyl methacrylate), and gold (Au) coating on both sides acts as an electrode. The fabricated nanowall nanogenerator produces the maximum output voltage and current of 2.5 V and 80 nA respectively, with maximum power output of $0.2 \mu\text{W}\cdot\text{cm}^{-2}$, when folding the device through the finger. Furthermore, we have studied the performance of the nanogenerator device with different load resistance. The voltage and current were linearly varied with the load resistance. The maximum power output ($37.7 \text{ nW}\cdot\text{cm}^{-2}$) was measured at load resistance of $75 \text{ M}\Omega$. The fabricated device showed the capability by driving a commercial green LED and LCD with the help of the capacitor.

4.1. Introduction

ZnO is a promising material for this application [1, 2] because it is easy to grow and control its shape in all substrates and is nontoxic and abundant in nature. Recently, much attention has been paid to growing low dimensional ZnO nanostructures, including 1D nanostructure such as nanowires, nanobelts, nanorods, and nanotubes as well as 0D nanostructures such as quantum dots due to their enhanced electronic, optical, and mechanical properties. When compared with 0D and 1D nanostructures, fewer reports came in the growth and application of 2D nanostructures such as nanowalls and nanosheets. Many methods have been used to grow nanowall structures on different substrates, such as metal organic chemical vapor deposition (MOCVD), pulsed vapor laser deposition (PLD), vapor-liquid-solid (VLS) method, molecular-beam epitaxy (MBE), thermal evaporation method on glass, and sapphire substrate [3-5]. Kim et al. reported the growth of ZnO nanowall network on GaN/c-Al₂O₃ substrates by Au catalyst-assisted epitaxial method. The grown ZnO nanowall network was used for hydrogen-sensing application [3]. Kumar et al. reported the growth of ZnO nanowall and nanowire structure on graphene-coated c-plane Al₂O₃ substrates through thermal CVD method, and they studied the interfacing property of graphene and ZnO nanostructure. Furthermore, they fabricated ZnO NG using ZnO nanowall and nanowire structure with graphene electrode [6]. Recently, Kim et al. reported the DC power generation using ZnO nanosheets and anionic heterojunction, and Gupta et al. also reported the DC power generation using vanadium-doped ZnO nanosheets [7].

To the best of our knowledge, it is the first report on the growth of ZnO nanowall structure of flexible substrate on both sides using the low-temperature hydrothermal method as well as the fabrication of the NG using this structure. Inspired by their pioneer work, we have developed a low temperature method to grow ZnO nanowall structure on both sides of the flexible substrate for energy harvesting application.

4.2. Experimental Section

4.2.1. Fabrication of Seed Layer

The ZnO seed layer was fabricated on the flexible substrate by a spin-coating method using seed solution. The seed solution was prepared as follows: 0.5 M of zinc nitrate hexahydrate was dissolved in deionized (DI) water; then, 3 M NaOH solution was added drop wise to that solution under vigorous stirring, and it started to precipitate. The precipitate was centrifuged repeatedly by three times to remove the Na^+ and NO_3^- from the sample. Finally, zinc hydroxide was redispersed in ammonia/water (1:0.2 v/v) mixture under bath sonicator for 20 min. The final zinc ammonia complex ($\text{Zn}(\text{NH}_3)_4^{2+}$) solution was used as a seed solution. The as-prepared seed solution was spin-coated at 2000 rpm for 20 s on flexible substrate and dried at 100 °C for 10 min in a hot air oven. This process was repeated three times to get 100 nm thicknesses. The seed layer was coated for both sides of the flexible substrate using the same procedure.

4.2.2. Hydrothermal Growth of ZnO Nanowall

The hydrothermal growth solution was prepared with an equimolecular (100 mM) aqueous solution of zinc nitrate ($\text{Zn}(\text{NO}_3)_2 \cdot 6\text{H}_2\text{O}$) and hexamethylenetetramine (HMTA, $(\text{CH}_2)_6\text{N}_4$) and 15 mM of polyethylenimine (PEI) dissolved in 50 mL of DI water. The prepared growth solution was transferred to a 100 mL Teflon container,

and seed-layer-coated substrate was hung in Teflon container. Then, hydrothermal reaction was performed at 90°C for 8 h. Finally, the samples were rinsed with DI water to remove the residual present on the surface and then dried in air at 100 °C overnight.

4.2.3. Fabrication of Nanogenerator Device

After drying, 1µm thick poly(methyl methacrylate) (PMMA) layer was coated on both sides of the substrate using the spin-coating method. The top and down Au electrodes with thickness of 100 nm were coated on both sides of the substrate using a thermal evaporator. Finally, two Cu wires were connected to the top and a bottom electrode; then, the whole device was packed with poly (dimethylsiloxane) (PDMS). The electrical output of the NG was measured by the semiconductor parameter analyzer (Agilent, 1500 A) without any external voltage. The typical bending deformation was given through the finger. The photocurrent measurement was carried on a probe station attached with semiconductor parameter analyzer with the help of a Prizmatix multiwavelength LED light source with intensity of 8 mW ·cm⁻².

4.3. Results and discussion

The seed-mediated hydrothermal method was successfully utilized to grow the controlled and well-aligned ZnO nanowall structure on the flexible substrate. The XRD pattern was measured to identify the phase and orientation of as-grown ZnO nanowall, which is shown in Fig.4.1.

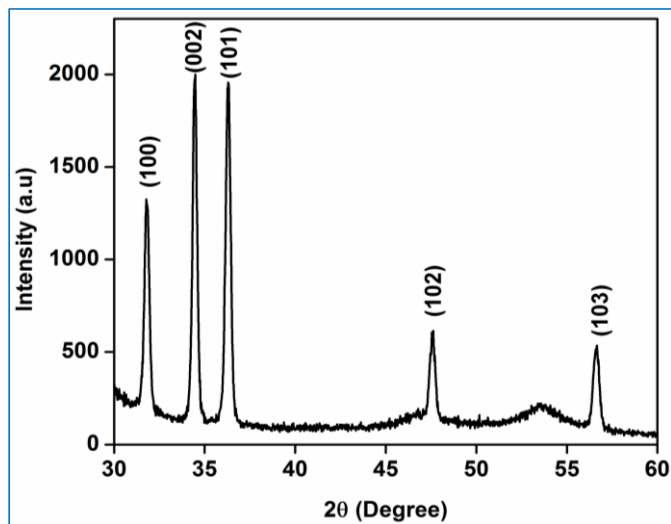


Fig.4.1. XRD pattern of ZnO nanowall on PET substrate.

From XRD pattern, all measured peaks are corresponding to the hexagonal wurtzite phase of ZnO, which is confirmed through the JCPDS file (89-1397) [8]. The higher intense diffraction peaks were found at (100), (002), and (101) planes, which indicate the in-plane and out-of-plane orientation of ZnO nanowall [9]. The prepared nanowall showed the preferred orientation along the c-axis orientation of (001) plane, and (100) orientation indicates the nanowall growth along the substrate. The (101) peak indicates that some of the c-axis-orientated nanowall is not perpendicular to the substrates that are bent (Fig.4.2a). In addition to strong peaks, other peaks were also observed at (102) and (103) planes, which are from the bent nanowall. The growth direction and morphology of the nanowall were imaged through FE-SEM and are shown in Fig.4.2.

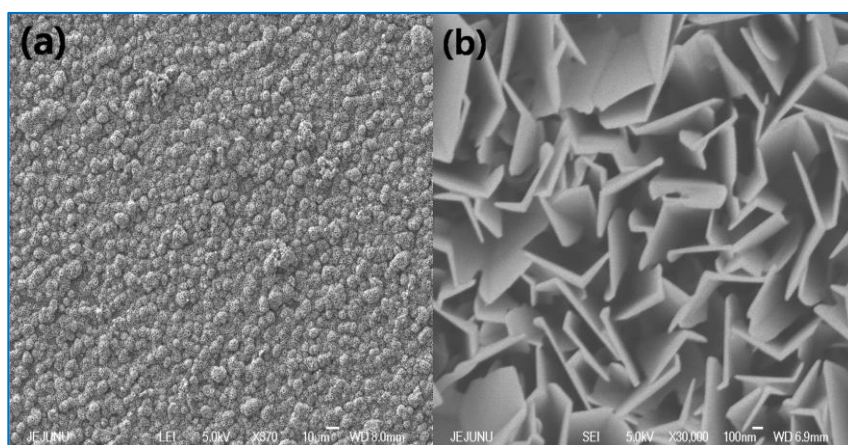


Fig.4.2. FE-SEM image of ZnO nanowall On PET substrate, a) lower (Scale bar: 10 μm), b) higher (Scale bar: 100 nm) magnification.

The typical FE-SEM image demonstrates that the ZnO nanowall structure was grown over the whole area of the substrate and grown perpendicular to the substrate, and a few of them are bent. The thickness (diameter) of 60–80 nm and the length of 2 to 3 μm is clearly seen from the magnified image (Fig.4.2b). The optical absorbance and transmittance spectrum of the ZnO nanowall on the flexible substrate was illustrated in Fig.4.3.

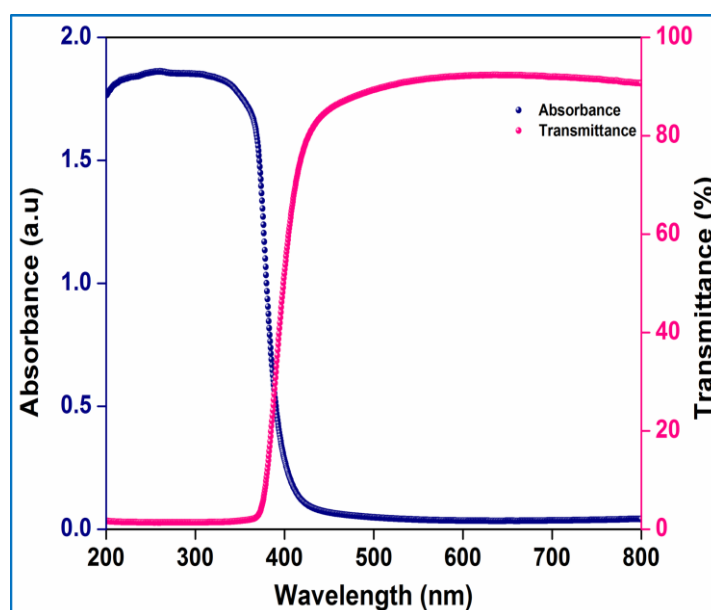


Fig.4.3. Optical absorbance and transmittance of the ZnO nanowall on both sides of flexible substrate

The grown nanowall film shows a high optical transmittance, ~92%, in the visible region that is due to the presence of oxygen vacancies in the nanowall [10]. The absorbance edge was observed at 389 nm, which corresponds to electron transfer from the valence band to the conduction band. The chemical compositions of ZnO nanowall film were investigated by XPS (Fig.4.4). The typical survey spectrum of ZnO nanowall film is shown in Fig.4.4a, which confirms the existence of Zn, O, and C, and there is no indication for the presence of impurity in the sample. The ZnO nanowall exhibits a double peak at 1023.4 and 1046.5 eV that corresponds to the Zn-2p level of p_{3/2} and p_{1/2}, respectively (Fig.4.4b) [10]. Fig.4.4c displays the asymmetric O 1s core spectrum deconvoluted with two peaks centered at 530.6 and 532.3 eV that correspond to the O₂⁻ ions in the wurtzite structure (O-Zn) and the presence of point defects or chemisorbed oxygen species [11].

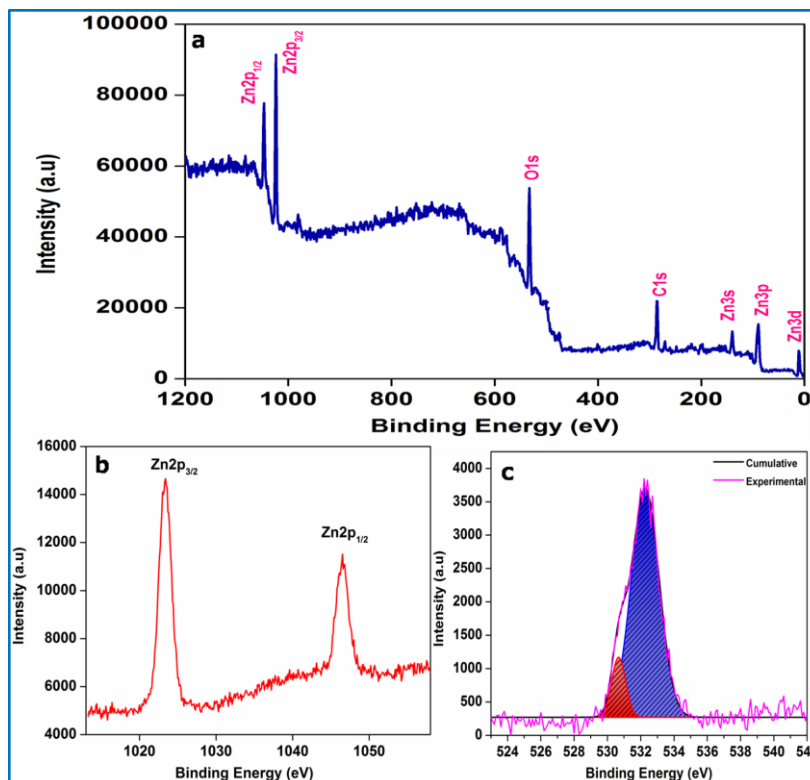


Fig.4.4. XPS spectrum of ZnO nanowall on flexible substrate, a) survey spectrum, b) Zn-2p, c) O-1s high resolution core level spectra.

The room-temperature PL spectrum of the as-grown ZnO nanowall is shown in Fig.4.5. The PL spectrum of as-grown ZnO nanowall exhibits several peaks covering the UV and visible regions. The UV emission arises due to the bound excitonic recombination, also referred to as near-band emission, which is observed at 389 nm [9]. In general, a broad visible emission, also referred to as defect level emission, was arisen due to the presence of defects such as oxygen vacancies, interstitial zinc, or zinc vacancies.

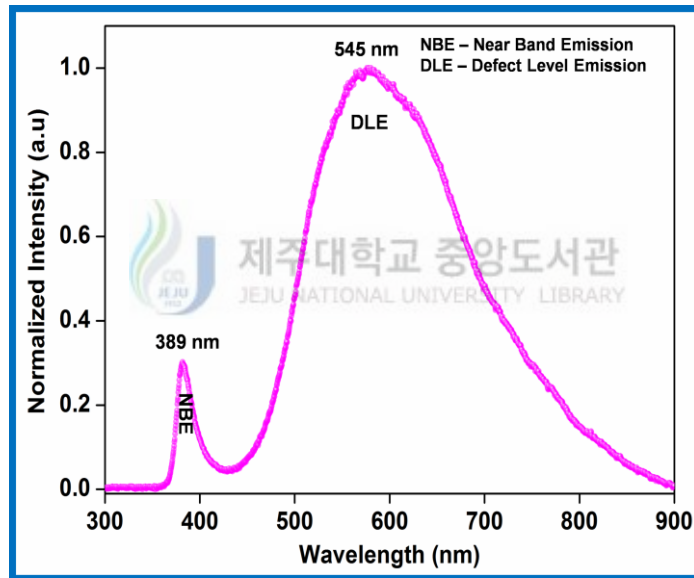


Fig.4.5. Room temperature photoluminescence spectra of ZnO nanowall

A broad visible emission observed at 540 nm belongs to the green emission, which arises due to recombination of photo generated hole with electrons generated from the oxygen vacancies like singly ionized oxygen, interstitial oxygen vacancies [9]. The intensity of the near-band emission was low when compared with defect emission because of the existence of higher interstitial oxygen vacancy, which is confirmed through XPS (Fig.4.4).

To verify the electrical property of the as-grown nanowall, we measured current–voltage (I–V) characteristics at dark and different illumination wavelength. The measured typical I–V characteristics showed the ohmic behavior at dark and illumination condition, which is shown in Fig.4.6.

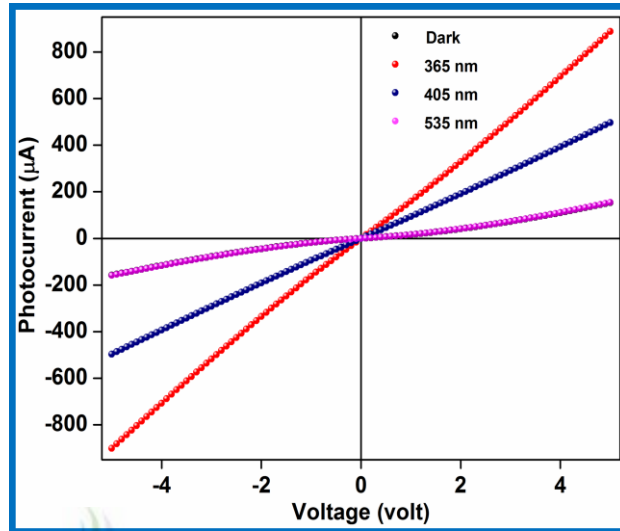


Fig.4.6. Electrical property of the ZnO nanowall under dark and under different illumination wavelength (365, 405, 535 nm)

The higher photocurrent response of 0.9 mA was observed under illumination wavelength of 365 nm when compared with dark, 535 nm (0.16 mA), and 405 nm (0.5 mA). The fabricated nanowall photo-detector showed the good response in 365 nm.

The NG was fabricated using the as-grown ZnO nanowalls. The active area of the fabricated NG was $1 \times 1 \text{ cm}^2$. The fabricated NG device consists of three layers, which are ZnO nanowall structure grown on the both sides of the flexible substrate and coated with PMMA layer. The top and bottom sides of the surface were coated with gold film for electrode. The electrical signal was generated in the NG measured under bending condition. The performance of the fabricated NG was tested under

periodic deformation through biomechanical movement of the human body by fingers.

The mechanism of the fabricated NG was explained through the piezoelectric effect of ZnO nanowall. When the NG was bending through the fingers, the ZnO nanowall layer felt tensile stress on the top and compressive stress on the bottom layer of the substrates. The tensile stress on the top of the substrate produced the compressive strain along the (002) plane of the nanowall, which created the piezo-potential distribution along the nanowall surface. At the same time, the bottom of the substrate underwent compressive stress, which generated the tensile strain along the nanowall growth direction (c axis). Tensile and compressive strain generated the piezo-potential distribution along the nanowall surface. The maximum piezo-potential was observed at the top of the nanowalls at both sides of the substrate. The generated piezo-potential distribution induces the charges on both sides of the electrode, which will derive the electron in the external load. The total potential of the device is the sum of the top and bottom sides of the substrate [12-14].

The generated output voltage and the closed-circuit current output of the fabricated NG device are shown in Fig. 4.7a, b. The measured peak voltage and current of the device were 2.5 V and 80 nA, respectively. The maximum output power of the NG is $0.2 \mu\text{W}\cdot\text{cm}^{-2}$. The enlarged view of the current and voltage peaks is shown in Fig.4.7c, d. The height of the voltage and current peaks is not uniform because of the different strain rate experienced by NG [12]. The fabricated device showed higher performance than previous reports [4].

The performance of the NG was directly related to load resistance of the external device. Here we tested the performance of the NG with different load

resistance, which is shown in Fig.4.8a. The output voltage and current of the NG were linearly varied with respect to the load resistance. The current was decreased with increasing load resistance, and at the same time voltage increased with increasing the load resistance [15]. The maximum output current density of the NG was observed at 150Ω , which is $73 \text{ nA} \cdot \text{cm}^{-2}$. The maximum output voltage of 2.1 V was observed at $125 \text{ M}\Omega$. The output power of the NG was linearly increased until $37.7 \text{ nW} \cdot \text{cm}^{-2}$ and decreased with increasing load resistance, which is shown in Fig.4.8b. The maximum output was observed at $75 \text{ M}\Omega$, which is $\sim 37.7 \text{ nW} \cdot \text{cm}^{-2}$. On the basis of the results, this device structure has potential in the real-world application like smart and wearable electronics.

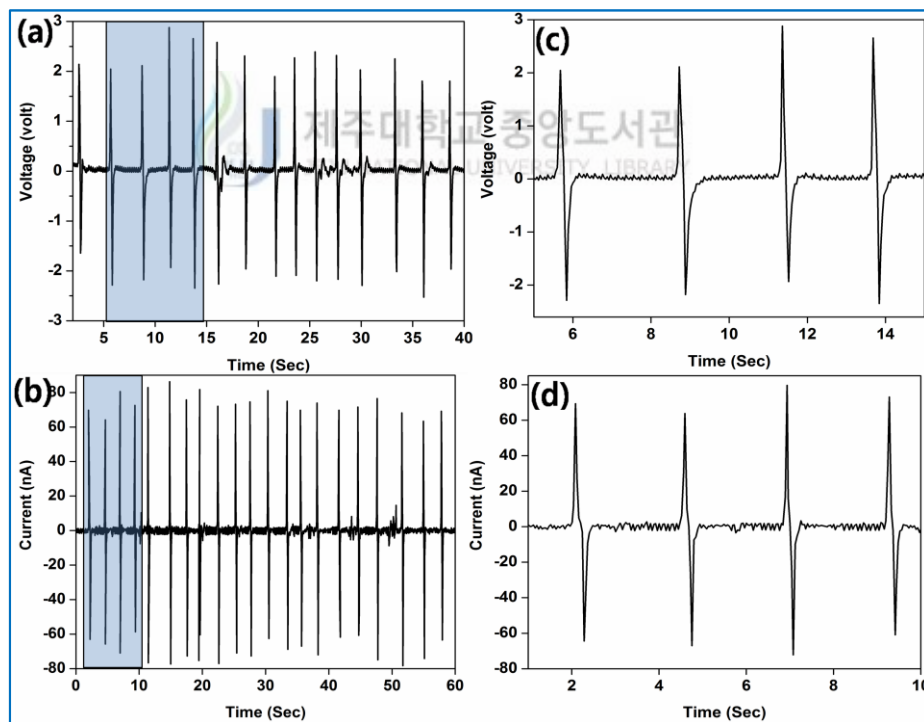


Fig.4.7. Electrical characteristics of nanowall based nanogenerator. a) Open-circuit output voltage of a nanogenerator, c) enlarged view of the marked output voltage. b) Closed- circuit output current, d) enlarged view of the marked output current.

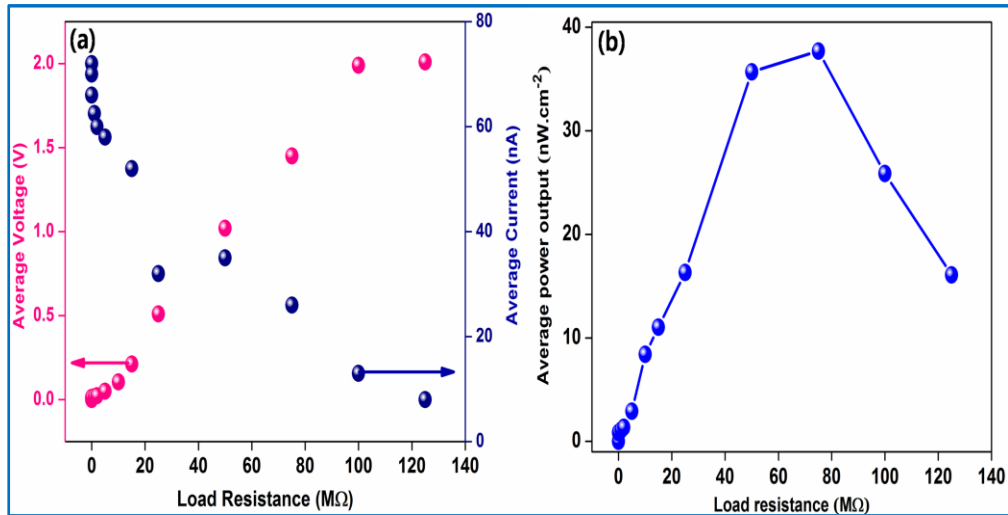


Fig.4.8. a) The voltage and current Vs external load resistance, b) power output Vs external load resistance.



To demonstrate the capability of NG, we have constructed the rectifier circuit (Fig.4.9a) with a capacitor and resistors for converting the AC signal into DC and stored the rectified electrical signals. The rectified voltage and current are shown in Fig.4.9b, c, which are ~ 1.8 V and 85 nA, respectively. The generated voltage was stored in the capacitor by close S1 key and open S2 until it reached an optimum voltage. After a multiple deformation cycle, the stored energy reached a maximum; S2 key was closed and S1 was opened, and this energy was used to light up a commercial green LED (3BG4UC00). The generated power is more than the threshold power of a commercial LCD (Penguin LCD) display, which is enough to operate the LCD display.

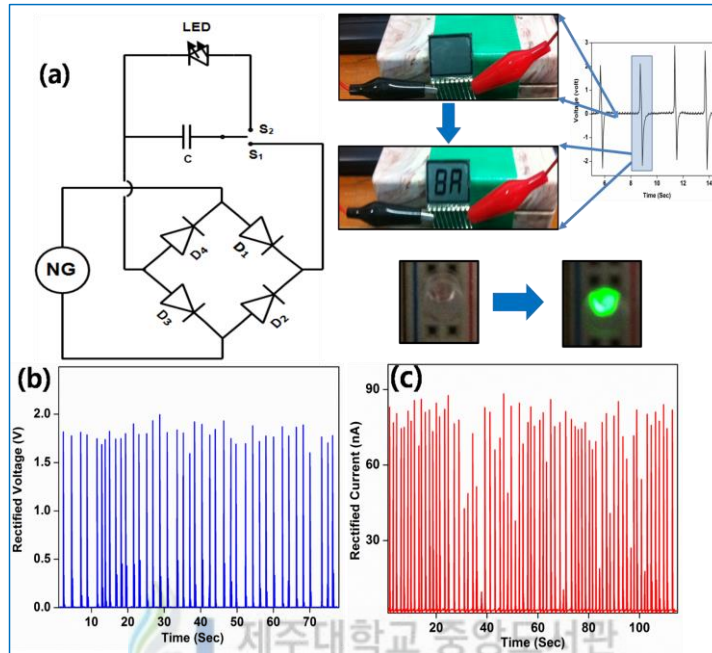


Fig.4.9. a) Circuit diagram of full wave bridge rectifier circuit. b) Rectified voltage. c) Rectified current. Top of the right corner indicates the snapshots of a driving LCD display and light up a commercial green LED.

The LCD display is a non-polar device that can operate under AC power, so we directly connected to this device with NG in parallel without any external circuit. The connected display was blinking at each deformation cycle, which is shown in Fig.4.9.

4.4. Conclusion

We have successfully grown vertically aligned ZnO nanowall structure on flexible substrate using facile low temperature hydrothermal method. The (002) orientation of the nanowall was confirmed through the X-ray diffraction pattern. The length and wall thickness of the nanowall was around 2 to 3 μm and 60–80 nm, respectively. The grown ZnO nanowall film showed better responses to UV light. The fabricated nanowall NG generated the maximum voltage and current of 2.5 V and 80 nA, respectively. Finally, we have constructed a bridge rectifier to store the harvested energy in the capacitor and to use to light up a commercial green LED. The energy harvested from NG was applied directly to drive the commercial LCD display without rectification and storage. The fabricated NG device has potential in smart and wearable electronic applications.



References

- [1] Z. Li, Z.L. Wang, Air/Liquid-Pressure and Heartbeat-Driven Flexible Fiber Nanogenerators as Micro/Nano-Power Source or Diagnostic Sensors. *Adv. Mater.* 23 (2011), 84–89.
- [2] H.K. Park, K.Y. Lee, J.S. Seo, J.A. Jeong, H.K. Kim, D. Choi, S.W. Kim, Charge-Generating Mode Control in High-Performance Transparent Flexible Piezoelectric Nanogenerators. *Adv. Funct. Mater.* 21 (2011), 1187–1193.
- [3] S.W. Kim, H.K. Park, M.S. Yi, N.M. Park, J.H. Park, S.H. Kim, S.L. Maeng, C.J. Choi, S.E. Moon, Epitaxial growth of ZnO nanowall networks on GaN/sapphire substrates. *Appl. Phys. Lett.* 90 (2007), 033107.
- [4] B. Kumar, K.Y. Lee, H.K. Park, S.J. Chae, Y.H. Lee, S.W. Kim, Controlled Growth of Semiconducting Nanowire, Nanowall, and Hybrid Nanostructures on Graphene for Piezoelectric Nanogenerators. *ACS Nano* 5 (2011), 4197-4204.
- [5] T.P. Chen, S.P. Chang, F.Y. Hung, S.J. Chang, Z.S. Hu, K.J. Chen, Simple Fabrication Process for 2D ZnO Nanowalls and Their Potential Application as a Methane Sensor. *Sensors* 13 (2013), 3941-3950.
- [6] K.H. Kim, B. Kumar, K.Y. Lee, H.K. Park, J.H. Lee, H.H. Lee, H. Jun, D. Lee, S.W. Kim, Piezoelectric Two-dimensional Nanosheets/anionic Layer Heterojunction for Efficient Direct Current Power Generation. *Sci. Rep.* 3 (2013), 2017.
- [7] M.K. Gupta, J.H. Lee, K.Y. Lee, S.W. Kim, Two-Dimensional Vanadium-Doped ZnO Nanosheet-Based Flexible Direct Current Nanogenerator. *ACS Nano* 7 (2013), 8932–8939.

- [8] B. Saravanakumar, R. Mohan, K. Thiyagarajan, S.J. Kim, Investigation of UV Photoresponse Property of Al, N Co-doped ZnO Film. *J. Alloys Compd.* 580 (2013), 538-543.
- [9] B.Q. Cao, T. Matsumoto, M. Matsumoto, M. Higashihata, D. Nakamura, T. Okada, ZnO Nanowalls Grown with High-Pressure PLD and Their Applications as Field Emitters and UV Detectors. *J. Phys. Chem. C* 113 (2009), 10975 – 10980.
- [10] A.A. Mosquera, D. Horwat, A. Rashkovskiy, A. Kovalev, P. Miska, D. Wainstein, J.M. Albella, J.L. Endrino, Exciton and Core-level Electron Confinement Effects in Transparent ZnO Thin Films. *Sci. Rep.* 3 (2013), 1714.
- [11] D. Deng, S.T. Martin, S. Ramanathan, Synthesis and Characterization of One-dimensional Flat ZnO Nanotower Arrays as High-efficiency Adsorbents for the Photocatalytic Remediation of Water Pollutants. *Nanoscale* 2 (2010), 2685–2691.
- [12] B. Saravanakumar, R. Mohan, K. Thiyagarajan, S.J. Kim, Fabrication of ZnO Nanogenerator for Eco-friendly Biomechanical Energy Harvesting. *RSC Adv.* 3 (2013), 16646-16656.
- [13] Y. Hu, Y. Zhang, C. Xu, L. Lin, R.L. Snyder, Z.L. Wang, Self-Powered System with Wireless Data Transmission. *Nano Lett.* 11 (2011), 2572–2577.
- [14] Y. Hu, C. Xu, Y. Zhang, L. Lin, R.L. Snyder, Z.L. Wang, A Nanogenerator for Energy Harvesting from a Rotating Tire and its Application as a Self-Powered Pressure/Speed Sensor. *Adv. Matter.* 23 (2011), 4068–4071.

- [15] S. Wang, L. Lin, Z.L. Wang, Nanoscale Triboelectric-Effect-Enabled Energy Conversion for Sustainably Powering Portable Electronics. *Nano Lett.* 12 (2012), 6339–6346.



CHAPTER – V

Organic- Inorganic Hybrid Composite Nanogenerator

In this chapter demonstrates the fabrication of hybrid composite nanogenerator using ZnO nanowire and piezoelectric polymer poly(vinylidene fluoride), through a simple, inexpensive solution-casting technique. The fabricated hybrid composite nanogenerator delivered a maximum open-circuit voltage of 6.9 V and a short-circuit current of 0.96 μA , with an output power of 6.624 μW under uniaxial compression, which was twofold higher than the values observed under bending conditions. This high-performance, electric poling free composite nanogenerator opens up the possibility of industrial-scale fabrication. The hybrid nanogenerator demonstrated its ability to drive five green LEDs simultaneously, without using an energy-storage device.

5.1. Introduction

The coexistence of semiconducting and piezoelectric properties in ZnO has germinated a new field of piezotronics, which take this material into further dimensions. Furthermore, it is utilized for harvesting the solar, thermal and mechanical energy in hybrid forms [1]. There are many reports on the fabrication of piezoelectric nanogenerator using vertical, laterally aligned ZnO micro/nanowires, nanotubes and micro/nanobelts using a variety of device tectonics [2]. However, the utility of these piezoelectric materials in this form is limited due to the brittleness and reduced strain levels, which limit large-scale fabrication. The first nanocomposite-based nanogenerator was proposed by Park et.al, [3] which overcomes the problem discussed earlier. However, the performance of this nanogenerator was not sufficient to self-drive the wearable electronic devices and sensors. Further explorations were required to improve the performance of the nanogenerator, which inspired us to design a flexible, paper-like, lightweight, large-scale nanogenerator that offered higher performance.

There have been several reports of composite nanogenerators based on polydimethylsiloxane (PDMS) and piezoelectric perovskites such as BaTiO₃, [4] PZT [5], NaNbO₃ [6], ZnSnO₃ nanostructures [7], and ZnO nanoparticles [8]. As of now, only a few reports are available for fabricating composite nanogenerators that use organic and which are small and have the potential for use inorganic piezoelectric materials [9]. The ferroelectric organic polymers, namely poly (vinylidene fluoride) (PVDF), [10] and its copolymers with trifluoroethylene (TrFE) [11] are used for energy harvesting applications because these materials possess both piezoelectric and

pyroelectric properties. The main advantages of using polymers are their low cost, chemical stability, flexibility, ease of fabrication in various forms, and durability under an applied strain. Among these, the PVDF polymer has a higher piezoelectric coefficient [12] and has been used in a variety of applications (e.g., soft-touch switches, strain gauges, piezoelectric transducers, actuators and ultrasound transducers) for more than two decades [13-15].

5.2. Experimental Section

5.2.1. Growth of ZnO nanowires

Fig.5.1 shows a schematic diagram of the experimental setup for the growth of the ZnO micro/nano wires. ZnO micro/nanowire growth was reported in our previous reports [11, 16, 17]. In typical growth, a horizontal quartz tube furnace was used. The source material consisted of a mixture of ZnO, metal Zn, and graphite, having a weight ratio of 1.5:0.5:1. The mixture of the source material with ethanol was continuously pulverized in a mortar to obtain the proper mixture. The mixed source material was then loaded into an alumina boat and dried in an oven overnight at 100°C. After, the alumina boat was placed inside a small quartz tube and then placed in the center of a long quartz tube (1.5 m). The source material was heated to 1100°C at a heating rate of 360°C/h under a constant argon flow of 350 sccm. Once the temperature reached 550–600°C, oxygen gas was introduced at a flow rate of 30 sccm. The furnace was maintained under these conditions for 1 h, and then cooled to room temperature. The ZnO nanowires were collected from the end of the quartz tube in the up flow direction of the gas flow.

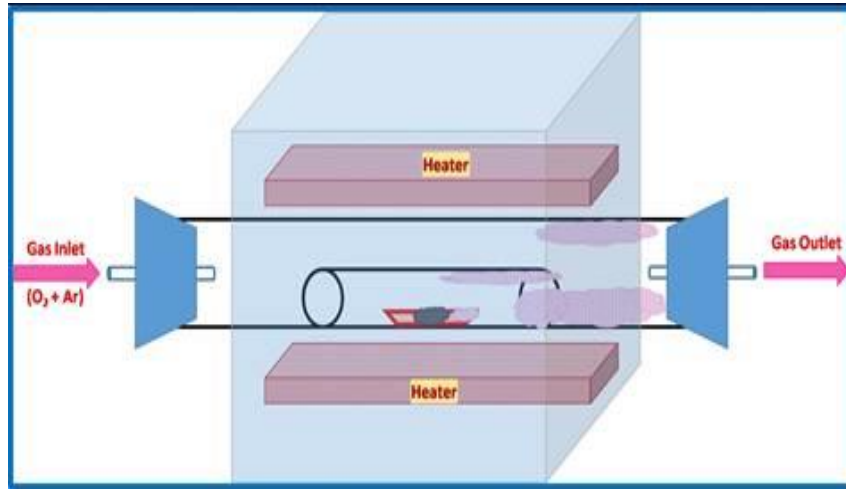


Fig.5.1. Schematic diagram of the experimental setup for the growth of ZnO micro/nanowires

5.2.2. Fabrication of the Hybrid Composite Nanogenerator

The ZnO nanowire and poly(vinylidene fluoride) (PVDF) (Sigma Aldrich) was dispersed in 15 mL of N,N-dimethylformamide at the weight percentage of 0.1/1 (w/w). The homogeneous mixer was prepared by the sonication process, using a probe sonicator for 30 min and was poured into a Petri dish and dried in a hot-air oven overnight at 80°C. The dried film was peeled off from the Petri dish. The nanogenerator was fabricated by coating Au electrodes on the top and bottom of the composite film through thermal evaporation. The electrical contact was taken from the top and bottom sides of the gold-coated composite, with Cu wires connected with silver paste. Finally, the entire device was covered with polydimethylsiloxane (PDMS) to avoid physical damage while under operation.

5.2.3. Characterization

The crystallinity and surface morphology of the as-grown nanowire and composite film were analyzed using X-ray diffraction (XRD, Rigaku) and field-emission scanning electron microscopy (FE-SEM, JEOL, JSM-6700F)

correspondingly. The chemical and surface composition of the composite film was analyzed through Fourier-transform infrared spectroscopy (FTIR, Nicolet 6700, and Thermo Scientific) and X-ray photoelectron spectroscopy (XPS, Theta Probe, and Thermo Scientific). The electrical measurement was carried out under continuous bending and uniaxial pressing conditions, using a Picoammeter (Keithley 6485) and Nanovoltmeter (Keithley 2182A). A bending tester (JIBT-200, Junil Tech) provided the uniaxial pressing/bending for the experimental testing.

5.3. Results and discussion

We have synthesized ZnO nanowire through vapor transport method. The crystal structure and morphology of the as synthesized ZnO nanowires were analyzed by X-ray diffraction (XRD), Fourier transform infrared spectroscopy (FTIR), field-emission scanning electron microscopy (FE-SEM). The XRD pattern of the ZnO nanowire was shown in Fig.5.2. The ZnO diffraction peaks films were in good agreement with standard file 3-1457. The diffraction peaks were confirmed the formation of wurtzite structure of the hexagonal ZnO and there is no impurity peak other than ZnO.

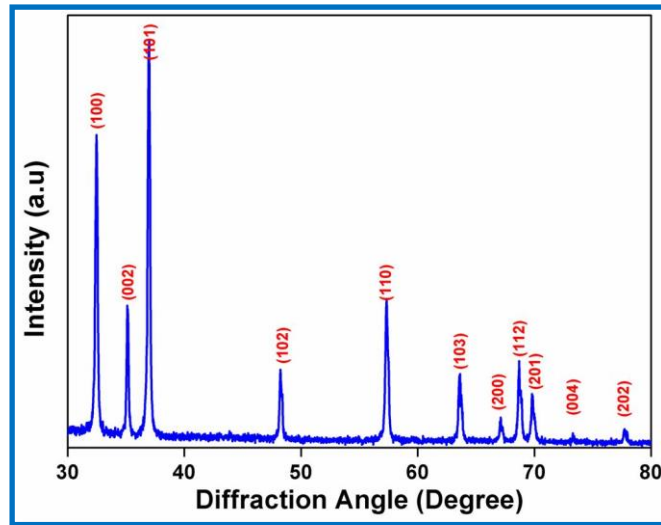


Fig.5.2. X-ray diffraction (XRD) pattern of as-grown ZnO nanowire

The morphology of the nanowire was confirmed from FE-SEM image and shown in Fig.5.3. The diameter and length of the grown ZnO nanowires are 60-80 nm and 6-8 μm respectively.

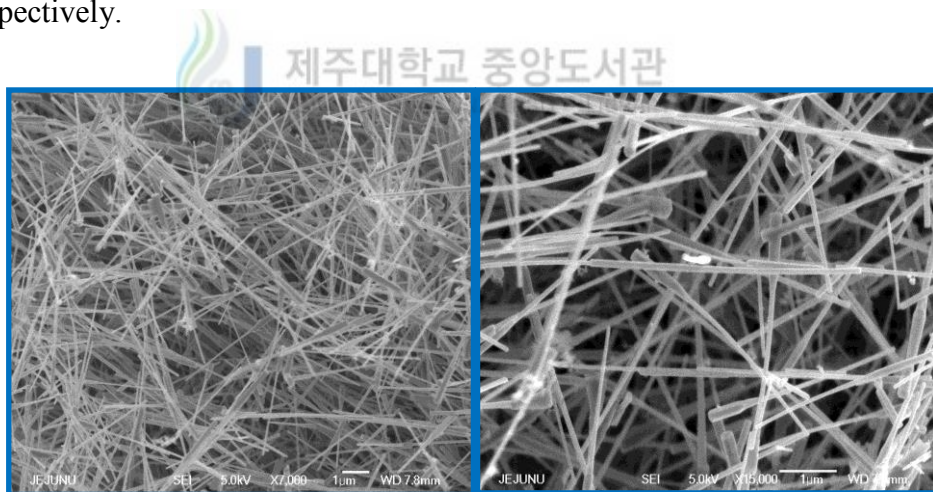


Fig.5.3. FE-SEM image of ZnO nanowire (Lower and Higher Magnification)

We fabricated a simple, low-cost, flexible hybrid composite nanogenerator, using PVDF and ZnO nanowire. PVDF plays a crucial role in this device, not only as a piezoelectric, but also by restricting aggregation between the ZnO nanowires. Fig.5.4 shows a schematic diagram of the detailed fabrication process. A simple

solution-casting process was used to fabricate the composite film; this technique is applicable to large-scale nanogenerator fabrication for real-world applications.

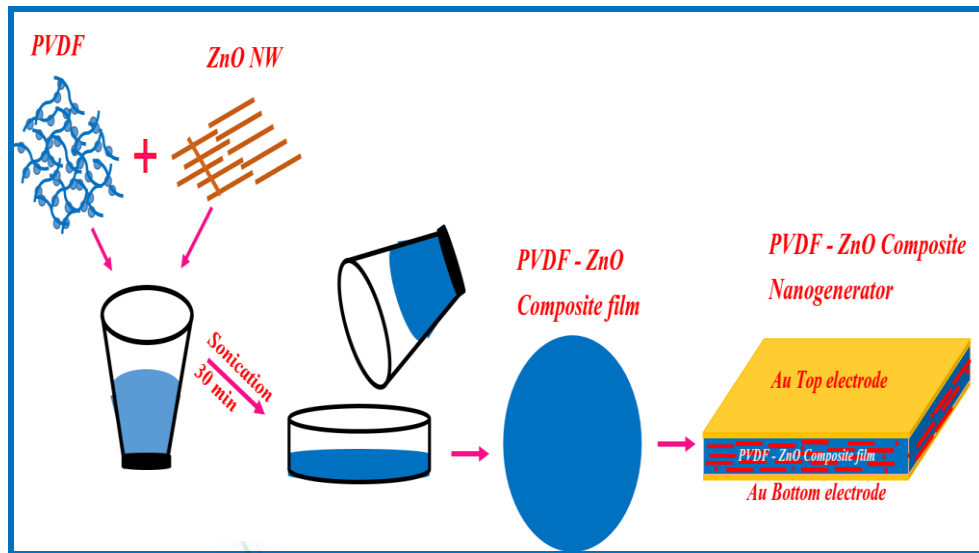


Fig.5.4. Schematic diagram of the fabrication process of the hybrid composite nanogenerator

X-ray diffraction (XRD), Fourier transform infrared spectroscopy (FTIR), field-emission scanning electron microscopy (FE-SEM), and X-ray photoelectron spectroscopy (XPS) were used to verify the crystallinity, phase, morphology, and composition of the composite film, respectively. The XRD pattern of the composite film confirmed the presence of ZnO and PVDF. The ZnO diffraction peaks in the composite film were in good agreement with standard file 3-1457, and also with as-grown ZnO nanowires [18] (Fig.5.5).

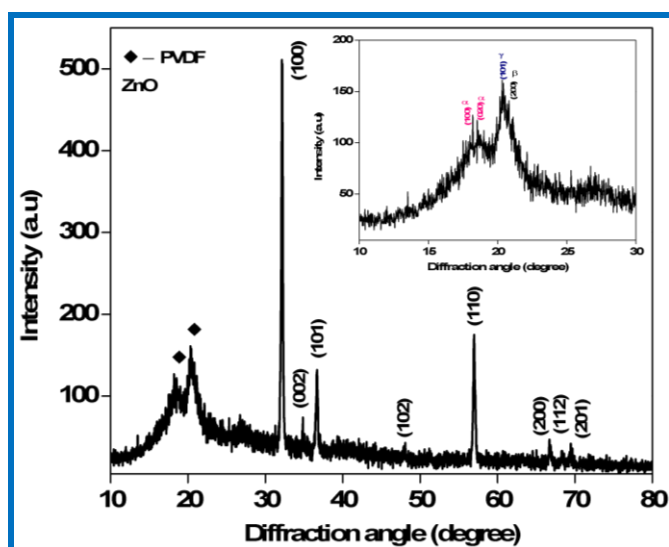


Fig.5.5. X-ray diffraction (XRD) pattern of the PVDF-ZnO nanowire composite film (the inset shows an enlarged view from 10–30°)

The inset shows an enlarged portion over 10–30°, corresponding to the crystalline phase of the PVDF film. XRD results showed a strong peak at $2\theta = 20.7^\circ$, corresponding to the (200) plane of the β -phase, and a small peak at $2\theta = 18.4^\circ$, corresponding to the (020) plane of α -PVDF [15].

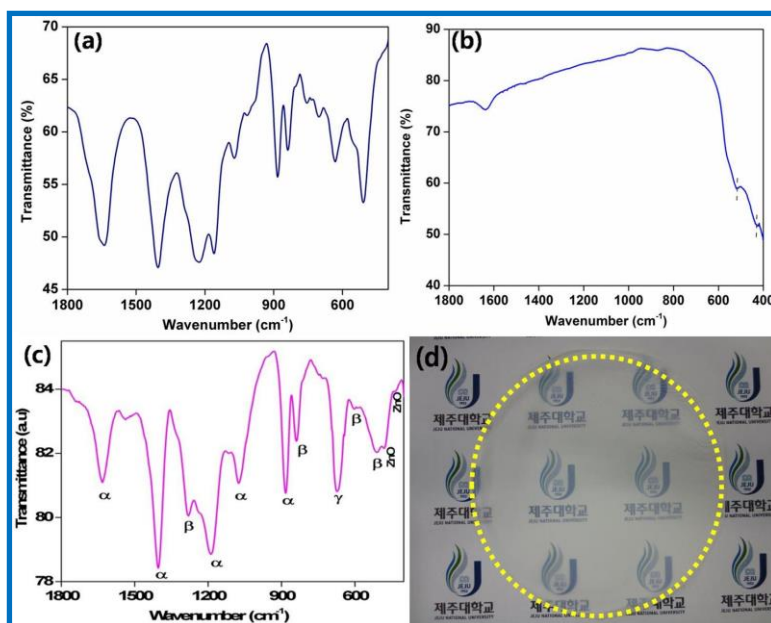


Fig.5.6. Fourier-transform infrared (FTIR) spectra of (a) PVDF, (b) ZnO nanowire, (c) PVDF-ZnO nanowire composite film (d) digital image of the composite film.

The FTIR results confirmed the existence of the β -phase of PVDF [15] at 512, 606, 838, and 1282 cm^{-1} , and ZnO stretching vibration mode peaks at 518 and 420 cm^{-1} ; the remaining peaks were related to other phases of PVDF (Fig.5.6a). The peaks that appeared in the composite film were in good agreement with the bare PVDF and ZnO nanowire results (Fig.5.6 b, c). The digital image of the fabricated composite film was clearly indicating the high transparency and it shown in Fig.5.6d.

The microscopic surface morphology of the composite film was investigated by FE-SEM, as shown in Fig.5.7a, b; the magnified image shows a homogeneous distribution of ZnO nanowires in crystalline superulites of the PVDF matrix [19].

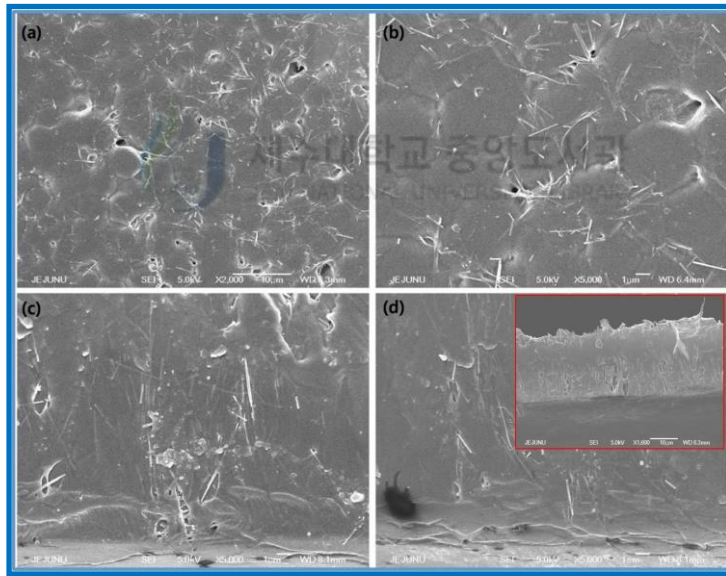


Fig.5.7. Field-emission scanning electron microscopy (FE-SEM) image of PVDF-ZnO nanowire composite film, (a) Lower, and (b) Higher magnification. Cross sectional image, (a) Lower, and (b) higher magnification.

For clear observation, we also measured the cross-sectional view of the composite film, from which we obtained the composite film thickness ($\sim 30 \mu\text{m}$) (Fig.5.7c, b). The homogeneous and disaggregated ZnO nanowires in the film are a good sign to ensure the highest performance.

The surface composition of the film was investigated using XPS. Fig.5.8a shows the XPS spectra, which confirmed the presence of O, C, F, and Zn in the composite film, as well as the high purity of the fabricated film. The inset shows the Zn 2p core-level spectra of the ZnO nanowire. The core level spectrum of C 1s consisted of three peaks at 284.57, 286.02, and 290.67 eV which corresponded to C=C, C–H, and C–F species, respectively (Fig.5.8b). An O 1s and F 1s peak were observed at 532.27 and 688 eV, respectively, which corresponded to the C–O and C–F bonds (Fig.5.8.c,d) [20].

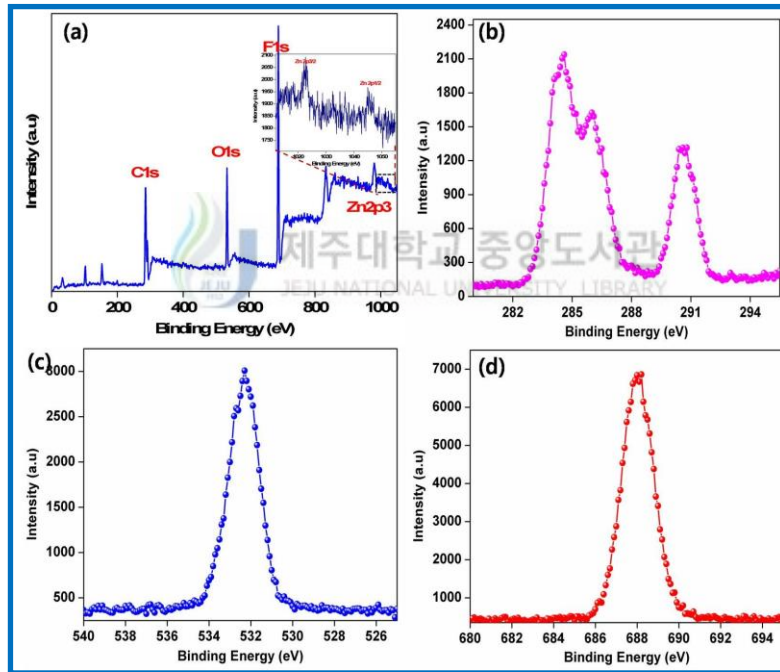


Fig.5.8. X-ray photoelectron spectroscopy (XPS), (a) survey spectrum (the inset shows the Zn 2p core-level spectrum). Core-level spectra of (b) C 1s, (c) O 1s, and (d) F 1s of the PVDF-ZnO nanowire composite film

To show the potential of the composite film, we fabricated a nanogenerator with gold as the top and bottom electrodes, having an active device area of $3 \times 3 \text{ cm}^2$. The electrical measurement was carried out under periodic deformation by bending

and pressing, using a bending tester. Fig.5.9 shows the performance of the nanogenerator under bending speeds of 25 mm.s^{-1} .

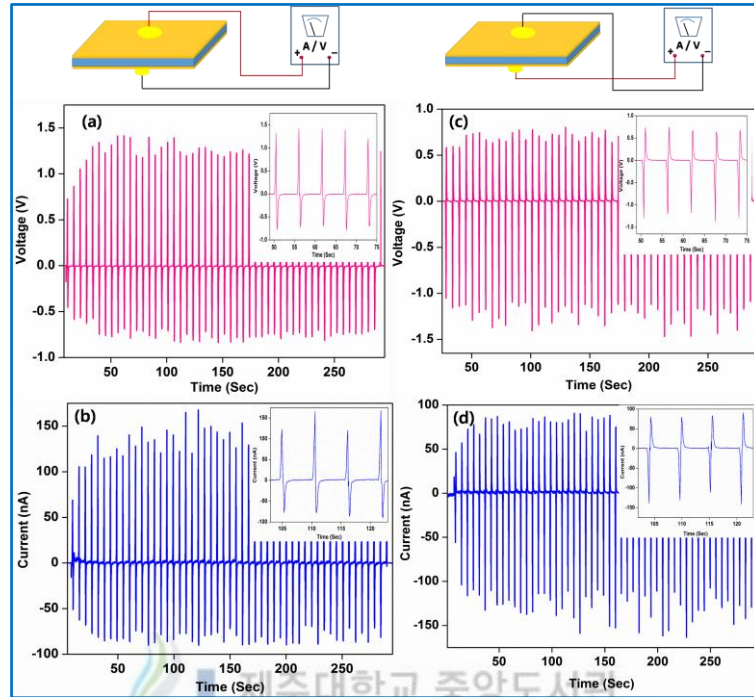


Fig.5.9. Measured open circuit voltage and short circuit current of hybrid composite nanogenerator under continuous bending condition, (a, b) at forward bias, (c, d) at reverse bias respectively. The insets are the enlarged view of the electrical output.

The average output voltage and current under bending and release conditions were 1.3 V, 0.16 μA and 0.77 V, 0.087 μA , respectively. The switching polarity test was used to verify the measured electrical output generated from the hybrid device. To check the polarity test, we connected the nanogenerator under reverse connection conditions. The measured outputs were the same; however, the polarity of the output signal was reversed in case of the reverse connection. The results conclude that the measured electrical signal generated from nanogenerator during bending and unbending condition. The output voltage and current of the device were not uniform for both forward and reverse connection conditions, which may be attributed to different strain rates [21]. The nanogenerator delivered an output voltage and current

of 1.3, 0.77 V and 0.162, 0.087 μA with an output power of 0.211, 0.072 μW for forward-connection conditions, and 0.75, 1.21 V and 0.157, 0.0875 μA with an output power of 0.066, 0.190 μW for reverse-connection conditions, under bending and release, respectively.

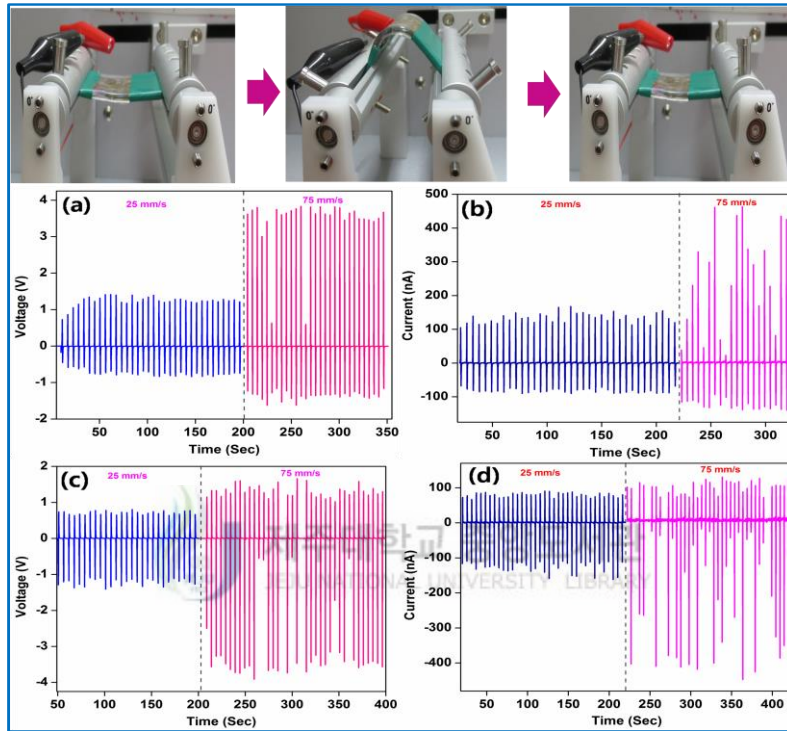


Fig.5.10. Measured open circuit voltage and short circuit current of hybrid composite nanogenerator under different speed of bending/ unbending condition, (a, b) at forward bias, (c, d) at reverse bias respectively.

To verify the effect of bending speed on the output performance of the nanogenerator, we measured the performance as a function of the bending speed. The results, shown in Fig.5.10, indicated that the output voltage and current increased with the bending speed. The maximum output voltage and current of 3.9 V and 0.48 μA , respectively, were measured at a bending speed of $75 \text{ mm}\cdot\text{s}^{-1}$, and corresponded to an output power of 1.856 μW ; these values are higher than those given in earlier reports [9, 19, 22, 23].

Most practical nanogenerator applications are based on uniaxial compression; as such, we tested our device under the periodic uniaxial compression force through a bending tester. The open-circuit voltage and short-circuit current of the hybrid device were measured under periodic uniaxial pressing and release conditions (Fig.5.11).

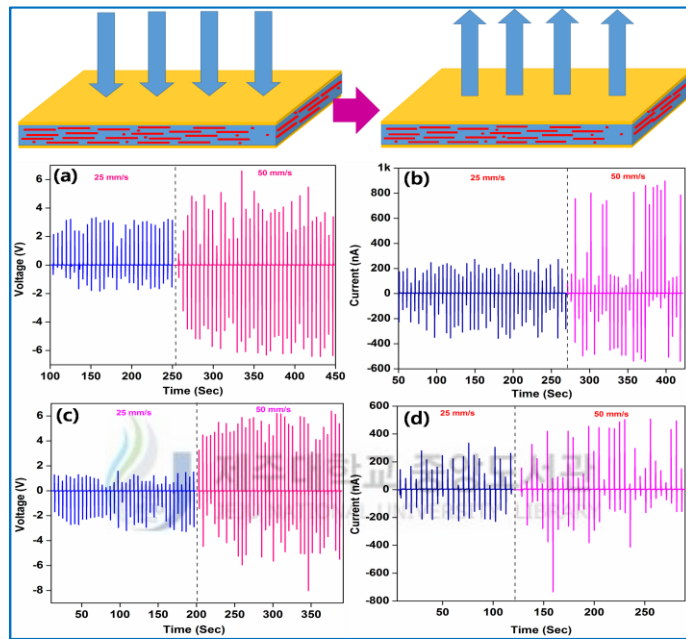


Fig.5.11. Measured open circuit voltage and short circuit current of hybrid composite nanogenerator under different speed of uniaxial pressing / unpressing condition, (a, b) at forward bias, (c, d) at reverse bias respectively.

At a compression speed of 25 mm.s^{-1} , we measured an average output voltage and current of 2.9 V and $0.263 \mu\text{A}$ respectively. The switching polarity test was used to verify the measured electrical output generated from the hybrid device. The nanogenerator delivered an output voltage and current of 2.9, 1.46 V and 0.193, $0.263 \mu\text{A}$ with an output power of 0.56, $0.384 \mu\text{W}$ for forward-connection conditions, and 1.15, 2.45 V and 0.174, $0.186 \mu\text{A}$ with an output power of 0.20, $0.456 \mu\text{W}$ for reverse-connection conditions, under compression and release, respectively.

To verify the effect of compression speed on the output performance of the nanogenerator, we measured the performance as a function of the compression speed. Increasing the compression speed up to 50 mm.s^{-1} increased the output; however, further increases in the compression speed reduced the electrical output. The maximum output voltage and current of 6.9 V and $0.96 \mu\text{A}$ with an output power of $6.624 \mu\text{W}$ was measured at a compression speed of 50 mm.s^{-1} . These results were higher than the values presented in previous reports based on composite nanogenerators, as summarized in Table. 5.1. [3, 10, 20, 23].

Table.5.1. Comparison of the performance of other reported PDMS based composite-nanogenerators

Materials	Composite	Applied stress	Output voltage	Reference
BaTiO₃	Nanotubes	PDMS	Bending	5.5 V
BaTiO₃	Nanoparticles with CNT dispersant	PDMS	Bending	3.2 V
PZT	Nanoparticles with CNT dispersant	PDMS	Bending	10 V
NaNbO₃	Nanowires	PDMS	Pressing	3.2 V
KNbO₃	Nanorods	PDMS	Pressing	3.2 V
ZnO	Nanoparticles with CNT dispersant	PDMS	Pressing	7.5 V
ZnSnO₃	Triangular Belts	PDMS	Pressing	5.5 V
ZnO	Nanowires	PVDF	Pressing	6.9 V

In our daily life, activities related to human body movement, such as walking, running, arm movements, finger typing, blood flow, and heartbeats, are ideal mechanical energy sources for human-based self-powered devices. To develop a human-based self-powered device, we tested the feasibility of our hybrid nanogenerator to harvest biomechanical energy.

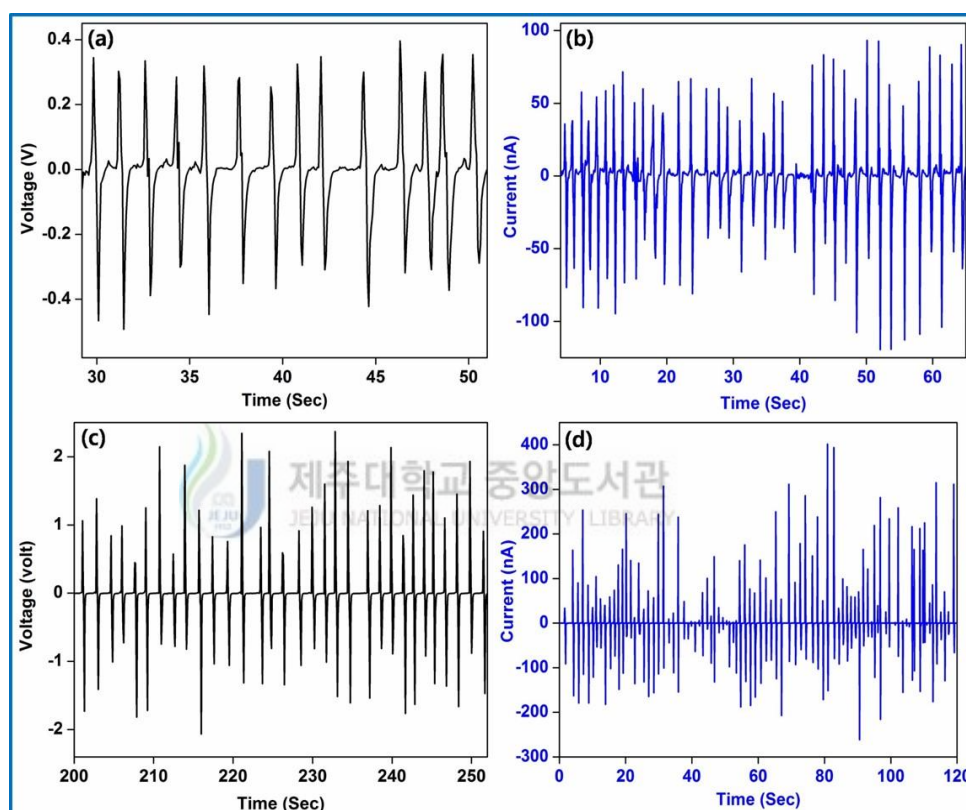


Fig.5.12. Measured open-circuit voltage and short-circuit current of the hybrid composite nanogenerator for (a, b) folding and (c, d) pressing with fingers.

Fig. 5.12 shows device testing under folding and pressing of fingers. When folding or pressing, the finger produces stress on the hybrid composite nanogenerator, which generates a piezo-potential across the device. The developed piezo-potential drives the electrons in the external circuit through Au electrodes. The measured average voltage and current under folding and pressing were 0.33 V, 0.062

μA and 1.3 V, 0.177 μA , respectively, which is higher than values cited in an earlier report [24]. The higher output may be due to the equal distribution of applied strain over the nanowire surface. The device performance was higher under uniaxial compression than bending (Fig.5.12c, d), which suggests that this device could be used to harvest the biomechanical energy while walking and running.

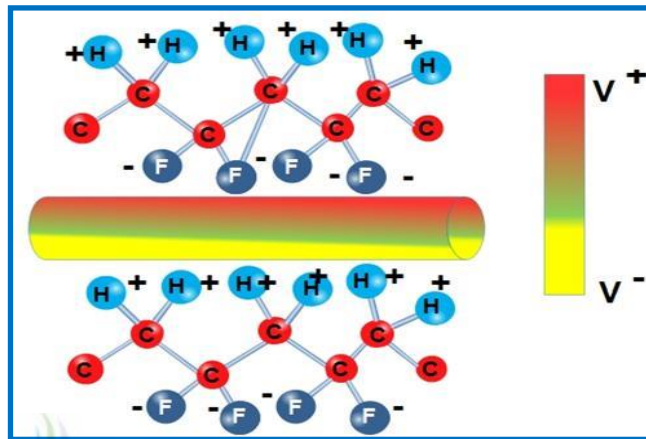


Fig.5.13. Schematic representation of self-polarization mechanism

The proposed working mechanism of the hybrid composite nanogenerator is the combined effect of PVDF and ZnO nanowire. In the hybrid nanogenerator, ZnO nanowires are uniformly distributed in the PVDF polymer matrix, which prevents agglomeration. The presence of oppositely charged polar surface in nanowire during the process, actively interact with CF_2 / CH_2 groups in PVDF build a negative and positive charge densities over the surface. The formation of dipole promotes the formation of piezoelectric PVDF β -phase through surface charge induced polarization [25] and nano confinement [26]. Both nano confinement and surface charge induced polarization results the self-polarized film, which was schematically represented in Fig.5.13. In addition to that the applied external mechanical force build a potential in the nanowire, which align the PVDF electric

dipole further along the unidirection through stress-induced polarization [7]. Finally, PVDF molecules are self-polarized along a single direction from the results of stress and surface charge induced polarization without external electric potential. The self-polarization mechanisms in piezoelectric and ferroelectric materials are unclear due to its complex nature. The self-polarization eliminates the complexity of poling process in MEMS and microstructure based energy harvesting devices, which is the additional advantage.

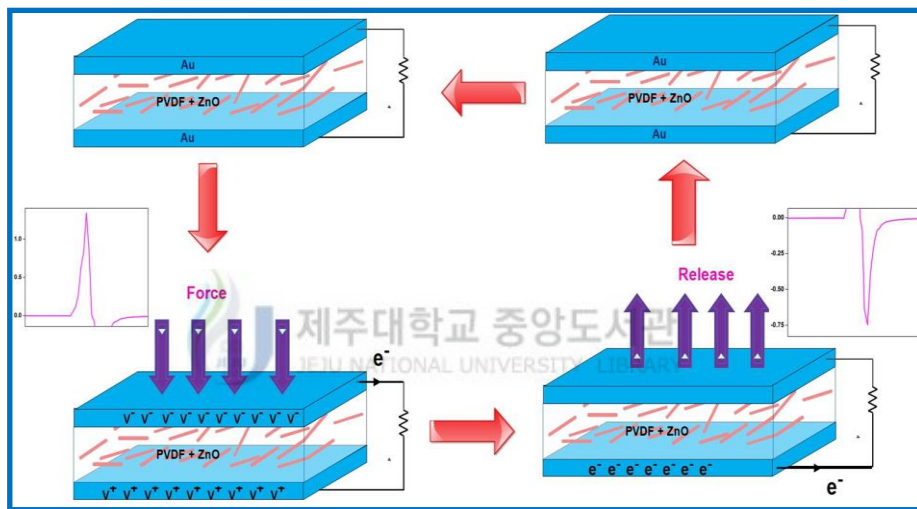


Fig.5.14. Power generation mechanism in the hybrid composite nanogenerator

Under bending/compression, the hybrid composite device experiences a strain over surface, which produces the piezo-potential in ZnO nanowires surface and as well as from the PVDF film and this combined effect contribute in the final output. The produced piezo-potential on either side of the composite film induces an inductive charge on the top and bottom electrodes. This potential difference will drive the electron in the external circuit and it's represented in Fig.5.14. To prove the self-polarization of the fabricated film, we have tested the device after electrical pole (5.5 kV, 36 hr). The result suggested that the electrical output was not much

improved than unpoled device, which defend the self-polarization behavior of PVDF-ZnO film (Fig.5.15) [26].

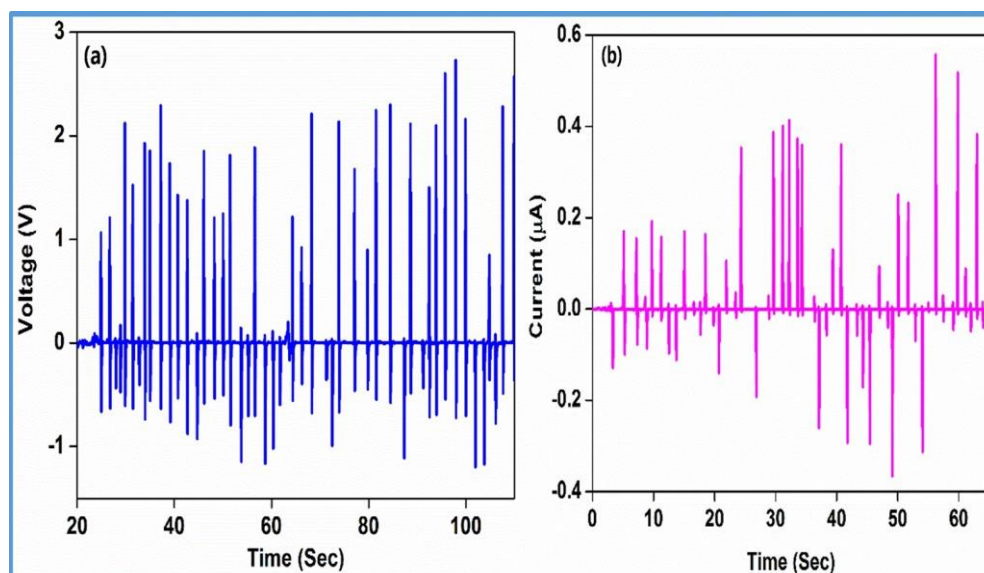


Fig.5.15. a) Open-circuit voltage and b) short-circuit current of the hybrid composite (PVDF-ZnO) nanogenerator after poling at 5.5 kV for 36 h under continuous pressing condition.

To check the effect of ZnO nanowires on the performance of hybrid nanogenerator, we measured the electrical output voltage and current of the PVDF nanogenerator; voltage and current values of 60 mV and 30 nA were observed, respectively (Fig. 5.16). The measured low output due to the random orientation of molecular dipoles in the PVDF film. To show the potential of hybrid device, we further compared with the ZnO nanoparticle based hybrid device. The results are clearly indicating that the fabricated hybrid device displayed higher performance than bare and ZnO nanoparticle based device (Fig.5.17).

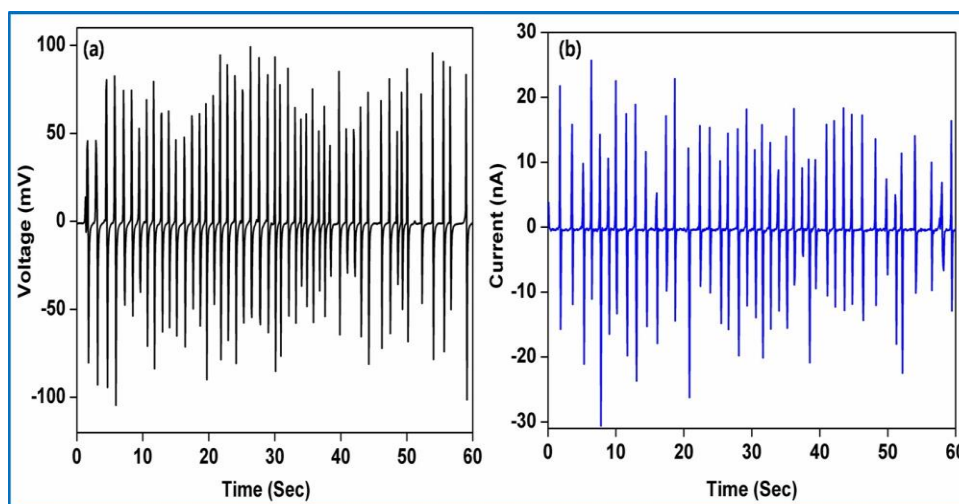


Fig.5.16. Measured electrical output of the PVDF nanogenerator: (a) open-circuit voltage, and (b) closed-circuit current.

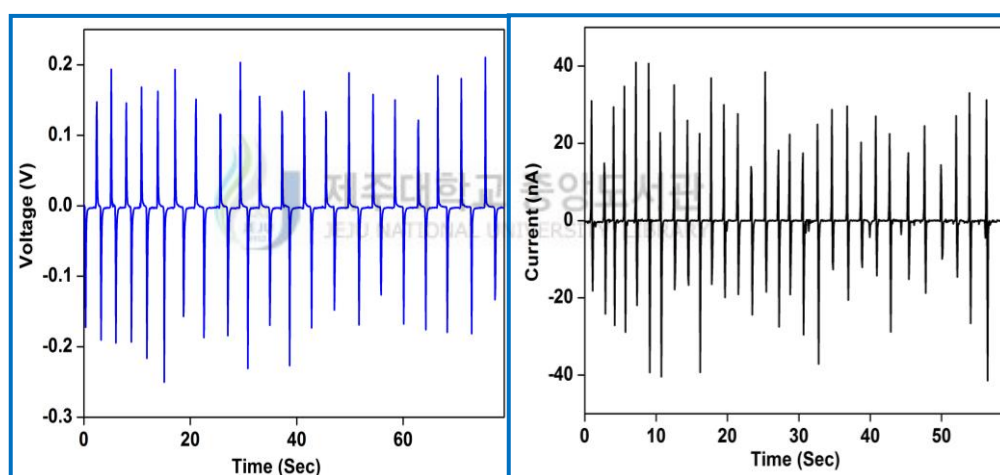


Fig.5.17. Measured electrical output of the hybrid nanogenerator with ZnO nanoparticle: (a) open-circuit voltage, and (b) closed-circuit current.

To demonstrate the application of the hybrid composite nanogenerator, we fabricated a full-wave bridge rectifier circuit (Fig.5.18). Using this circuit, we rectified the electrical signal generated in the nanogenerator, shown in Figure 3b and c. The rectified electrical signal generated by one press/ release cycle was directly used to drive five green LEDs simultaneously, without any storage device, see Fig.5.18.

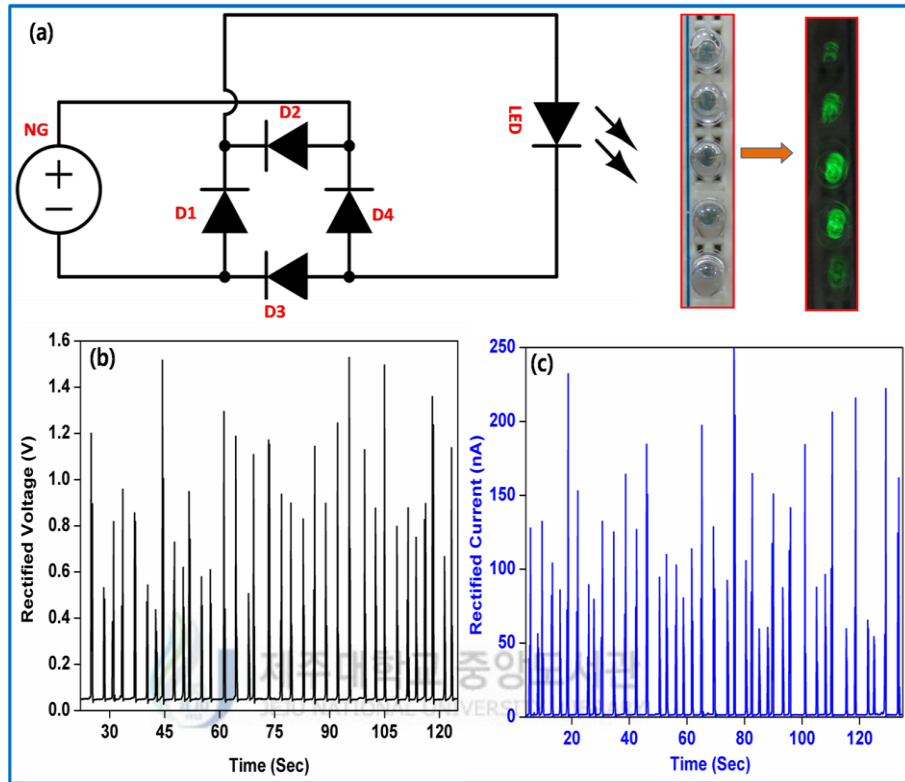


Fig.5.18. (a) Schematic diagram of the full-wave Bridge rectifier circuit. (b) Measured rectified open-circuit voltage. (c) Short-circuit current by pressing the fingers. The rectified output was used to drive five green LEDs, which is shown in the top left corner.

The fabricated hybrid composite nanogenerator exhibited several advantages. First, the fabrication process was simple, cost-effective, and easily transferred to mass production. Second, electric poling was not required to align the piezoelectric domains, which increases the possibility for mass production. Third, the device is non-toxic, flexible, and lightweight. Finally, a higher output performance was observed under uniaxial compressive stress, which facilitates real-life applications of the device. The integration of other piezoelectric nanomaterials with PVDF polymer gives the new research area to enhance the output performance.

5.4. Conclusion

A hybrid composite nanogenerator was developed with ZnO nanowires and a PVDF polymer, using a simple, low-cost solution-casting method. The simplicity of the process and electric poling free composite nanogenerator provided the possibility of producing a thin, large-scale, lightweight nanogenerator of any shape. The hybrid composite nanogenerator delivered a maximum voltage, current, and output power of 6.9 V, 0.96 μA , and 6.624 μW . Finally, we used the hybrid composite nanogenerator to build a self-powered ZnO microwire-based pH sensor that was capable of operating five green LEDs simultaneously, without the need for a storage device.



References

- [1] Z.L. Wang, W. Wu, Nanotechnology-Enabled Energy Harvesting for Self-Powered Micro-/Nanosystems. *Angew. Chem. Int. Ed.* 51 (2012), 11700 – 11721.
- [2] Z.L. Wang, G. Zhu, Y. Yang, S. Wang, C. Pan, Progress in Nanogenerators for Portable Electronics. *Mater. Today* 15 (2013), 532-543.
- [3] K.I. Park, M. Lee, Y. Liu, S. Moon, G.T. Hwang, G. Zhu, J.E. Kim, S.O. Kim, D.K. Kim, Z.L. Wang, K.J. Lee, Flexible Nanocomposite Generator Made of BaTiO₃ Nanoparticles and Graphitic Carbons. *Adv. Mater.* 24 (2012), 2999–3004.
- [4] Z.H. Lin, Y. Yang, J.M. Wu, Y. Liu, F. Zhang, Z.L. Wang, BaTiO₃ Nanotubes-Based Flexible and Transparent Nanogenerators. *J. Phys. Chem. Lett.* 3 (2012), 3599–3604
- [5] K.I. Park, C.K. Jeong, J. Ryu, G.T. Hwang, K.J. Lee, Flexible and Large-Area Nanocomposite Generators Based on Lead Zirconate Titanate Particles and Carbon Nanotubes. *Adv. Energy Mater.* 3 (2013), 1539-1544.
- [6] Y. Yang, J.H. Jung, B.K. Yun, F. Zhang, K.C. Pradel, W. Guo, Z.L. Wang, Flexible Pyroelectric Nanogenerators using a Composite Structure of Lead-Free KNbO₃ Nanowires. *Adv. Mater.* 24 (2012), 5357–5362.
- [7] K.Y. Lee, D. Kim, J.H. Lee, T.Y. Kim, M.K. Gupta, S.W. Kim, Unidirectional High-Power Generation via Stress-Induced Dipole Alignment from ZnSnO₃ Nanocubes/Polymer Hybrid Piezoelectric Nanogenerator. *Adv. Funct. Mater.* 24 (2013), 37-43.

- [8] H. Sun, H. Tian, Y. Yang, D. Xie, Y.C. Zhang, X. Liu, S. Ma, M. Zhao Hai, T.L. Ren, A Novel Flexible Nanogenerator Made of ZnO Nanoparticles and Multiwall Carbon Nanotube. *Nanoscale* 5 (2013), 6117-6123.
- [9] W. Zeng, X.M. Tao, S. Chen, S. Shang, H.L.W. Chan, S.H. Choy, Highly Durable All-Fiber Nanogenerator for Mechanical Energy Harvesting. *Energy Environ. Sci.* 6 (2013), 2631-2638.
- [10] S.N. Cha, S.M. Kim, H.J. Kim, J.Y. Ku, J.I. Sohn, Y.J. Park, B.G. Song, M.H. Jung, E.K. Lee, B.L. Choi, J.J. Park, Z.L. Wang, J M. Kim, K. Kim, Porous PVDF As Effective Sonic Wave Driven Nanogenerators. *Nano Lett.* 11 (2011), 5142–514.
- [11] S.H. Bae, O. Kahya, B.K. Sharma, J. Kwon, H.J. Cho, B. Özyilmaz, J.H. Ahn, Graphene-P(VDF-TrFE) Multilayer Film for Flexible Applications. *ACS Nano* 7 (2013), 3130–3138.
- [12] H. Kawai, The Piezoelectricity of Poly(vinylidene fluoride). *J. Appl. Phys.* 8 (1969), 975–976.
- [13] Q.M. Zhang, V.V. Bharti, X. Zhao, Giant Electrostriction and Relaxor Ferroelectric Behavior in Electron-Irradiated Poly(vinylidene Fluoride–trifluoroethylene) Copolymer. *Science* 280 (1998), 2101–2104.
- [14] Q.M. Zhang, H. Li, M. Poh, F. Xia, Z.Y. Cheng, H. Xu, C. Huang, An All-Organic Composite Actuator Material with a High Dielectric Constant. *Nature* 419 (2002), 284–287.
- [15] H. Yu, T. Huang, M. Lu, M. Mao, Q. Zhang, H. Wang, Enhanced Power Output of an Electrospun PVDF/MWCNTs-based Nanogenerator by Tuning Its Conductivity. *Nanotechnology* 24 (2013), 405401-09.

- [16] S. Priya, D.J. Inman, *Energy Harvesting Technologies*. Springer Science, New York 2009.
- [17] S.P. Beeby, M.J. Tudor, N.M. White, *Energy Harvesting Vibration Sources for Microsystems Applications*. *Meas. Sci. Technol.* 17 (2006), R175.
- [18] R. Mohan, K. Krishnamoorthy, S.J. Kim, *Enhanced Photocatalytic Activity of Cu-Doped ZnO Nanorods*. *Solid State Commun.* 152 (2012), 375–380.
- [19] Jr.R. Gregorio, M. Cestari, *Effect of Crystallization Temperature on the Crystalline Phase Content and Morphology of Poly(vinylidene fluoride)*. *J. Polym. Sci. Part B: Polym. Phys.* 32 (1994), 859-870.
- [20] Y. Hu, Y. Zhang, C. Xu, G. Zhu, Z.L. Wang, *High-Output Nanogenerator by Rational Unipolar Assembly of Conical Nanowires and Its Application for Driving a Small Liquid Crystal Display*. *Nano Lett.* 10 (2010), 5025–5031.
- [21] Z.L. Wang, G. Zhu, Y. Yang, S. Wang, C. Pan, *Progress in Nanogenerators for Portable Electronics*. *Mater. Today* 15 (2013), 532-543.
- [22] Z.L. Wang, W. Wu, *Nanotechnology-Enabled Energy Harvesting for Self-Powered Micro-/Nanosystems*. *Angew. Chem. Int. Ed.* 51 (2012), 11700 – 11721.
- [23] G. Zhu, R. Yang, S. Wang, Z.L. Wang, *Flexible High-Output Nanogenerator Based on Lateral ZnO Nanowire Array*. *Nano Lett.* 10 (2010), 3151–3155.
- [24] S.Y. Chung, S. Kim, J.H. Lee, K. Kim, S.W. Kim, C.Y. Kang, S. J. Yoon, Y.S. Kim, *All-Solution-Processed Flexible Thin Film Piezoelectric Nanogenerator*. *Adv. Mater.* 24 (2012), 6022–6027.
- [25] Y. Mao, P. Zhao, G. McConohy, H. Yang, Y. Tong, X. Wang, *Sponge-Like Piezoelectric Polymer Films for Scalable and Integratable Nanogenerators*

and Self-Powered Electronic Systems. *Adv. Energy Mater.* 4 (2014), 1301624, doi: 10.1002/aenm.201301624.

- [26] V. Cauda, S. Stassi, K. Bejtka, G. Canavese, Nanoconfinement: An Effective Way to Enhance PVDF Piezoelectric Properties. *ACS Appl. Mater. Interfaces* 5 (2013), 6430–6437.



CHAPTER-VI

Carbon based Composite nanogenerator

In this chapter describes the fabrication of composite nanogenerator, which consisted of ZnO nanowires and reduced graphene oxide in a polydimethylsiloxane matrix, generated an average peak-to-peak output voltage and current of 15.5 V and 2.26 μ A, respectively, with an output power of 35.03 μ W under palm impact. Under a periodic foot stamp, an output voltage and current of 5.5 V and 0.63 μ A, respectively, were observed. A large-area composite nanogenerator ($11 \times 10 \text{ cm}^2$) was fabricated; the device delivered a maximum output voltage and current of 35 V and 4 μ A, respectively. Further, we have demonstrated the capability of the composite nanogenerator to power light-emitting diodes, segmented displays, and liquid-crystal displays.

6.1. Introduction

The ZnO is lead-free, biocompatible, and has piezo and semiconducting properties [1, 2]; its non-centrosymmetric nature has proven to be advantageous for nanogenerator applications. Specifically, ZnO played an important role in the nanogenerator progress with diverse nanogenerator device configurations (*e.g.*, lateral, vertical, radial, integration, stacked, and composite nanogenerator forms) [3]. The composite-based nanogenerator has significantly impacted in nanogenerator progress, due to its flexibility and stretchability, in addition to its low-cost and simple fabrication method that can be easily scaled to industrial applications. However, the composite nanogenerator based on piezo-materials has encountered problems with aggregation, limiting device performance. To overcome this problem and achieve higher outputs, various fillers have been used to evenly disperse the piezoelectric material in the composite layer. These fillers include carbon materials [4], metal nanowires [5], and two-dimensional (2-D) materials (*e.g.*, boron nitrate and molybdenum sulfide). Among these, graphene has attracted much attention as a filler material, due to the added advantage of improved conductivity and higher surface area. Graphene is a single hexagonal carbon layer that possesses a large surface area and enhanced electrical, thermal conductivity, higher surface area and mechanical stability [6–8]. Due to its exceptional properties, graphene-based composites have been used in a wide range of applications, such as energy harvesting [9], storage [10], and as catalysts.[11] Recently, Kumar et al. reported on a graphene vertically aligned ZnO nanostructure-based energy harvester [9]; here, graphene was used as a buffer layer and substrate to grow the ZnO nanostructure. Inspired by the pioneer

research, we developed a composite nanogenerator design that included one-dimensional ZnO nanowires and 2-D reduced graphene oxide (rGO) in a polydimethylsiloxane (PDMS) matrix; the rGO provided conducting paths, in addition to acting as a filler to disperse the ZnO nanowires throughout the PDMS matrix.

6.2. Experimental Section

6.2.1. Preparation of Graphene Oxide (GO)

The detailed experimental procedure for graphene oxide (GO) was given as, 2 g of natural graphite powder and 2 g of NaNO₃ was added in 50 mL of concentrated H₂SO₄. The mixture was vigorously stirred in an ice bath for 30 min. Further, 7 g of KMnO₄ was gradually added into that solution and then the mixer was stirred until the color change into brown. The color change indicates that the completion of exfoliation reaction. After completion of the reaction, 100 mL of distilled water was added gradually into the mixture, and 10 mL of H₂O₂ was added to that solution to increase the oxidation level and terminated the reaction. After 30 min, the mixture was diluted by the addition of 300 mL of DI water. Then, the solution was centrifuged and washed consecutively with 5% HCl solution until to reach a neutral pH value by centrifuge. After reaching neutral pH, the sample was dried at 70°C in hot air oven for overnight [12, 13].

6.2.2. Preparation of Reduced Graphene Oxide (rGO)

Reduced graphene oxide (rGO) was synthesized from graphene oxide through chemical reduction followed by thermal reduction. The prepared GO (0.1 g; 1 mg mL⁻¹) was dissolved in 100 mL of deionized water; the solution was sonicated for 30

min. Sodium borohydride and hydrazine mixtures were added to the solution under constant stirring at 70°C overnight. The prepared rGO was centrifuged several times in a deionized water/ethanol mixture to remove the residue and unreacted component. Finally, the sample was dried at 70°C for 12 h and then heat-treated at 250°C for 15 min under an Argon atmosphere.

6.2.3. Preparation of rGO-ZnO nanowire composites

ZnO nanowires were synthesized using a vapor transport method, as described in chapter-5 [13]. The rGO-ZnO nanowire composite was prepared by dispersing rGO and ZnO nanowire in an ethanol solution at a weight ratio of 0.1:1. The mixed solution was sonicated for 30 min to homogeneously disperse the ZnO nanowires and rGO, and then dried in an oven at 80°C overnight to obtain a composite powder.

6.2.4. Fabrication of the rGO-ZnO composite nanogenerator

The prepared rGO-ZnO composite (0.2 g) and 10 g of polydimethylsiloxane (PDMS) (Sylgard 184, Dow Corning at 10:1) were mixed well and then cast into a Petri dish. The composite film was cured at 80°C for 5 h in an oven. The composite nanogenerator was fabricated by sandwich the composite film between the Al foil/polyethylene terephthalate (PET) substrate as the top and bottom electrodes.

6.2.5. Characterization

The crystallinity and surface morphology of the as-grown nanowire, rGO, and composite were analyzed using X-ray diffraction (XRD, Rigaku) and field-emission scanning electron microscopy (FE-SEM, JEOL, JSM-6700F), respectively. The functional groups present in the composite and nanowire were analyzed through Fourier transform infrared spectroscopy (FTIR, Nicolet 6700, Thermo Scientific).

The electrical measurement was carried out under continuous pressing/release conditions using a Keithley Picoammeter (6485) and Nanovoltmeter (2182A). Periodic mechanical deformation was applied to the nanogenerator by palm impact and stamping of the foot.

6.3. Results and Discussion

The graphene oxide (GO) was synthesized by modified hummers method and synthesized graphene oxide was characterized by X-ray diffraction (XRD) pattern, raman spectrum and field emission scanning electron microscopy (FE-SEM) to measure the interlayer spacing, structure and morphology, it is displayed in Fig.6.1.

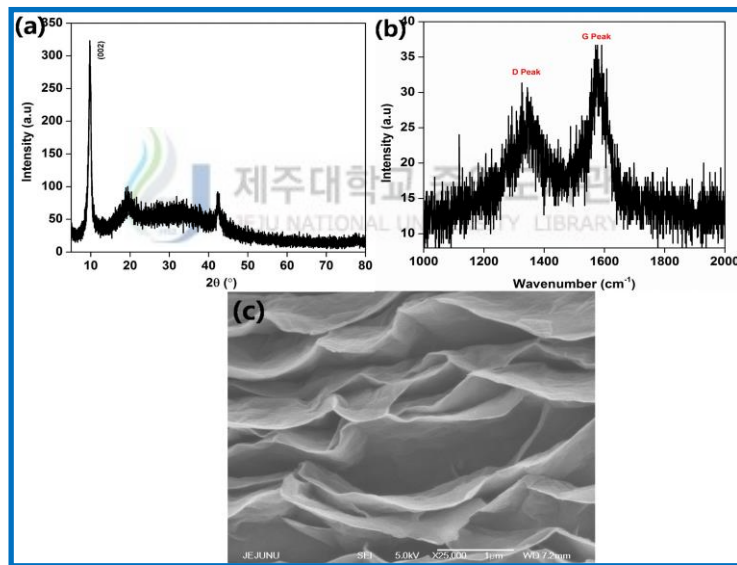


Fig.6.1. Graphene Oxide (GO) a) X-ray diffraction (XRD) pattern, b) Field emission scanning electron microscopy (FE-SEM) image, c) Raman spectrum

In XRD pattern (Fig.6.1a), the strong and sharp peak observed at $2\theta = 10^\circ$, which corresponds to the (002) plane of graphene oxide with interlayer distance of 0.880 nm. The two broad peaks at 1347, 1576 cm^{-1} are observed in the Raman spectrum of the graphene oxide samples, which are D and G bands of the carbon based materials (Fig.6.1b). The G band assigned to the first-order scattering of the

E_{2g} phonon from sp^2 carbon (graphite lattice), and the D band resulting from the structural imperfections created by the hydroxyl and epoxy groups on the carbon basal plane. The sheet like morphology of the graphene oxide was confirmed through FE-SEM image (Fig.6.1c). Further, the prepared graphene oxide was successfully reduced to reduced graphene oxide (rGO) by two steps, in which chemical reduction followed by thermal reduction at inert atmosphere.

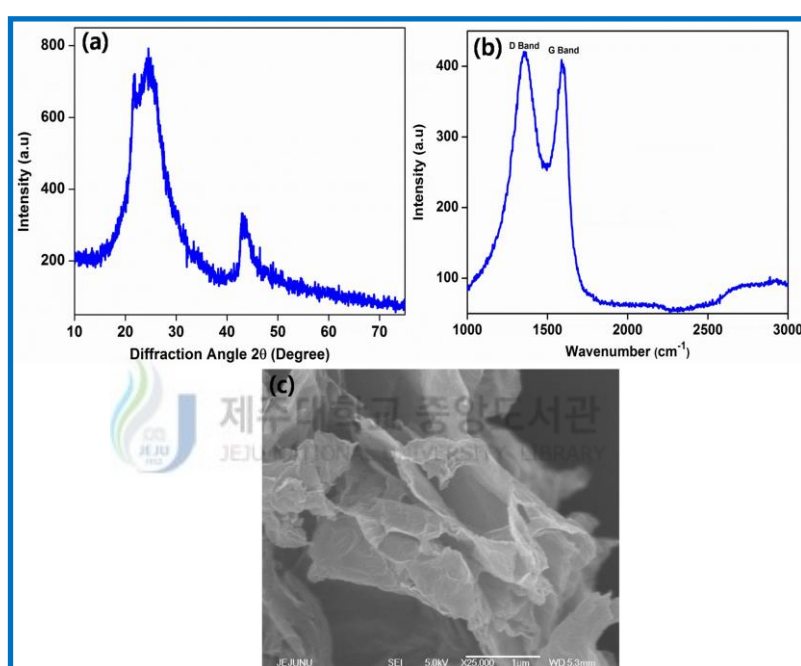


Fig.6.2. reduced graphene oxide (rGO), (a) X-ray diffraction (XRD) pattern, (b) Raman spectrum, (c) Field-emission scanning electron microscopy (FE-SEM) image

The quality of the synthesized rGO was evaluated using XRD, Raman spectroscopy, and FE-SEM. The XRD pattern (Fig.6.2a) revealed the existence of a broad peak at $2\theta = 24.6^\circ$, corresponding to the (002) peak of graphene. In the Raman spectra, two intense peaks were observed at 1593 and 1359 cm^{-1} , corresponding to the G and D bands of rGO, as shown in Fig.6.2b. The intensity of the D peak was slightly higher than that for the G peaks, due to the presence of defects or structural disorder in the basal plane of graphene during the reduction from graphene oxide

[12]. Fig.6.2c shows the surface morphology of the prepared rGO, confirming a loosely bound, fluffy, sheet-like structure.

We fabricated a lead-free, eco-friendly, biocompatible rGO-ZnO nanowire composite nanogenerator, using a simple, low-cost method. The fabrication process is shown in the schematic diagram in Fig.6.3. To prepare the rGO-ZnO nanowire composite, ZnO nanowires were grown using the vapor transport method (chapter-5) and rGO was synthesized from graphene oxide.



Fig.6.3. Schematic representation of composite nanogenerator fabrication

XRD, FTIR and Raman spectroscopy, and FE-SEM measurements were performed on the prepared composite. The XRD pattern indicated a wurtzite structure corresponding to hexagonal ZnO, which is shown in Fig.6.4a. All of the diffraction peaks observed in the composite were well matched with the standard Joint Committee on Powder Diffraction Samples (JCPDS) file (3-1457) [13]. No obvious peak related to rGO was observed in the composite, which may be due to presence of small amounts of rGO, as well as the emergence of high intensity peaks related to ZnO. The FTIR spectrum of the composite confirmed the presence of a

skeletal vibration peak for graphene at 1565 cm^{-1} and the characteristic peak of Zn-O at 514 cm^{-1} (Fig.6.4b).

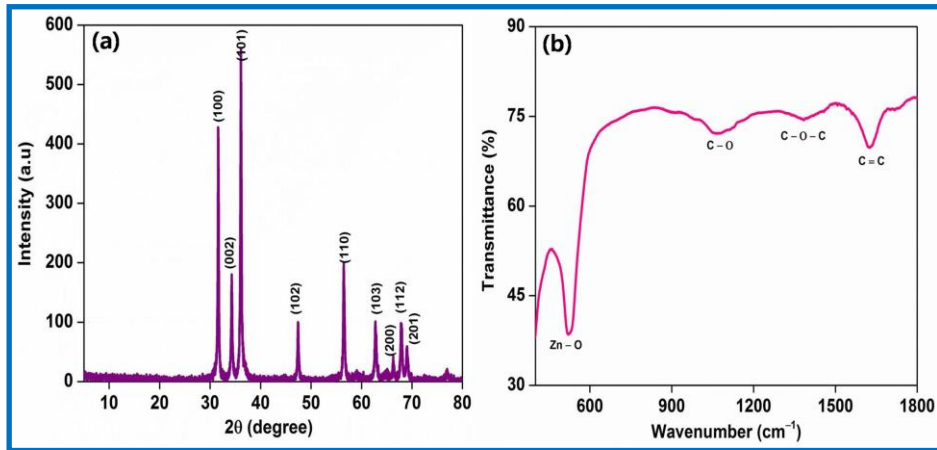


Fig.6.4. Reduced graphene oxide (rGO)-ZnO nanowire composite, (a) X-ray diffraction (XRD) pattern, (b) Fourier transform infrared (FTIR) spectrum.

The structure of the as-prepared rGO-ZnO composite was evaluated by Raman spectroscopy (Fig.6.5). Peaks were observed at 98, 201, 327, 434, and 577 cm^{-1} corresponding to ZnO, specifically, E_2 (low), B_1 (low), A_1 (TO), E_2 (high), and A_1 (low), respectively. The peaks at 1355 and 1596 cm^{-1} corresponded to the D and G bands of rGO.

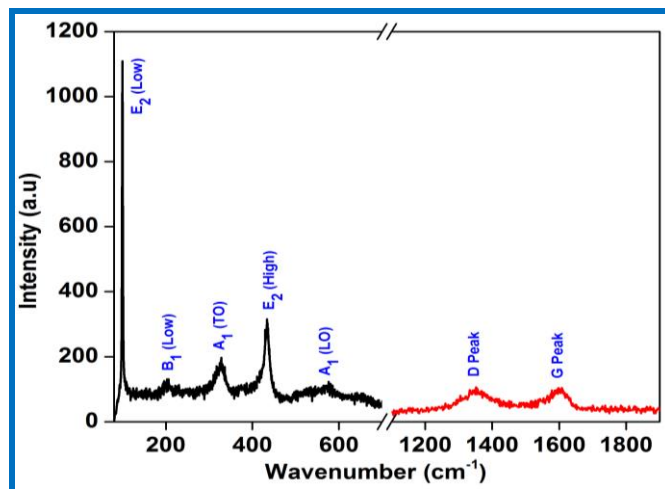


Fig.6.5. Raman Spectrum of rGO-ZnO composite

The FE-SEM images confirmed the distribution of ZnO nanowires and intercalation with rGO in the prepared composite. The presence of rGO prevents agglomeration and distributes the ZnO nanowires. From the homogeneous distribution of ZnO nanowires and intercalated rGO sheets (Fig.6.6 a, b), we expected improved electrical performance for the nanogenerator. Here, rGO played an important role as a dispersing agent, stress reinforcement, and conduction path between nanowires for enhanced piezo-potential extraction from the nanowires. The composite film was fabricated by mixing the rGO-ZnO composite with PDMS having a film thickness of $\sim 220 \mu\text{m}$; the thickness was confirmed in cross-sectional images (Fig.6.6 c, d).

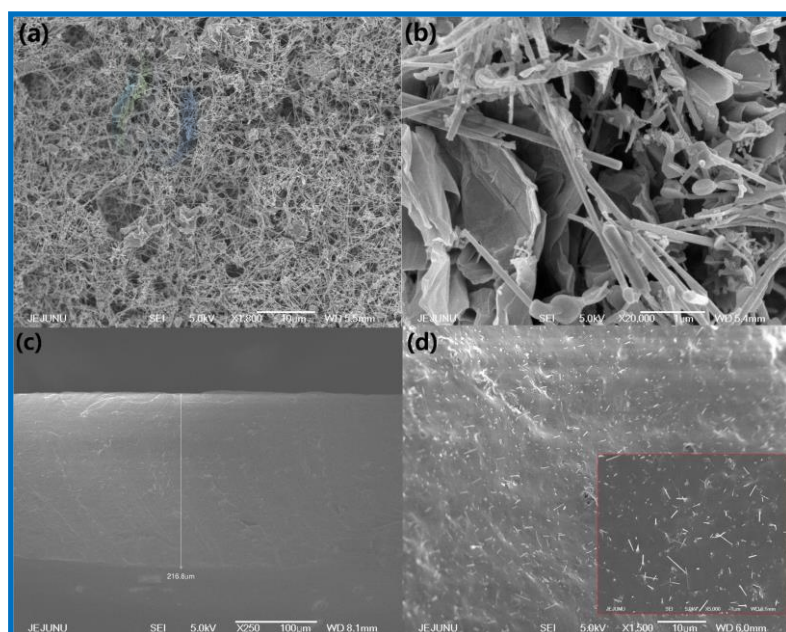


Fig.6.6. Field-emission scanning electron microscopy (FE-SEM) image, (a) and (b) lower and higher magnified image of rGO-ZnO composite. Cross Sectional view of PDMS- rGO-ZnO composite film, (c) lower, and (d) higher magnification.

To characterize the electrical performance of the composite film, we fabricated a nanogenerator device with an active area of $4 \times 4 \text{ cm}^2$. The electrical

measurement was carried out under continuous periodic mechanical deformation by pressing through palm impact and foot stamp. Fig.6.7 shows the electrical output performance of the composite nanogenerator under continuous palm impact in forward and reverse connection conditions. To check that the measured output was only from the piezoelectric effect of the device, we performed polarity-switching tests. Fig.6.7a shows a schematic diagram of the device connection configuration with measurement unit. The device delivered an average peak-to-peak voltage and current of 13.6 V and 2.33 μA , respectively, with an output power of 31.69 μW under forward connection. Under a reverse connection, the measured output signals were inverted, with an average peak-to-peak output voltage and current of 15.5 V and 2.26 μA , respectively, and an output power of 35.03 μW ; these values were higher than those reported previously [4,5,14 16].

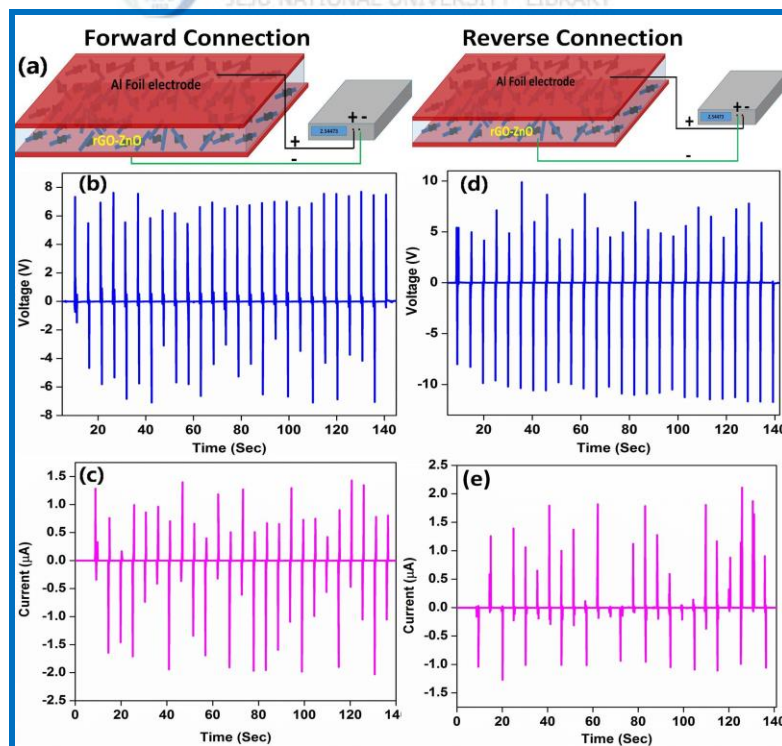


Fig.6.7. Measured output performance of the composite nanogenerator under palm impact. a) Schematic representation of the polarity test. The voltage and current under forward connection (b, c) and reverse connection (d, e).

An enlarged view of the voltage curve under forward and reverse connection conditions is shown in Fig.6.8. The variation in the output voltage and current under forward and reverse conditions was attributed to the different strain rate experienced in the device.

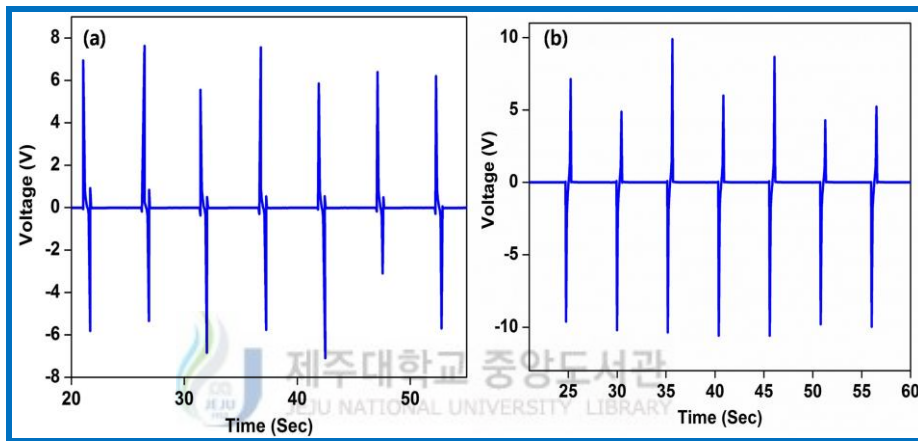


Fig.6.8. Enlarged view of the voltage curve of the composite nanogenerator under forward (a), and reverse (b) connections.

To demonstrate the capability of the device to harvest biomechanical energy during human body movements, such as walking and running, we tested our device under foot stamp (walking) conditions, using the device connection shown in Fig.6.9a. The output voltage and current were measured during foot stamp (human walking); an average voltage and current of 5.5 V and 0.63 μ A, respectively, were recorded (Fig.6.9). These values were higher than the reported values [17]. Based on these results, the rGO-ZnO based composite nanogenerator is a promising device for harvesting mechanical energy during walking, running, or vehicle transport.

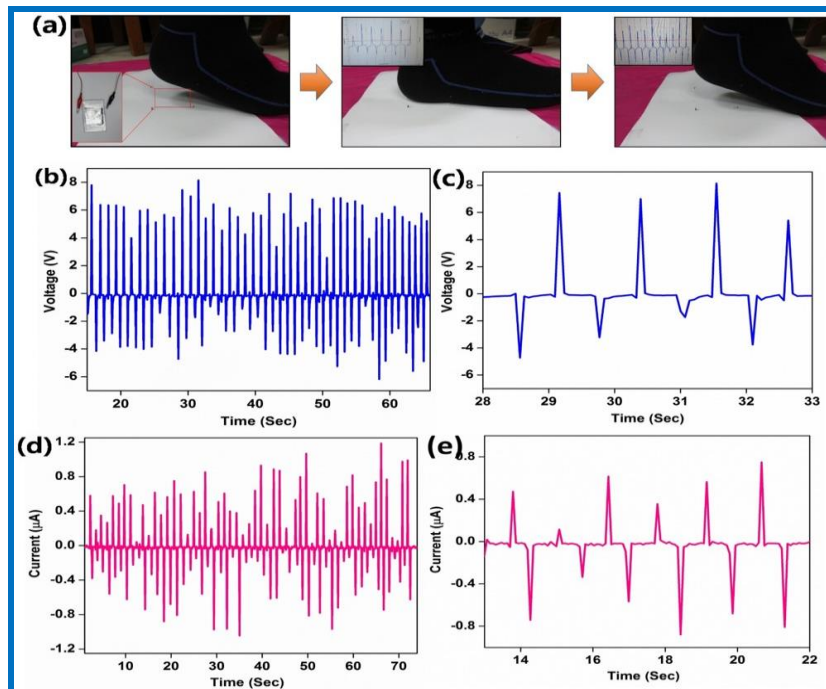


Fig.6.9. Measured output performance of the composite nanogenerator under foot stamp: a) digital image of the foot stamp at different stages, b) output voltage, and c) enlarged view of the voltage signal. d) Output current and e) enlarged view of the current signal.

The enhanced power generation mechanism in the composite nanogenerator can be explained by the piezoelectric effect. The ZnO nanowires undergo compressive strain via the PDMS polymer, when subjected to external mechanical deformation perpendicular to the device. Under this condition, a separation of the static ionic charge centers occurs in the wurtzite ZnO crystal along the nanowire surface; this results in a piezoelectric potential gradient along the nanowire surface [18]. The resultant piezo-potential induces a potential difference across the electrode surface, which drives the electrons in the external circuit. The applied compressive strain on the nanowire vanishes when the external force is removed, eliminating the piezo-potential in the nanowire. As a result, electrons flow in the opposite direction via an external circuit for charge neutrality, resulting in the reverse (negative) signal.

To show the potential of the composite nanogenerator, we performed control experiments with only PDMS and PDMS-ZnO devices. The output of these devices, shown in Fig.6.10, clearly indicated that the output power of the composite nanogenerator was higher than the bare ZnO nanowire device.

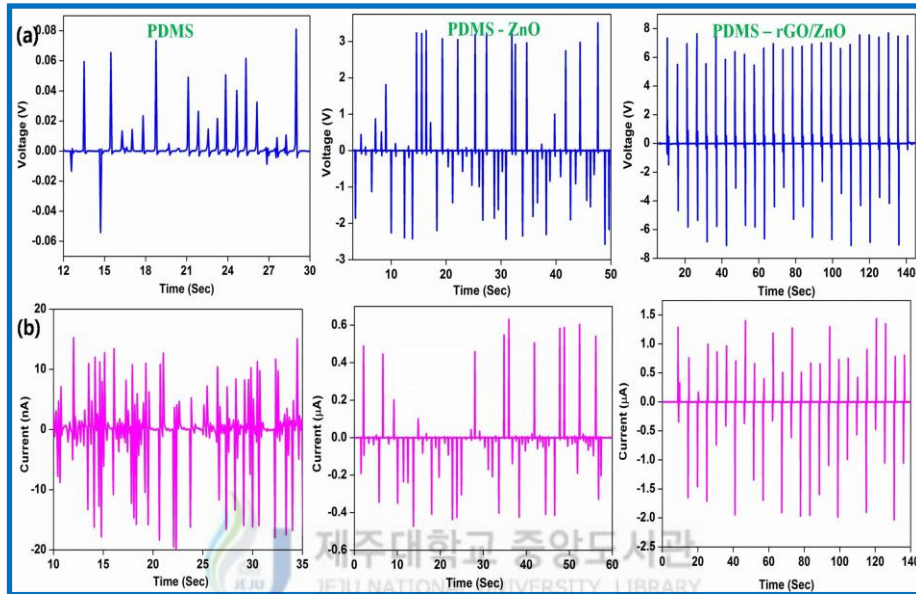


Fig.6.10.The output performance of the only PDMS, PDMS-ZnO, PDMS-rGO-ZnO composite device with same device size and thickness (a) Voltage, (b) Current. The graphene in the composite enhanced the output voltage and current of the composite device, compare to only ZnO device.

The higher output of the composite nanogenerator was attributed to the following. The presence of rGO in the composite reduced nanowire aggregation, and the higher aspect ratio of rGO distributed the nanowires uniformly throughout the polymer matrix, compared with the PDMS-ZnO device. Moreover, rGO acted as filler that enhanced the stress over the ZnO nanowire in the device and improved its mechanical stability, compared with the bare ZnO device. Finally, rGO formed an electrical bridge between the nanowires and varied the dielectric constant of the device via Maxwell–Wagner–Sillars (MWS) polarization and microcapacitance

effects [19]. The generated open-circuit voltage of the device can be calculated as follows [20]:

$$V_{OC} = g_{33}\sigma Yt \text{ ----- (1)}$$

where σ is the strain in the perpendicular direction, g_{33} is the piezoelectric voltage constant ($g_{33} = d_{33} / \epsilon_0 K$), d_{33} is the piezoelectric charge constant, ϵ_0 is the permittivity of free space, K is the dielectric constant or relative permittivity, Y is Young's modulus, and t is the thickness of the device. From Eq. (1), the piezoelectric output voltage depends mainly on g_{33} and σ . The presence of rGO improved the strain over the nanowire and the dielectric constant of the composite film.

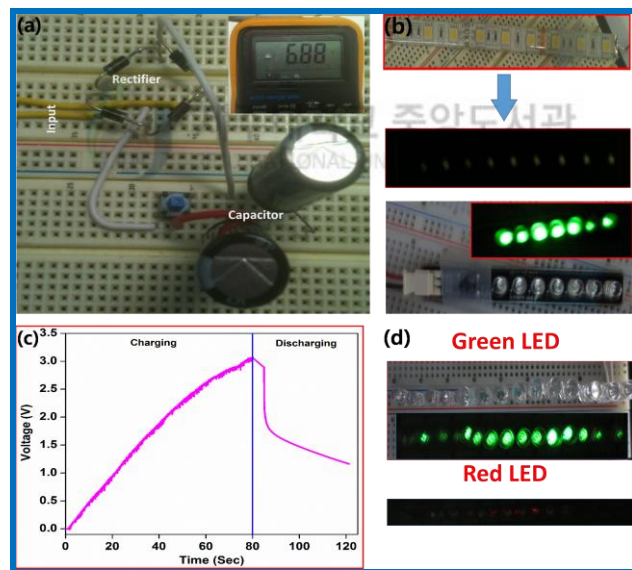


Fig.6.11. (a) Digital image of the constructed bridge rectifier circuit and capacitors. Inset show the digital image of stored voltage in the capacitors (top) b) Snapshot of the LEDs (warm white, green) before and after power up c) Capacitor charging curve under mechanical deformation. d) Snapshot of glowing 15 green and 10 red without storage using large-area nanogenerator.

To show the potential of the composite nanogenerator, we used this nanogenerator to power commercial LEDs, LCDs, and segmented displays. To demonstrate these applications, we constructed a bridge rectifier circuit (Fig.6.11a)

for the harvested energy, which was then stored in a commercial capacitor (100 μF). Fig.6.12a, b shows the rectified voltage and current of the composite nanogenerator, 14.3 V and 2.46 μA , respectively, in agreement with the peak-to-peak values of the device. The insets in Fig.6.11a show the voltage value stored in the two commercial capacitors connected in series and Fig.6.11a shows the charging curve of the capacitor (3.2 V in 80 s). The stored energy was used to power a commercial serial warm-white LED (length: 0.3 m) (Fig.6.11b). Further, we used this rectified power to drive directly seven green LEDs, without storage (Fig.6.11d).

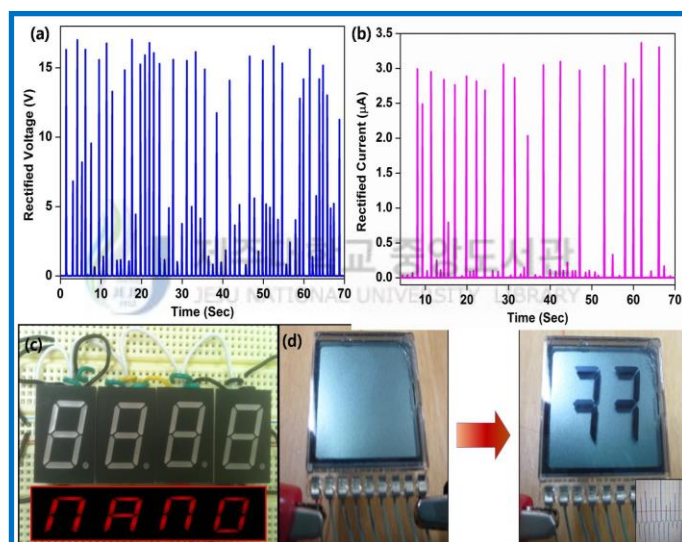


Fig.6.12. Composite nanogenerator, (a) rectified voltage, and (b) rectified current.(c) Snapshot of the segmented display, (d) Snapshot of the LCD display.

We constructed a series of four seven-segmented displays to spell the word “NANO”. These displays were powered by harvested energy (capacitor), as shown in Fig.6.12c. Finally, a LCD was directly operated by the composite nanogenerator during pressing/release, without rectification and storage. The LCD display is a non-polar device that can operate under an alternating current (AC) signal when the signal is greater than the turn-on voltage of the LCD device (Fig.6.12d).

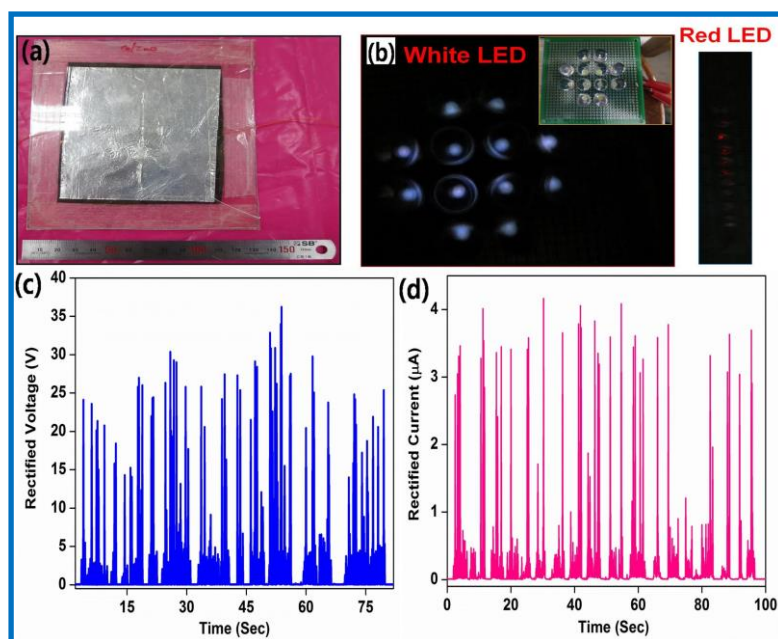


Fig.6.13. Large-area nanogenerator, (a) digital image, (b) snapshots of 12 white and 10 red LEDs glowing, (c) rectified voltage, and (d) rectified current.

The method used to fabricate the composite-based nanogenerator was simple; thus, this method could easily be applied to large-scale production. To demonstrate this, we fabricated a large-area composite nanogenerator (area: $11 \times 10 \text{ cm}^2$) by casting the composite in a Petri dish. The thickness and size of the film were controlled by adjusting the mass of the composite and the size of the Petri dish. To reduce the cost and facilitate scale-up, we used commercially available Al foil as an electrode. A digital image of the fabricated large-area composite nanogenerator is shown in the inset of Fig.6.13. The large-area composite nanogenerator produced a maximum rectified voltage and current of 35 V and 4 μA , respectively, under palm impact (Fig.6.13c, d). The harvested energy was directly applied to simultaneously lighting 12 commercial white (Fig.6.13b), 15 green, and 10 red LEDs, without storage, under continuous impact (Fig.6.13b). These results demonstrate that the fabricated composite nanogenerator is a good candidate for self-powered personal

electronic device applications. The fabricated composite nanogenerator exhibited several advantages. First, the fabrication process was simple, inexpensive, and could be easily adapted to large-scale production. Second, the materials used were non-toxic, lead-free, and biocompatible.

6.4. Conclusion

We fabricated a biocompatible, lead-free, eco-friendly composite nanogenerator using ZnO nanowires and rGO. The fabricated device showed a higher response to palm impact, delivering a maximum voltage and current of 15.5 V and 2.26 μ A, respectively, with a higher output power of 35.03 μ W. The composite nanogenerator generated an output voltage and current of 5.5 V and 0.63 μ A, respectively. We successfully fabricated a large-area composite nanogenerator that displayed higher output performance. This composite nanogenerator was then used to power LEDs of various colors (green, white, warm white, and red); further, this nanogenerator was used to operate segmented displays and LCDs, without the need for external power.

References

- [1] B. Saravanakumar, R. Mohan, S. J. Kim, An Investigation of the Electrical Properties of p-type Al:N Co-doped ZnO Thin Films. *J. Korean Phys. Soc.* 61 (2012), 1737-1741.
- [2] B. Saravanakumar, R. Mohan, K. Thiyagarajan, S. J. Kim, Investigation of UV Photoresponse Property of Al, N Co-doped ZnO Film. *J. Alloys Compd.* 580 (2013), 538–543.
- [3] Z. L. Wang, W. Wu, Nanotechnology-Enabled Energy Harvesting for Self-Powered Micro-/Nanosystems. *Angew. Chem. Int. Ed.* 51 (2012), 11700-11721.
- [4] K.I. Park, M. Lee, Y. Liu, S. Moon, G.T. Hwang, G. Zhu, J.E. Kim, S.O. Kim, D.K. Kim, Z.L. Wang, K.J. Lee, Flexible Nanocomposite Generator Made of BaTiO₃ Nanoparticles and Graphitic Carbons. *Adv. Mater.* 24 (2012), 2999.
- [5] C. Jeong, K. Park, J. Ryu, G. Hwang, K. J. Lee, Large-Area and Flexible Lead-Free Nanocomposite Generator Using Alkaline Niobate Particles and Metal Nanorods Filler. *Adv. Funct. Mater.* 24 (2014), 2620-2629.
- [6] K. Thiyagarajan , A. Ananth, B. Saravanakumar, Y.S. Mok, S.J. Kim, Plasma-induced Photoresponse in Few-layer Graphene. *Carbon* 73 (2014), 25-33.
- [7] K. Thiyagarajan, B. Saravanakumar, R. Mohan, S.J. Kim, Self-Induced Gate Dielectric for Graphene Field-Effect Transistor. *ACS Appl. Mater. Interfaces* 5 (2013), 6443–6446.

- [8] K. Thiyagarajan, B. Saravanakumar, R. Mohan, S.J. Kim, Thickness-Dependent Electrical Transport Properties of Graphene. *Sci. Adv. Mater.* 5 (2013), 542-548.
- [9] B. Kumar, K.Y. Lee, H.K. Park, S.J. Chae, Y.H. Lee, S.W. Kim, Controlled Growth of Semiconducting Nanowire, Nanowall, and Hybrid Nanostructures on Graphene for Piezoelectric Nanogenerators. *ACS Nano* 5 (2011), 4197–4204.
- [10] A. Ramadoss, G.S. Kim, S.J. Kim, Fabrication of Reduced Graphene oxide/TiO₂ Nanorod/Reduced Graphene Oxide Hybrid Nanostructures as Electrode Materials for Supercapacitor Applications. *Cryst. Eng. Comm.* 15 (2013), 10222-10229.
- [11] B. Saravanakumar, R. Mohan, S.J. Kim, Facile Synthesis of Graphene/ZnO Nanocomposites by Low Temperature Hydrothermal Method. *Mater. Res. Bull.* 48 (2013), 878-883.
- [12] A. Ramadoss, S. J. Kim, Improved Activity of a Graphene–TiO₂ Hybrid Electrode in an Electrochemical Supercapacitor. *Carbon* 63 (2013), 434-445.
- [13] R. Mohan, K. Krishnamoorthy, S.J. Kim, Enhanced photocatalytic activity of Cu-doped ZnO nanorods. *Solid State Commun.* 152 (2012), 375–380.
- [14] Y. Hu, Y. Zhang, C. Xu, G. Zhu, Z.L. Wang, High-Output Nanogenerator by Rational Unipolar Assembly of Conical Nanowires and Its Application for Driving a Small Liquid Crystal Display. *Nano Lett.* 10 (2010), 5025–5031.
- [15] K.I. Park, C.K. Jeong, J. Ryu, G.T. Hwang, K.J. Lee, Flexible and Large-Area Nanocomposite Generators Based on Lead Zirconate Titanate Particles and Carbon Nanotubes. *Adv. Energy Mater.* 3 (2013), 1539.

- [16] H. Sun, H. Tian, Y. Yang, D. Xie, Y.C. Zhang, X. Liu, S. Ma, H. M. Zhao, T.L. Ren, A Novel Flexible Nanogenerator Made of ZnO Nanoparticles and Multiwall Carbon Nanotube. *Nanoscale* 5 (2013), 6117-6123.
- [17] S. Lee, J.I. Hong, C. Xu, M. Lee, D. Kim, L. Lin, W. Hwang, Z.L. Wang, Toward Robust Nanogenerator Using Aluminum Substrate. *Adv. Mater.* 24 (2012), 4398-4402.
- [18] Z.L. Wang, Piezopotential Gated Nanowire Devices: Piezotronics and Piezo-Phototronics. *Nano Today* 5 (2010), 540–552.
- [19] D. Wang, Y. Bao, J.W. Zha, J. Zhao, Z.M. Dang, G.H. Hu, Improved Dielectric Properties of Nanocomposites Based on Poly (vinylidene fluoride) and Poly (vinyl alcohol) Functionalized Graphene. *ACS Appl. Mater. Interfaces* 4 (2012), 6273–6279.
- [20] S. Xu, G. Poirier, N. Yao, PMN-PT Nanowires with a Very High Piezoelectric Constant. *Nano Lett.* 12 (2012), 2238–2242.

CHAPTER -VII

Triboelectric Nanogenerator

This chapter presents the fabrication of triboelectric nanogenerator with vertical contact mode. The triboelectric nanogenerator was fabricated using Kapton and aluminium electrification layer to create the charges. The performance of the fabricated device discussed in details.

7.1. Introduction

Recent years, new types of energy harvesting methods were developed based on contact electrification and electrostatic induction processes and it is named as “triboelectric nanogenerator”. Contact electrification is considered as a negative effect in olden days, because it creates an external electric field which destroys the performance of the devices. The electrification creates the following problems over the years, (i) damage to microelectronics, (ii) explosions during transfer of flammable liquids (e.g., during fueling of vehicles), (iii) damage caused by discharges of ungrounded helicopters, and (iv) explosions of dust in silos.[1-7] The scientists are effectively used this negative effect into some useful potential application for harvesting [8] mechanical vibration into electrical signals and other than this it is used for chemical sensors,[9, 10] electrostatic charge patterning,[11, 12] metal-ion reduction,[13–15] and laser printing[16]. In traditionally, Wimshurst

machine and Van de Graaff generator was developed to produce voltage by the process of triboelectrification and electrostatic induction.

The Fig.7.1 shows the traditional triboelectric generator generated based on Wimshurst machine and Van de Graaff generator and with working mechanisms. The fundamental mechanism in the triboelectric nanogenerator was contact induced electrification between the two different materials during contact. The polarity of the charge generated in the materials are purely depends on their triboelectric charge which is shown in Fig.7.2. The triboelectric effect is a common one it is happen every one's life, which is frequently happen in daily life. For achieving higher triboelectrification, the Materials should have few qualities that are likely less conductive or insulators, it have tendency to capture the transferred charges and retain them for an extended period of time.

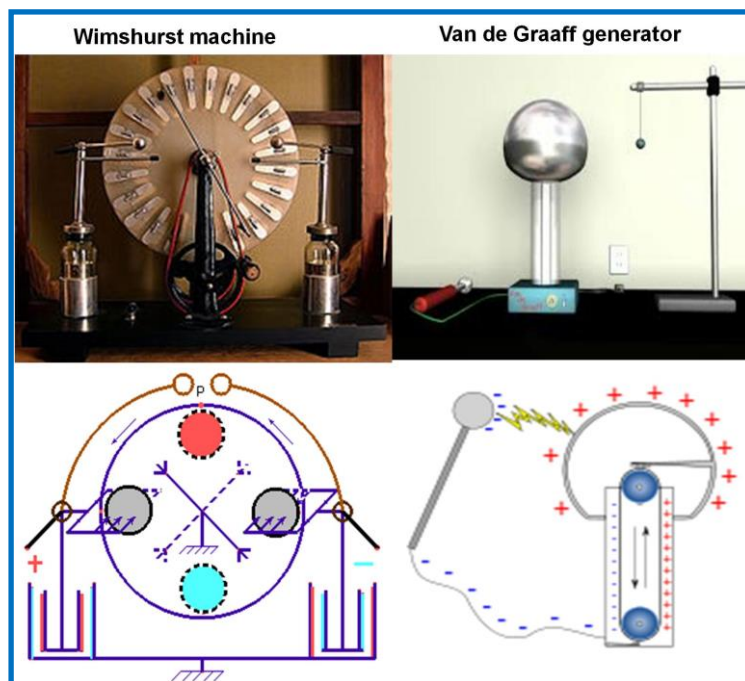


Fig.7.1. Traditional Trioelectric generator based on Wimshurst machine and Van de Graaff generator



POSITIVE CHARGE	NEUTRAL	NEGATIVE CHARGE		
	Dry Human skin		Wood	
	Leather		Cotton	Amber
	Rabbit Fur		Steel	Hard rubber
	Glass			Nickel, Copper
	Quartz			Brass, Silver
	Human hair			Gold, Platinum
	Nylon			Polyester
	Wool			Saran Wrap
	Lead			Polyurethane
	Fur			Polyethylene
	Lead			Polypropylene
	Silk			Vinyl (PVC)
	Aluminum			Silicon
	Paper			Teflon

Fig.7.2. Trioelectric series

The clear mechanisms for triboelectric charge creation in the materials are under debate, which is basically come into contact with other surface, a chemical bond was formed between these two surfaces. Due to chemical bonding, the charges move from one material to the other to equalize their electrochemical potential [17]. During separation, few bonded atoms have a tendency to leave free electrons or keep the electrons in the atom, possibly makes the charges over the surfaces. Based on this concept, there are many mode were proposed to generate the surface charges over the polymers.

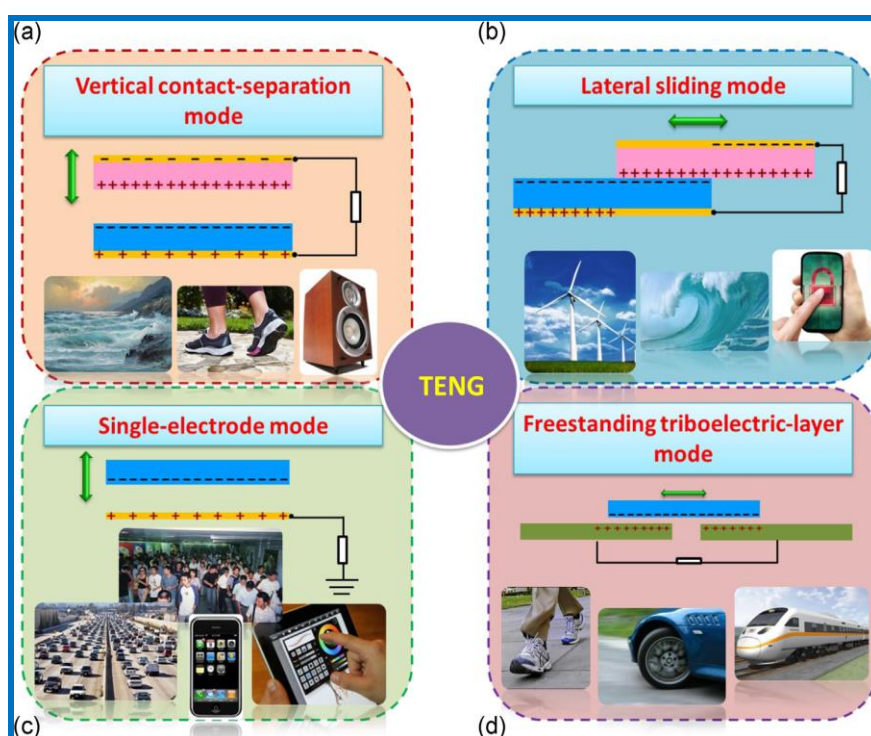


Fig.7.3. Four fundamental modes of triboelectric nanogenerators: (a) vertical contact-separation mode; (b) lateral-sliding mode; (c) single-electrode mode; and (d) free standing triboelectric-layer mode [18].

When two different triboelectric surfaces with opposite charges come into contact with each other, the triboelectric charges are generated over the surface of the concern triboelectric surfaces. Based on the triboelectric charges the concern electric charges are induced over their electrode surfaces. Due to induced charges in the electrodes create potential difference between the electrodes which drives the electron through external circuit. Based on the contact mode the triboelectrification varied and the schematic of those methods are represented [18] in Fig.7.3. There are four modes to harvest mechanical energy into electrical energy using triboelectric effect. It is vertical contact-separation, sliding, single electrode configuration and freestanding modes. The first triboelectric nanogenerator was demonstrated based on the vertical contact-separation method. In which two triboelectric materials with opposite polarity was come into contact and separated periodically. During the

contact, the tribo-charges created over the surface of the materials which is under equilibrium condition. Under the released condition, the surface charges are separated by small distance which generates the potential difference between the electrodes by induced charge over the electrodes by generated tribo-charges. Due to the potential difference electron will flow in the external circuit to compensate potential difference. At next pressing, the two charge surfaces come into contact, which forms the equilibrium between two tribosurfaces, which creates again unequilibrium in the electrodes. To compensate, the electrons are flown back through external circuit. The electron flows in the both side produce the signal in the measurement unit.

Second sliding mode, in which two surface are in contact when sliding the separation was takes place at in-plane direction. The periodic sliding produces an electrical signal by continues contact and separation at in-plane. These types of sliding motion harvest the energy from planar motions, disc rotation, or cylindrical rotation. In single electrode mode, only one triboelectric layer was used to generate the energy. In this method, the one layer induces the potential during the sliding or contact to the electrode, which is simple and applicable for many applications. At final free standing mode, the potential was in two stationary symmetry electrodes through moving (or) other tribosurface, which creates the potential difference between this electrode and electron flow through circuit due to the potential difference.

7.2. Fabrication of Triboelectric nanogenerator

The triboelectric nanogenerator was fabricated using kapton tape and aluminum, here kapton act as triboelectric material and aluminum act as an electrode as well as triboelectric layer. The kapton film was attached with aluminum foil and other surface of the kapton was rapped with salt paper to make surface roughness. The aluminum was used as a top electrode and here also rapped with salt paper. The kapton layer and aluminum was assembled like arc shape through PET substrate. The contact was made from top and bottom aluminum foil through Cu wires.

7.3. Results and discussion

We have fabricated triboelectric nanogenerator very simple by assembling kapton and aluminum in arc shape. The digital image of fabricated device structure and schematic diagram was shown in Fig.7.4.

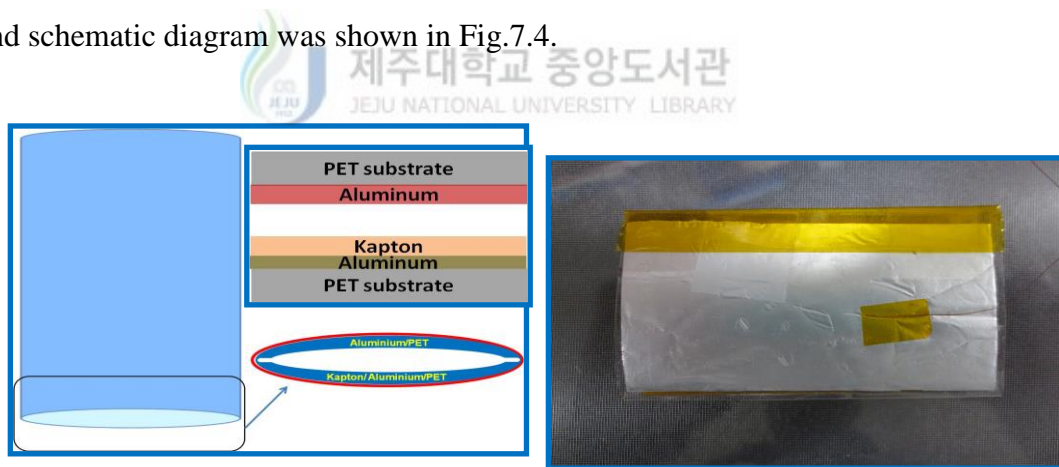


Fig.7.4. Schematic diagram and digital image of the fabricated triboelectric nanogenerator

Fig.7.5. represents the schematic diagram of energy conversion mechanism. The working mechanism basically constructed based on contact electrification and electrostatic induction. In originally there is no electric charge over the triboelectric materials (kapton, aluminum). When top aluminium electrode come to contact with down kapton due to applied external force, it will create the triboelectric charge

(negative) over kapton surface and positive on aluminium through contact electrification. At contact state the charge equilibrium was maintained by top aluminium and kapton. When release the force, the top aluminium separated from the kapton, i.e., positive charge and negative charges are separated by some distance. The separation of positive and negative charges creates the field over the surfaces. The negative field over the kapton surface induces the positive charge in the bottom aluminium electrode.

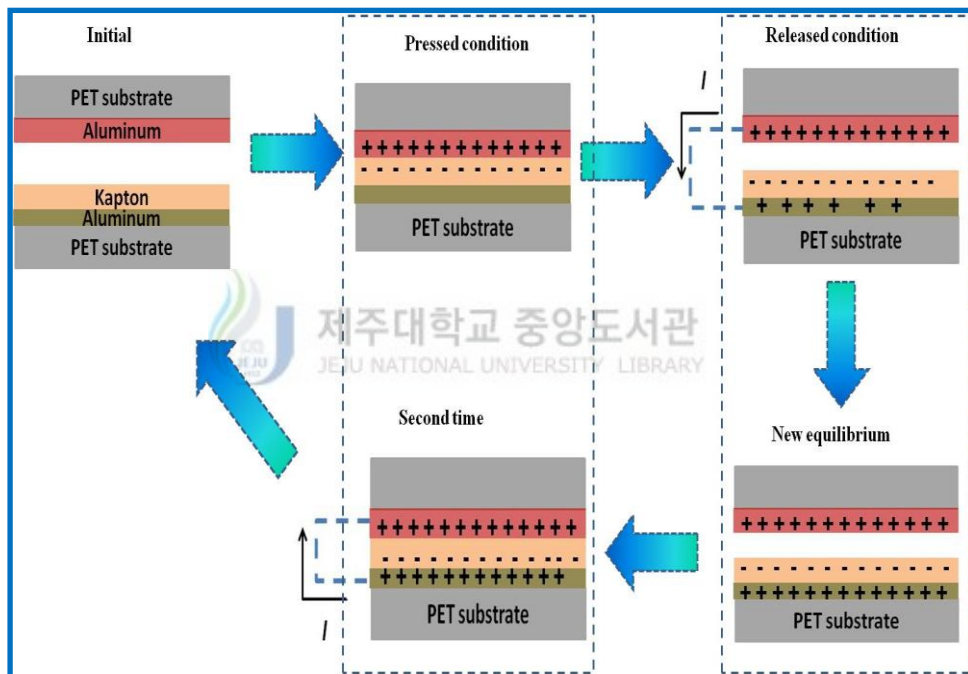


Fig.7.5. Working mechanism of the triboelectric nanogenerator

The potential difference between the top and bottom aluminium drives the electron through external circuit through load. Until to reach new equilibrium state, the electrode will flows through external circuit. At equilibrium, again pressing the device, second time aluminium is contact with kapton. At this moment surface induced charges over kapton and aluminium surfaces breaks the equilibrium state. To attain equilibrium, again electron flows through the external circuit in opposite

direction. This process will continue and electron will flows in forward and reverse the direction in the external circuit produces AC signal in load resistance.

The measured output signals from the fabricated triboelectric nanogenerator were shown in Fig.7.6. The maximum output voltage and current was measured around 2.3 V and 0.6 μA under forward connection. When reverse the connection configuration the signal are inverted and output was measured as 0.2 V and 0.03 μA

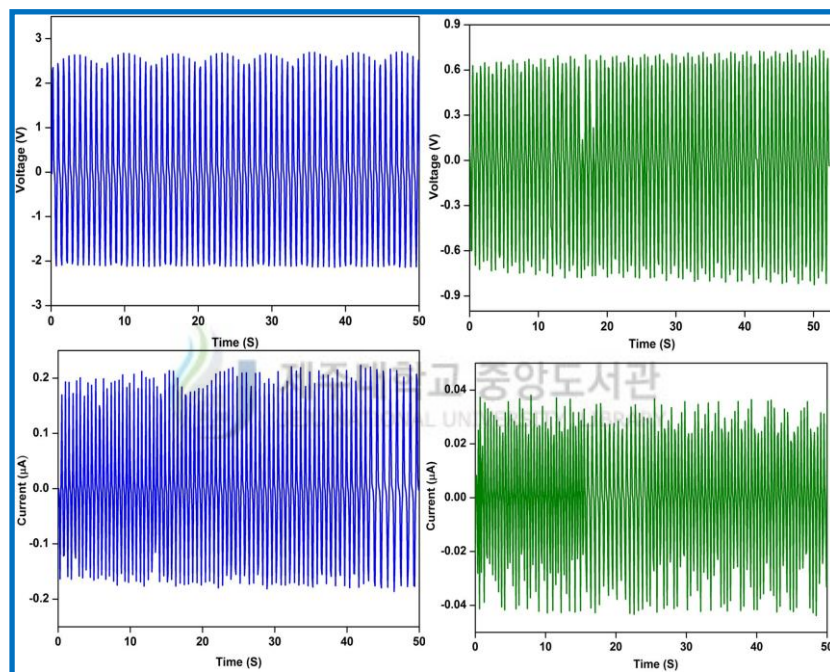


Fig.7.6. The measured open-circuit voltage and short circuit current under forward and reverse connection

7.4. Conclusion

We have successfully fabricated triboelectric nanogenerator using kapton and aluminum. Here kapton and aluminium have negative and positive triboelectric series. The fabricated device worked under vertical contact –separation method. The electric signal generation mechanism was discussed in detail. The fabricated device generated the maximum open circuit voltage and short circuit current of 2.3 V and 0.6 μ A respectively.



References

- [1] L.S. McCarty, G.M. Whitesides, Electrostatic Charging Due to Separation of Ions at Interfaces: Contact Electrification of Ionic Electrets, *Angew. Chem., Int. Ed.* 47 (2008), 2188–2207.
- [2] A.F. Diaz, Contact Electrification of Materials. The Chemistry of Ions on Polymer Surfaces, *J. Adhes.* 67 (1998), 111–122.
- [3] S.W. III. Thomas, S.J. Vella, G.K. Kaufman, G.M. Whitesides, Patterns of Electrostatic Charge and Discharge in Contact Electrification, *Angew.Chem., Int. Ed.* 47 (2008), 6654–6656.
- [4] L.S. McCarty, A. Winkleman, G.M. Whitesides, Ionic Electrets: Electrostatic Charging of Surfaces by Transferring Mobile Ions upon Contact, *J. Am. Chem. Soc.* 129 (2007), 4075–4088.
- [5] N. Gibson, Static Electricity — an Industrial Hazard Under Control?, *J. Electrostat.* 40 (1997), 21–30.
- [6] M. Glor, K. Schwenzfeuer, Occurrence of Cone Discharges in Production Silos, *J.Electrostat.* 40 (1997), 511–516.
- [7] J. Paasi, H. Salmela, J. Smallwood, Electrostatic Field Limits and Charge Threshold for Field-Induced Damage to Voltage Susceptible Devices, *J. Electrostat.* 64 (2006), 128–136.
- [8] F.R. Fan, Z.Q. Tian, Z.L. Wang, Flexible Triboelectric Generator, *Nano Energy* 1 (2012), 328–334.
- [9] Z.H. Lin, G. Zhu, Y.S. Zhou, Y. Yang, P. Bai, J. Chen, Z.L. Wang, A Self-Powered Triboelectric Nanosensor for Mercury Ion Detection, *Angew. Chem.* 125 (2013), 5169–5173

- [10] Z.H. Lin, Y. Xie, Y. Yang, S. Wang, G. Zhu, Z.L. Wang, Enhanced Triboelectric Nanogenerators and Triboelectric Nanosensor Using Chemically Modified TiO₂ Nanomaterials, *ACS Nano* 7 (2013), 4554–4560.
- [11] X. Ma, D. Zhao, M. Xue, H. Wang, T. Cao, Selective Discharge of Electrostatic Charges on Electrets Using a Patterned Hydrogel Stamp, *Angew. Chem.* 122 (2010), 5669–5672
- [12] D. Zhao, L. Duan, M. Xue, W. Ni, T. Cao, Patterning of Electrostatic Charge on Electrets Using Hot Microcontact Printing, *Angew. Chem.* 121 (2009), 6827–6831
- [13] C.Y. Liu, A.J. Bard, Electrostatic Electrochemistry at Insulators, *Nat. Mater.* 7 (2008), 505–509
- [14] C.Y. Liu, A.J. Bard, Chemical Redox Reactions Induced by Cryptoelectrons on a PMMA Surface, *J. Am. Chem. Soc.* 131 (2009), 6397–6401
- [15] B. Baytekin, H.T. Baytekin, B.A. Grzybowski, What Really Drives Chemical Reactions on Contact Charged Surfaces? *J. Am. Chem. Soc.* 134 (2012), 7223–7226
- [16] D.M. Pai, B.E. Springett, Physics of Electrophotography, *Rev. Mod. Phys.* 65 (1993), 163–211
- [17] Z.L. Wang, Triboelectric Nanogenerators as New Energy Technology for Self-Powered Systems and as Active Mechanical and Chemical Sensors, *ACS Nano*, 7 (2013), 9533–9557.
- [18] S. Wang, L. Lin, Z.L. Wang, Triboelectric Nanogenerators as Self-powered Active Sensors, *Nano Energy* 11 (2015), 436–462

CHAPTER - VIII

Self-powered Device Applications

This chapter demonstrates that the fabrication and operation of self-powered devices by integrating with nanogenerator and sensors. In first, I fabricated single ZnO microwire based pH sensor and characterized the device. Then, I carried out detailed electrical measurement under different pH environment. Finally, I integrated pH sensor with PVDF- ZnO nanowire composite nanogenerator for self-powered operation. The result of the fabricated self-powered device was clearly indicating the output variation with pH variation. Secondly, I fabricated UV photo sensor using ZnO nanowire and characterized the fabricated device. Then, I measured electrical output of the device with different illumination wavelength (365, 405 and 535 nm) and dark conditions. Finally, I integrated the photo sensor with reduced graphene oxide (rGO) - ZnO nanowire composite nanogenerator to perform the self-powered UV sensing application. Based on this results, nanogenerator based self-powered nanosensors are good candidature for future self-powered sensor application in hazardous environment.

8.1. Introduction

The tremendous growth in the electronics industry has resulted in the steady reduction of the operating voltages and sizes of electronic devices. At the same time, development of miniaturized power sources are highly demanded to operate those electronic devices. Due to limitation of size reduction and operation time hinders their developments [1-4]. To overcome those problems, the self-powered concept was developed, in which required energy was harvested from the environment. The integrated self-powered system provides an independent, sustainable, maintenance-free operation for long time. The self-powered device has created a huge technological impact on smart and portable nanoelectronic for environmental monitoring and sensing, or as implantable biomedical devices in small, wearable electronic applications [1]. The self-powered operation is achieved by the integration of the energy harvester with electronic devices [5, 6]. A nanogenerator is one of energy harvester, which converts low-frequency vibration and environmental activities (e.g., wind, sound, friction, and thermal energy) into electrical energy through piezoelectric, triboelectric, and pyroelectric effects [3]. The harvested energy is sufficient for the operation of small electronic devices in an aperiodic manner. The self-powered operation was achieved in two ways by, i) integrating the sensor with nanogenerator, ii) nanogenerator itself acts as a sensor. In this work, I have fabricated ZnO microwire based pH sensor and ZnO nanowire based UV photo sensor. The fabricated pH sensor and UV photo sensor/commercial sensor was integrated with PVDF - ZnO hybrid composite nanogenerator and composite nanogenerator (rGO-ZnO) respectively, for self-powered operation. The integrated

self-powered sensors successfully monitor pH and UV light without external power by utilizing from nanogenerator.

8.2. Experimental Section

8.2.1. Fabrication of the pH Sensor

The pH sensor was fabricated using a ZnO microwire, which was grown using the vapor transport method and detailed growth process was given in Chapter-2. A single ZnO microwire was positioned across a glass substrate, and both ends of the wire were affixed with silver paste. A very thin poly(methyl methacrylate) (PMMA) layer of around 100 nm was coated on the microwire surface to protect the microwire from dissolving in the buffer solution. Electrical contact was made through Cu wires; both electrical contacts were covered with epoxy. The buffer solution pH was varied from 12 to 6 by adding sodium dihydrogen phosphate (5 M NaH_2PO_4). The fabricated pH sensor was connected in parallel with a hybrid composite nanogenerator to measure the response as a function of pH value.

8.2.2. Fabrication of the UV photo sensor

The UV photo sensor was fabricated using a ZnO nanowire, which was grown using the vapor transport method and detailed growth process was given in Chapter-5. To fabricate the UV photo sensor, ZnO nanowires were dispersed in a polyvinyl alcohol (PVA) polymer solution through probe sonication. The dispersed ZnO-PVA solution was drop casting onto a patterned indium tin oxide (ITO)-coated glass substrate. The drop-cast film was dried at 100°C for 30 min and annealed at 300°C for 1 h to remove the polymer (PVA) and other impurities (physisorbed molecules on the nanowire) from the film. The connection was taken from both sides of the ITO

substrate through Cu wire using Ag paste. The fabricated UV photo sensor was connected in parallel with the composite nanogenerator to measure the response as a function of the light intensity. Also, we fabricated a self-powered UV photo sensor, using a commercial photo resistor (gl5528).

8.3. Results and discussion

8.3.1. Self-Powered pH sensor

Fig.8.1 shows the digital and optical image of the fabricated ZnO microwire based pH sensor. Further, I have measured FE-SEM, which clearly indicating that the length of the channel around 1 mm and shown in Fig.8.2.

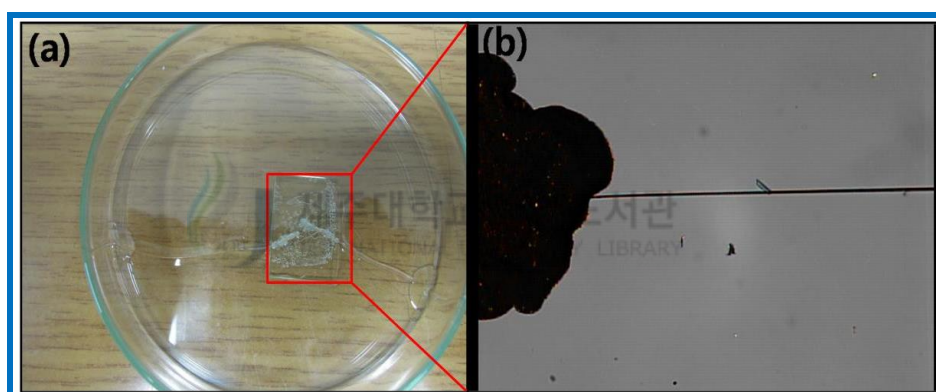


Fig.8.1.Single ZnO microwire based pH sensor, a) digital image and b) optical image

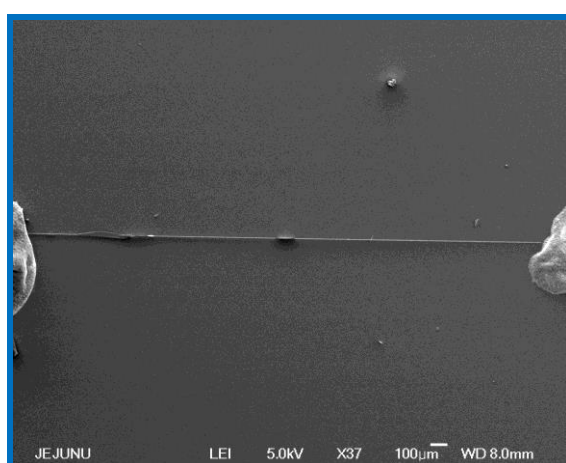


Fig.8.2. Field emission scanning electron microscopy (FE-SEM) of ZnO microwire device

We have measured the electrical behavior of the fabricated single microwire sensor under different pH environment. In this experiment, I have used phosphate buffer solution with different pH value. Initially, 50 ml of 0.1 M Na_2HPO_4 solution was prepared which have the pH of 9.2 and I have adjusted the pH value to 12 by adding NaOH. Then, I have varied the pH from 12 to 6 adding the different amount of 5 M NaH_2PO_4 solution and I have monitored I-V characteristics at each pH value which was shown in Fig.8.3.

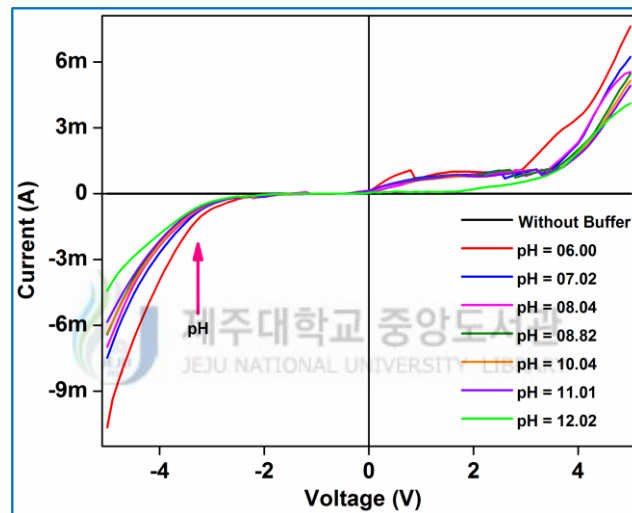


Fig.8.3. Current-voltage (*I-V*) characteristics of a ZnO microwire as a function of pH.

Under normal conditions (without buffer solution), the device showed a very low current (in the pA range), which confirmed the existence of higher resistance. Upon addition of buffer solution increased the conductivity significantly compared to bare device which is because of change in chemical environment to higher base condition (pH = 12.02) over the ZnO surface which reduced depletion layer thickness considerably and it results decrease in resistivity of the device. Further, reducing the pH values from 12 to 6 alter the chemical environment from base to acidic condition. When the solution pH changed from basic to acidic, the chemical environment

around the ZnO surface become altered, which lead to an increase in the output current. In addition, we have carried out stability measurement test at different pH value with constant bias voltage of - 0.5 V to check the device stability over time and chemical environment. The results indicate that the fabricated device has stability under basic and acidic condition over this period, which displayed in Fig.8.4. From this result, the fabricated device was good stability and which can be extent to self-powered application.

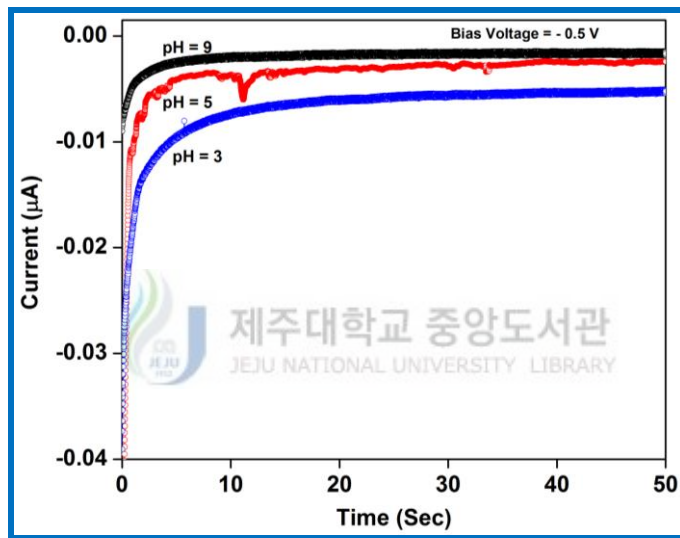


Fig.8.4. Current-time ($I-t$) characteristics of the fabricated ZnO microwire at different pH with constant bias voltage on - 0.5 V

Further, to show the self-powered operation, we fabricated a pH sensor using a ZnO microwire, connected in parallel to a hybrid nanogenerator. Fig.8.5 shows a schematic diagram of the pH sensor. The fabricated hybrid composite nanogenerator was used to drive the ZnO microwire-based pH sensor without external power.

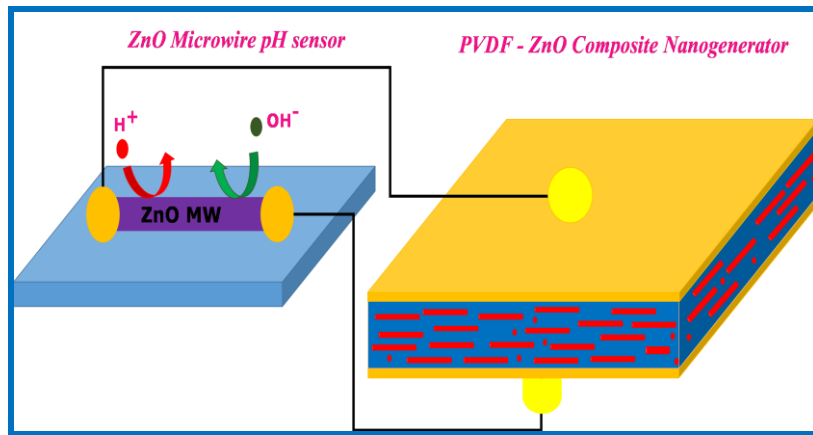


Fig.8.5. Schematic representation of the self-powered pH sensor device

When there was no buffer solution, the measured potential drop across the microwire pH sensor was ~ 0.34 V (Fig.8.6), due to the high resistance across the ZnO microwire (Fig.8.6). The introduction of a buffer solution changed the chemical environment (H^+ , OH^-) around the microwire, which altered the output voltage by changing the depletion region [7]. The measured output voltage as a function of pH value is presented in Fig.8.7; the change from basic to acidic conditions reduced the output voltage. At higher pH (base) values, a hydroxyl group on the ZnO surface combined with OH^- ions to form $Zn-O^-$ ($Zn-OH + OH^- \leftrightarrow ZnO^-$). The existence of negatively charged species ($-O^-$) produced a depletion region at the ZnO surface, and increased the resistance of the microwire. This leads to developing a potential drop across the microwire for a pH value of 12.2.

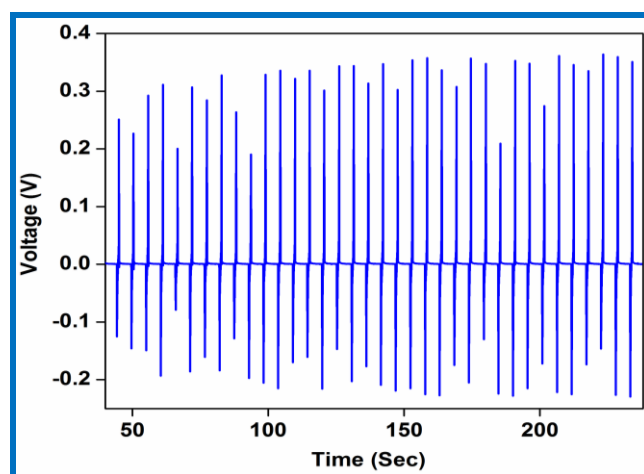


Fig.8.6. Measured electrical output voltage of self-powered pH sensor without any buffer solution.

Under lower pH conditions (acidic), the surface was modified into Zn-OH_2^- ($\text{Zn-OH}^+ + \text{H} \leftrightarrow \text{ZnOH}_2^-$) by H^+ ion adsorption, which lead to a reduction of the depletion region thickness. The pH changed from basic to acidic (12.2 to 6.02) and the O^- species were converted into OH_2^- , which reduced the output voltage by lowering the resistance across the microwire [5, 8-10]. The mechanism of the pH sensing was schematically represented in Fig.8.8. The chemical environment over the microwire surface was highly sensitive and changed the depletion layer thickness according to H^+ , OH^- ion concentration. The change of resistance across the microwire changes nanogenerator output. Simply, here pH sensor acts as a variable resistance according to pH value (Fig.8.8).

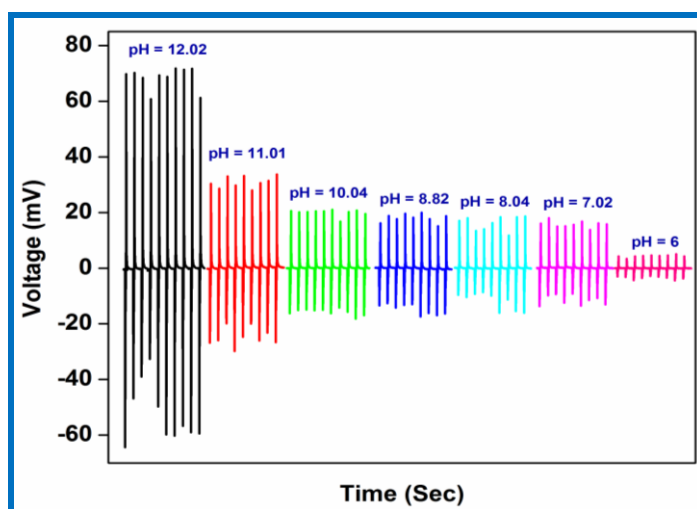


Fig.8.7. Electrical output as a function of pH across the pH sensor

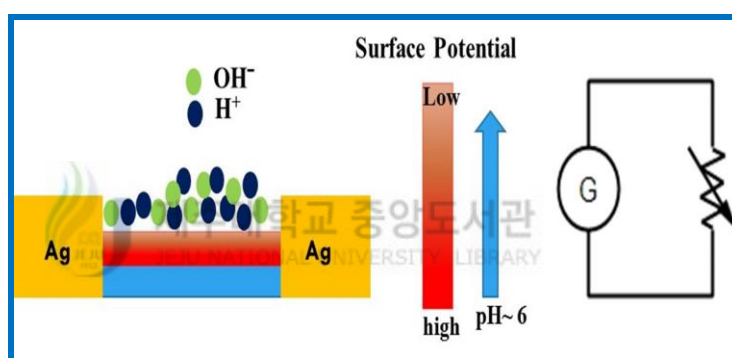


Fig.8.8. Schematic representation of pH mechanism of the self-powered device

Non-linear behavior was observed in the response current as a function of pH value, which may be due to small variations in the depletion layer at lower pH levels, it shown in Fig.8.9. A similar behavior was observed in the self-powered device, as well as in the bare ZnO device, indicating that the fabricated self-powered device could be used as a pH sensor. This study demonstrates the potential of the hybrid composite nanogenerator as a self-powered device for portable, wearable electronic device applications.

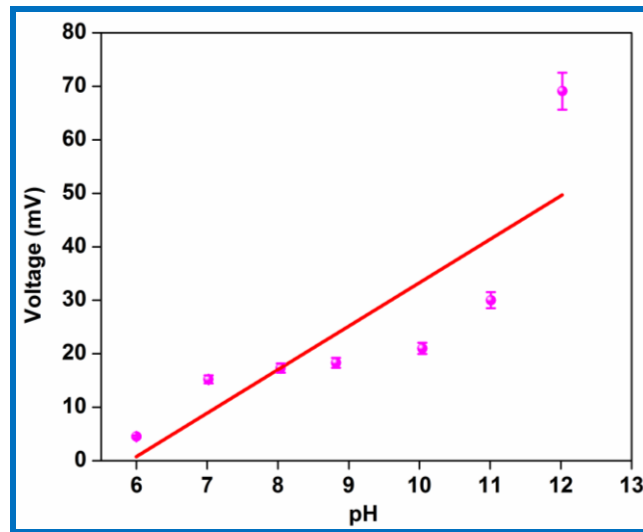


Fig.8.9. Self-powered pH sensor output voltage as a function of different pH values

8.3.2. Self-Powered UV photosensor

The Fig.8.10 shows the digital image and optical image of the fabricated ZnO nanowire photosensor.

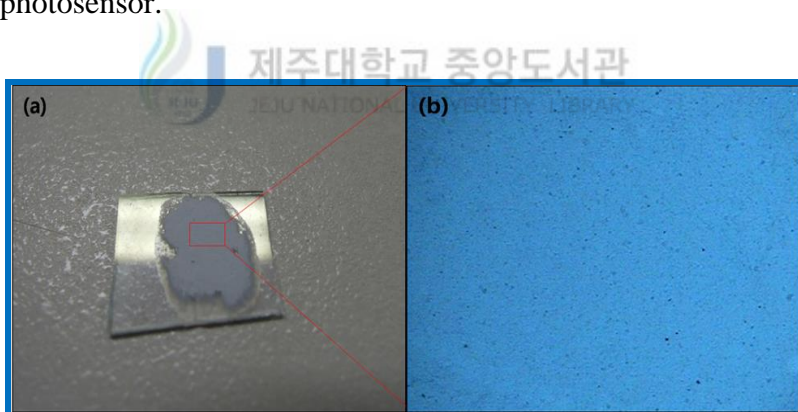


Fig.8.10. ZnO nanowire film, a) Digital image, and b, c) Optical image of the device

The film FE-SEM image (Fig.8.11) confirmed the presents of ZnO nanowire without any morphological changes during process. From this results, we confirmed that the ZnO nanowire have diameter of ~ 100 nm and length of \sim several micrometer.

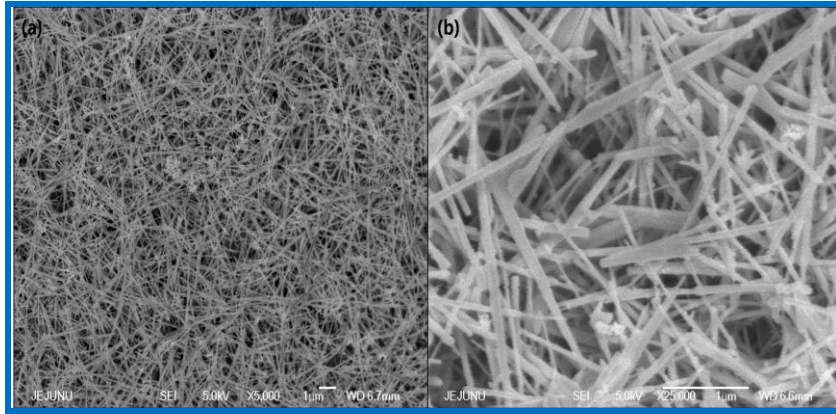


Fig.8.11. FE-SEM image of the ZnO nanowire film, a) Lower, and b) Higher magnification

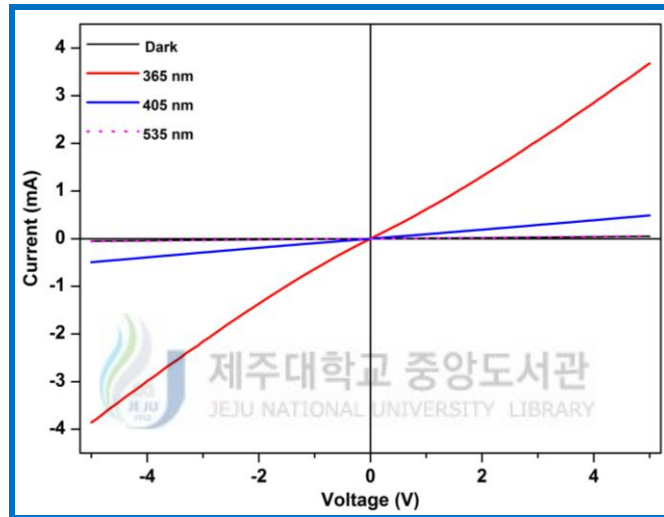


Fig.8.12. Current – Voltage (I - V) characteristic of the ZnO nanowire photo sensor with different illumination wavelength

Further, the electrical measurement was performed on the device, to confirm the electrical behavior of the device with different illumination wavelength and shown in Fig.8.12. The device showed the higher resistance under dark condition because of the chemisorbed oxygen species on the nanowire surface. The free electron present in the nanowire was draped by chemisorbed oxygen molecules which increase the resistance of the nanowire. When expose to high energy photons, the conductivity of the device increased drastically and higher response was observed for 365 nm wavelength. The detailed photocurrent generation mechanism of ZnO nanowire was schematically represented in Fig.8.13. When ZnO device expose to

environment, oxygen molecules (O_2 , O , O^{2-}) chemisorbed over the ZnO surface and deplete the free electrons from ZnO conduction band (CB) to form the depletion layer over the ZnO surface. The increase of depletion layer increased the resistance across the device. The reaction at the surface of device under dark condition given as,

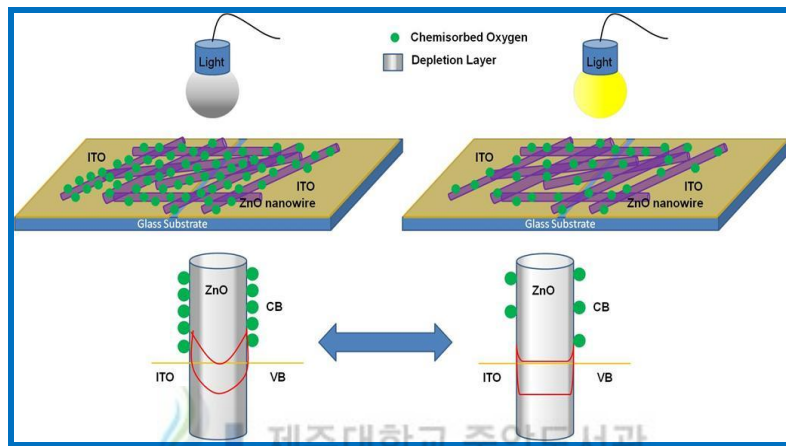
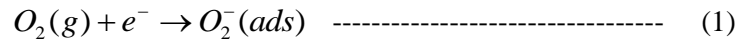
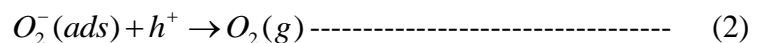


Fig.8.13. Schematic representation of the photocurrent generation mechanism in ZnO nanowire photo sensor

Upon expose the light with higher energy than band gap (3.3 eV), the electron – hole pair was created in the device, the hole migrate towards the surface and neutralize with chemisorbed oxygen species, reduces the depletion layer thickness. As a result, the unpaired electrons are generated in the device which reduced the resistance across device [11]. The neutralization reaction at ZnO surface was represented as follows,



We designed and fabricated a self-powered UV photo detector by connecting the composite nanogenerator to a UV photo detector [12]. Fig.8.14 shows a

schematic diagram of the photo detector, in which ZnO nanowire photo detector connected in parallel to the composite nanogenerator.

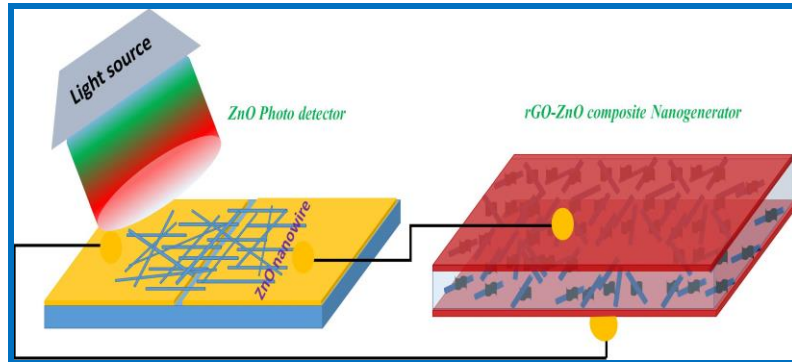


Fig.8.14. Schematic diagram of the self-powered UV photo sensor

The composite nanogenerator was used to drive the UV photo detector without external power. The response was measured as a voltage across the nanowire/photo resistor sensor. Without UV light, the voltage drop across the sensor was 60 and 80 mV at the positive and negative sides, respectively; note the higher resistance across the nanowire sensor.

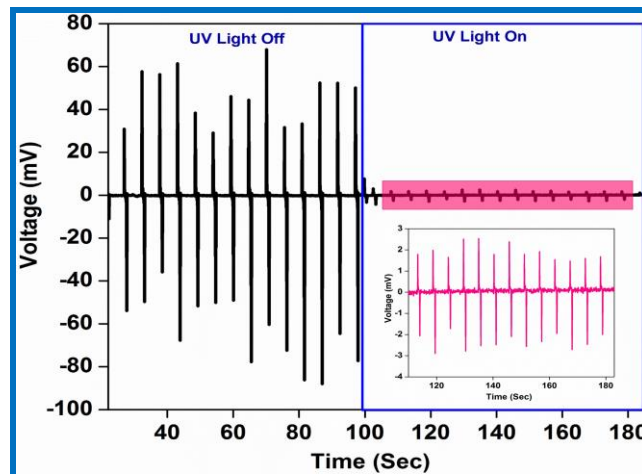


Fig.8.15. The measured response with and without UV exposes. Inset enlarged portion of pink color mark.

Hereafter, we considered only the positive side of the output to simplify the explanation. When illuminated with UV light (λ : 365 nm; intensity: 8 mW cm^{-2}), the

resistance across the sensor was reduced due to the photo generated free electrons, which reduced the voltage to 2 mV (Fig.8.15). To assess the selectivity of the device, we conducted an illumination test using various wavelengths (Fig.8.16). The measured voltage drop increased with increasing exposure wavelength, due to the change in the resistance across the sensor. The increase in the wavelength reduced the number of photo generated carriers, due to the lower photo excitation energy, in good agreement with the inherent properties of ZnO [13].

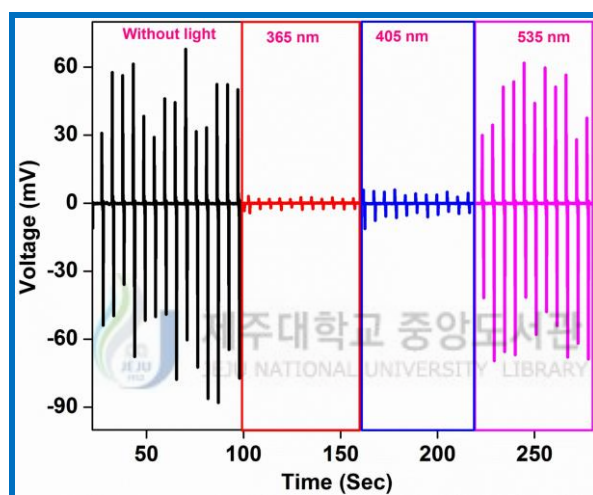


Fig.8.16. The measured response as a function of exposure wavelength.

Our composite nanogenerator was then connected to a commercial photo detector to validate our results; the results were similar to those obtained using a ZnO nanowire-based photo sensor (Fig.8.17). The self-powered UV sensor circuit consisted of a nanogenerator, a photo detector and an LED, as shown in Fig.8.18; the actual experimental set-up is shown in Fig.8.18. The rectified signal output from the nanogenerator was connected in series to the photo detector and LED. In the absence of UV light, the circuit was open, and no light was emitted under palm impact. When exposed to UV light, the circuit was shorted and the LED emitted light under impact. Thus, UV sensing was achieved via the self-powered photo detector.

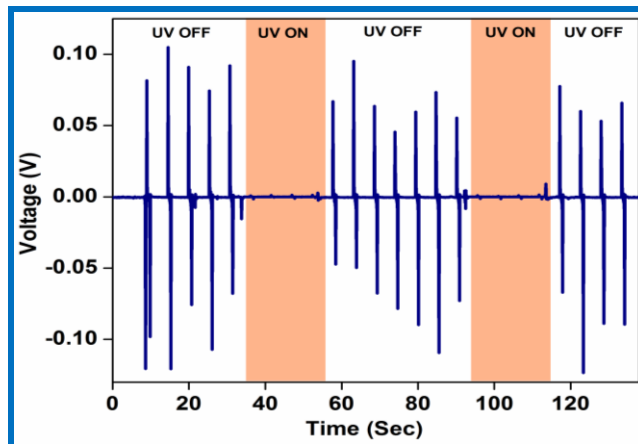


Fig.8.17. The measured response for the commercial photo sensor

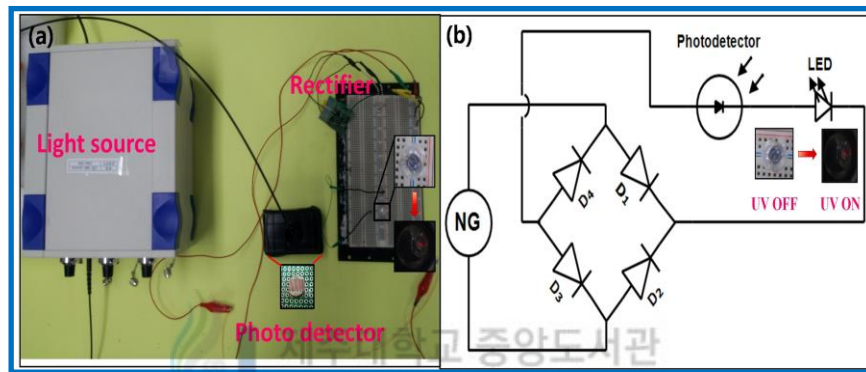


Fig.8.18. a) The digital image of the experimental setup. Inset indicates the glowing red LED during UV expose. b) Circuit diagram of the self-powered UV photo sensor.

8.4. Conclusion

We have successfully fabricated nanosensors for pH and UV sensing applications using ZnO micro and nanowires. The fabricated device was highly response to both pH variation and light illumination wavelength. Finally, we have coupled ZnO based sensors and composite nanogenerator (PVDF-ZnO and rGO-ZnO) for self-powered device application. The constructed self-powered device provided an output voltage in response to light exposure and pH variation. From this result, we concluded that the fabricated device can be used for self-powered device applications, in particular, as an environmental/hazardous material sensor.

References

- [1] Y. Yang, H. Zhang, J. Chen, S. Lee, T.C. Hou, Z.L. Wang, Simultaneously Harvesting Mechanical and Chemical Energies by a Hybrid Cell for Self-powered Biosensors and Personal Electronics. *Energy Environ. Sci.* 6 (2013), 1744-1749.
- [2] Z.L. Wang, G. Zhu, Y. Yang, S. Wang, C. Pan, Progress in Nanogenerators for Portable Electronics. *Mater. Today* 15 (2013), 532-543.
- [3] Z.L. Wang, Toward Self-powered Sensor Networks. *Nano Today* 5 (2010), 512-514.
- [4] Z. Li, G. Zhu, R. Yang, A.C. Wang, Z.L. Wang, Muscle-Driven In-vivo Nanogenerator. *Adv. Mater.* 22 (2010), 2534–2537.
- [5] S. Xu, Y. Qin, C. Xu, Y. Wei, R. Yang, Z.L. Wang, Self-powered Nanowire Devices. *Nat. Nanotechnol.* 5 (2010), 366–373.
- [6] Z.H. Lin, G. Zhu, Y.S. Zhou, Y. Yang, P. Bai, J. Chen, Z.L. Wang, A Self-Powered Triboelectric Nanosensor for Mercury Ion Detection. *Angew. Chem., Int. Ed.* 52 (2013), 1–6.
- [7] F. Patolsky, C.M. Lieber, Nanowire Nanosensors. *Mater. Today* 8 (2005), 20.
- [8] S. Al-Hilli, M. Willander, The pH Response and Sensing Mechanism of n-Type ZnO/Electrolyte Interfaces. *Sensors* 9 (2009), 7445.
- [9] B.J. Hansen, Y. Liu, R. Yang, Z.L. Wang, Hybrid Nanogenerator for Concurrently Harvesting Biomechanical and Biochemical Energy. *ACS Nano* 4 (2010), 3647.

- [10] Y. Cui, Q. Wei, H. Park, C.M. Lieber, Nanowire Nanosensors for Highly Sensitive and Selective Detection of Biological and Chemical Species. *Science* 293 (2001), 1289.
- [11] B. Weintraub, Z. Zhou, Y. Li, Y. Deng, Solution Synthesis of One-dimensional ZnO Nanomaterials and Their Applications. *Nanoscale* 2 (2010), 1573–1587.
- [12] S. Bai, L. Zhang, Q. Xu, Y. Zheng, Y. Qin, Z L. Wang, Two Dimensional Woven Nanogenerator. *Nano Energy* 2 (2013), 749–753.
- [13] B. Saravanakumar, R. Mohan, K. Thiyagarajan, S.J. Kim, Investigation of UV Photoresponse Property of Al, N Co-doped ZnO Film. *J. Alloys Compd.* 580 (2013), 538–543.



CHAPTER -IX

Summary and future direction

This chapter describes the summary of overall thesis. The thesis mainly focuses on the development of piezoelectric and triboelectric nanogenerator for energy harvesting application using ZnO micro/nanostructures. The main part of the thesis provides the development of piezoelectric nanogenerator using different ZnO micro/ nanostructures and composites such as ZnO microwire, vertically aligned ZnO nanowire array, nanowall array, PVDF-ZnO and rGO-ZnO. The second part of the thesis presents the development of self-powered devices and self-powered operation of commercial electronic devices such as light emitting diodes, liquid crystal displays etc.,. The overall outcome the thesis was schematically shown in Fig.9.1. It clearly presents the achievement and outcome the whole research during the thesis time. In future, further improvements are required in the output performance to operate real time devices for monitoring environment and biomedical health care application. I will focus to integrate energy harvesting devices with those sensors for sustainable operation with the help of energy storage devices.

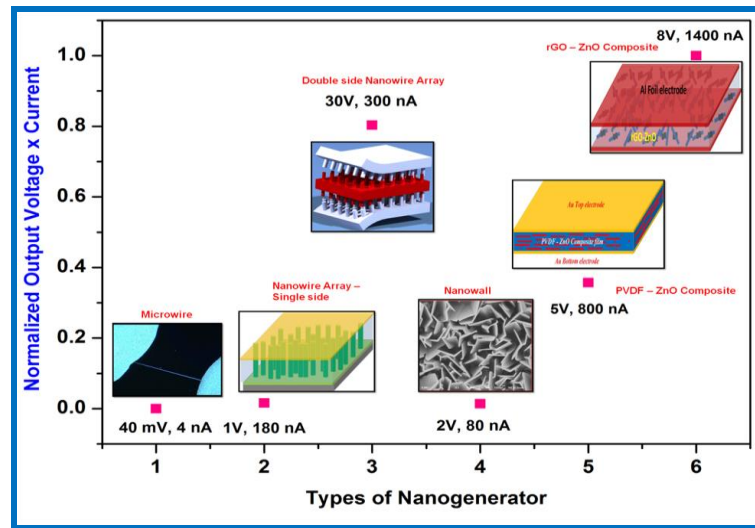


Fig.9.1. Overall outlook of the thesis

Publication and Conference

List of publications:

1. ***Balasubramaniam Saravanakumar***, Kaliannan Thiyagarajan, Nagamalleswara Rao Alluri, Shin SoYoon, , Kim Taehyun, Zong-Hong Lin and Sang-Jae Kim, Fabrication of an Eco-friendly Composite Nanogenerator for Self-powered Photosensor Applications
Carbon, 2015, 84, 56 –65.
2. ***Balasubramaniam Saravanakumar***, Shin Soyoon, and Sang Jae Kim
Self-Powered pH Sensor based on a Flexible Organic- Inorganic Hybrid Composite Nanogenerator
ACS Applied Materials & Interfaces, 2014, 6 (16), 13716-13723.
3. ***Balasubramaniam Saravanakumar*** and Sang-Jae Kim
Growth of 2D ZnO Nanowall for Energy Harvesting Application
Journal of Physical Chemistry C, 2014, 118 (17), 8831–8836
4. ***Balasubramaniam Saravanakumar***, Rajneesh Mohan, Kaliannan Thiyagarajan, Sang-Jae Kim
Fabrication of a ZnO Nanogenerator for Eco-Friendly Biomechanical Energy Harvesting
RSC Advances, 3 (37), 2013, 16646-16656
5. ***Balasubramaniam Saravanakumar***, Rajneesh Mohan, Kaliannan Thiyagarajan, Sang-Jae Kim
Investigation of UV Photoresponse Property of Al, N co-doped ZnO Film
Journal of Alloys and Compounds, 580 (15), 2013, 538-543
6. ***Balasubramaniam Saravanakumar***, Rajneesh Mohan, Sang-Jae Kim
Facile Synthesis of Graphene/ZnO Nanocomposites by Low Temperature Hydrothermal Method
Materials Research Bulletin, 48 (2), 2013, 878–883
7. ***Balasubramaniam Saravanakumar***, Rajneesh Mohan, Sang-Jae Kim

An Investigation of the Electrical Properties of p-Type Al: N Co-doped ZnO Thin Films

Journal of the Korean Physical Society, 61 (10), 2012, 1737-1741

Communicated papers:

1. Investigation of Resistive Switching Behavior of Vertically Aligned ZnO Nanorods Array

Balasubramaniam Saravanakumar and Sang-Jae Kim

Patent

1. Fabrication of new ZnO nanogenerator device structure for Eco-friendly Energy harvesting

Patent No: 10-1327876

Sang-Jae Kim, Jea-Yun Lim, In-Seok Kang, *Balasubramaniam Saravanakumar*



Papers presented in International / National conferences:

1. Fabrication of PVDF-ZnO Hybrid Composite Nanogenerator for Self-powered pH Sensor Application (Oral Presentation)

Balasubramaniam Saravanakumar, Sang Jae Kim

The 2nd International Conference on Nanogenerators and Piezotronics (NGPT-2014), Georgia Institute of Technology, Atlanta, Georgia, USA on June 9 - 11, 2014.

2. Fabrication of piezoelectric ZnO nanogenerator

Balasubramaniam Saravanakumar, Shin SoYoon, Sang Jae Kim

The 2nd International Symposium on Advanced Electromaterials (ICAE-2013), Jeju, Republic of Korea on November 12 - 15, 2013.

3. Highly Sensitive ZnO microware based UV photo detector

Rajneesh Mohan, *Balsubramaniam Saravanakumar*, Shin SoYoon, Sang Jae Kim

The 2nd International Symposium on Advanced Electromaterials (ICAE-2013), Jeju, Republic of Korea, November 12 - 15, 2013.

4. Energy harvesting using ZnO microwire nanogenerator

Balsubramaniam Saravanakumar, Shin SoYoon, Rajneesh Mohan, Sang Jae Kim

The 16th International Symposium on the Physics of Semiconductors and Applications (ISPSA-2013), Jeju, Republic of Korea, July 2 - 5, 2013.

5. Development of ZnO Nanogenerator for eco-friendly Energy Harvesting application (Oral Presentation)

Balsubramaniam Saravanakumar, Rajneesh Mohan, Kaliannan Thiyagarajan, Sang-Jae Kim,

12th Jeju- Nagasaki University Joint symposium on Science and Technology (JSST), Jeju, Republic of Korea, June, 5-7 – 2013.

6. Fabrication of triboelectric nanogenerator for self-sufficient power source application(Oral Presentation)

Shin SoYoon, *Balsubramaniam Saravanakumar*, Sang-Jae Kim,

12th Jeju- Nagasaki University Joint symposium on Science and Technology (JSST), Jeju, Republic of Korea, June, 5-7 – 2013.

7. Electrochemical properties of non-enzymatic glucose sensor using ZnO/CuO heterostructure

Shin SoYoon, Ananthakumar Ramadoss, *Balsubramaniam Saravanakumar*, Rajneesh Mohan, Sang Jae Kim

The 15th Korean MEMS Conference (KMEMS), Jeju, Republic of Korea, April 4-6, 2013.

8. Photoelectric properties of prepared Al doped ZnO thinfilms by Sol-gel method

Hong Eui Yong, *Balasubramaniam Saravanakumar*, Sang-Jae Kim

The 15th Korean MEMS Conference (KMEMS), Jeju, Republic of Korea, April 4-6, 2013.

9. Piezoelectric nanogenerator for vibration sensor

Balasubramaniam Saravanakumar, Rajneesh Mohan, Eui Young Hong and Sang-Jae Kim

Korean Sensors Society conference, Jeju, Republic of Korea, November 16-17, 2012

10. Fabrication of CuO / ZnO heterostructure for non-enzymatic glucose sensor application

Shin SoYoon, Ananthakumar Ramadoss, *Balasubramaniam Saravanakumar*, Sang Jae Kim

Korean Sensors Society conference, Jeju, Republic of Korea, November 16-17, 2012



11. VUV Responses of few layer graphene irradiated by atmospheric plasma

Kaliannan Thiyagarajan, Antony Ananth, *Balasubramaniam Saravanakumar*, Young Sun Mok, Sang-Jae Kim

Korean Sensors Society conference, Jeju, Republic of Korea, November 16-17, 2012

12. Vertically aligned n-ZnO nanorods array/p-Si heterojunction for photocurrent measurement

Balasubramaniam Saravanakumar, Rajneesh Mohan, Sang-Jae Kim

The 14th Korean MEMS Conference (KMEMS), Jeju, Republic of Korea, April 5-7, 2012.

13. Fabrication of hybrid p-n junction of vertically aligned ZnO nanorods and PEDOT: PSS structure for light emitting diode applications

Balasubramaniam Saravanakumar, Rajneesh Mohan, Sang-Jae Kim

5th National Korea institute of solid state lighting conference (SISSI), Busan,
Republic of Korea, February 23, 24, 2012.

14. Electrical and optical studies of p type ZnO thin films

Balasubramaniam Saravanakumar, Rajneesh Mohan, Sang-Jae Kim

The 7th International conference on Advanced Materials and Devices (ICAMD-2011), Jeju, Republic of Korea, December 7-9, 2011.

